Charles University
Faculty of Science

Study program: Biology
Field of study: Cell and Developmental Biology

Róbert Zach

The phenomenon of mitotic catastrophe in *Δcbf11* mutant

Fenomén mitotickej katastrofy u mutanta *Δcbf11*

Diploma Thesis

Supervisor: Martin Převorovský, Ph.D.

Prague, 2017

Prehlásenie

Prohlašuji, že jsem závěrečnou práci zpracoval samostatně a že jsem uvedl všechny použité informační zdroje a literaturu. Tato práce ani její podstatná část nebyla předložena k získání jiného nebo stejného akademického titulu.

V Prahe, 27.04. 2017

Róbert Zach

Acknowledgments

I would like to express my gratitude to my supervisor, M. Prevorovsky, and all members of Gene Expression Regulation group, who significantly contributed to my personal development and improved my chances to succeed in highly competitive scientific environment. Additional thanks go to Beata Grallert, Erik Boye and all associated laboratory members who were kind enough to accept me as a trainee at the Institute for Cancer Research, Oslo and showed me scientific work from completely different perspective. Special thanks go to Christiane Rothe who managed to introduce me to procedure of cell cycle synchronization by lactose gradient centrifugation.

Abstract [Eng]

Fission yeast, *Schizosaccharomyces pombe,* represents a key model organism for studies of cell cycle regulation. Even though the biology of *S. pombe* is described to a great detail, certain aspects of crucial importance regarding cell cycle governing regulatory circuits are still unclear. In this study, we investigate a fission yeast CSL homologous transcription factor, Cbf11, the function of which is important for successful mitosis. *Δcbf11* mutants are characterized by growth retardation and display a broad range of defects, of which we focus on catastrophic mitosis, also known as the cut (cell untimely torn) phenotype. We show the growth defects and the cut phenotype prevalence are conditional, being severe in *Δcbf11* populations grown in the rich YES medium, but significantly less pronounced, when cultured in the minimal EMM medium. Our data indicate that the EMM-mediated cut phenotype rescue is caused by the excessive availability of nitrogen source (ammonium chloride in EMM), though we do not provide any molecular explanation. According to our data, mitotic defects observed in *Δcbf11* mutants arise from transcriptional deregulation of lipid anabolism genes, *cut6* and *vht1*, respectively encoding acetyl coenzyme A carboxylase and biotin transporter. Since Cut6 performance is biotin-dependent, we argue that the lower levels of Cut6 combined with the insufficient biotin transport results in downscaling of Cut6 activity, impairment of fatty acid synthesis and mitotic failure. Employing different synchronization techniques, including Cdc10-M17 block/release, hydroxyurea block/release and synchronization by lactose gradient centrifugation, we disproved that *cut6*, *vht1* and functionally related *bio2* (biotin synthase) display cell cycle contextual periodicity of transcription. We tested, whether the complete biotin withdrawal induces mitotic defects in WT cells, finding that the biotin-starved yeasts arrest the cell cycle, rather than commit catastrophic mitosis. To enrich our experimental toolset, we aspired to construct a conditional *cbf11* mutant, using a plant-derived auxin inducible protein degradation system. According to the basic genotyping, *cbf11:3HA:aid:kanR* allele has been constructed and successfully transformed. Detection of expression at the protein level, however, has not been successfully conducted, leaving construction procedure unfinished.

Abstract [SK]

Kvasinka, *Schizosaccharomyces pombe,* predstavuje kľúčový modelový organizmus pre výskum regulácie bunkového cyklu. Aj keď je biológia *S. Pombe* popísaná do veľkých detailov, určité kriticky dôležité aspekty týkajúce sa regulačných okruhov riadiacich bunkový cyklus sú stále nejasné. V rámci tejto štúdie, skúmame *S. pombe* CSL-homologický transckripčný faktor, Cbf11, ktorého funkcia je dôležitá pre úspešnú mitózu. Mutant *Δcbf11* je charakteristický spomaleným rastom a širokou škálou defektov, z ktorých sa zameriavame na katastrofickú mitózu, taktiež známu ako cut (cell untimely torn) fenotyp. Ukazujeme, že rastové defekty a výskyt cut fenotypu sú podmienené, vykazujúc veľkú závažnosť v populáciách *Δcbf11* buniek pestovaných v bohatom YES médiu a významné potlačenie v minimálnom EMM médiu. Naše dáta nasvedčujú, že EMM médiom indukované potlačenie cut fenotypu, je spôsobené nadbytkom zdroja dusíku (v prípade EMM, chlorid amónny), avšak neprichádzame so žiadnym molekulárnym vysvetlením. Podľa našich výsledkov, mitotické defekty pozorované u mutanta *Δcbf11* vyplývajú z transkripčnej deregulácie génov anabolismu lipidov, *cut6* a *vht1*, kódujúcich acetyl koenzým A karboxylásu a biotínový transportér. Keďže funkcia Cut6 je závislá na biotíne, tvrdíme, že znížená hladina Cut6 v kombinácii s nedostatočným transportom biotínu má za následok redukciu aktivity Cut6, narušenie produkcie acetylu koenzým A a mitotické zlyhanie. S využitím rôznych synchronizačných techník, vrátane Cdc10-M17 block/release, hydroxyurea block/release a synchronizácie prostredníctvom centrifugácie v laktózovom gradiente, sme vyvrátili, že *cut6*, *vht1* and funkčne súvisiaci *bio2* (biotín syntáza) vykazujú periodickú transkripciu v kontexte bunkového cyklu. Otestovali sme či kompletné odstránenie biotínu indukuje vznik mitotických defektov u WT buniek, zistiac, že bunky hladujúce na biotín zastavujú bunkový cyklus a neprechádzajú katastrofickou mitózou. Aby sme obohatili našu kolekciu experimentálnych nástrojov, s využitím auxínom indukovaného proteín degradačného systému odvodeného od rastlín sme chceli skonštruovať podmieneného mutanta *cbf11*. Na základe genotypizácie bola alela *cbf11:3HA:aid:kanR* úspešne skonštruovaná a transformovaná, avšak, detekcia expresie na úrovni proteínu nebola úspešná, ponechávajúc konštrukciu nedokončenú.

List of abbreviations

AB	Aniline blue
Ac-CoA	Acetyl coenzyme A
aid	Auxin inducible degron
AP	Alkaline phosphatase
ATP	Adenosine triphosphate
BF	Bright field
BTD	β-trefoil domain
cAMP	Cyclic adenosine monophosphate
cdc	Cell division cycle
cDNA	Complementary DNA
CTP	Cytidine triphosphate
cut	Cell untimely torn
DAPI	4',6-Diamidine-2'-phenylindole dihydrochloride
DIC	Differential interference contrast
DMSO	Dimethylsulfoxid
dNTP	Deoxynucleoside triphosphate
DT	Doubling time
DTT	Dithiotreitol
EMM	Edinburgh minimal medium
FA	Fatty acid
G	Glucose
GFP	Green fluorescence protein
HU	Hydroxyurea
kan	kanamycin
LiAc	Lithium acetate
MAPK	Mitogene activated protein kinase
NE	Nuclear envelope
NICD	Notch intracellular domain
no-RT	No reverse transcriptase
NTC	No template control
OD	Optical density
PA	Phosphatidic acid
Page	Polyacrylamide gel electrophoresis
PCR	Polymerase chain reaction
PDC	Pyruvate dehydrogenase complex
PEG	Polyethylenglykol
PI	Propidium iodide
PL	Phospholipid
PMG	Pombe minimal glutamate
PVDF	Polyvinylidenfluorid
qPCR	quantitative PCR
rcf	Relative centrifugal force
RHR	Rel homology region
RNR	Ribonucleotide reductase
RT	Reverse Transcription
SDS	Sodium dodecyl sulfate
SPB	Spindle pole body
ssDNA	Salmon sperm DNA
TAE	Tris base, acetic acid, EDTA
TAG	Triacylglycerol
TBS	Tris buffered saline
TBSt	Tris buffered saline + tween
TCA	Trichloroacetic acid
TE	Tris base EDTA
UTP	Uridine triphosphate
WT	Wild type
YES	Yeast extract with supplements
YPD	Yeast extract peptone dextrose

Contents

1 INTRODUCTION

Fission yeast, *Schizosaccharomyces pombe*, has been widely used as a model organism for studies of cell cycle regulatory circuits. *S. pombe* is characterized by the employment of closed mitosis and medial fission mediated cell division. To avoid mitotic failure, processes of karyokinesis and cytokinesis must be properly coordinated. If such coordination is impaired, unseparated nuclear mass is intersected by developing septum, ultimately resulting in cut (cell untimely torn) phenotype. Up to date, several *S. pombe* cut mutants have been characterized. Apart from factors, the function of which is directly connected to processes governing separation of chromosomes, development of cut phenotype is characteristic for lipid metabolism defective mutants. Such a phenomenon is only partially understood and indicates the existence of unknown mitosis related signalling platforms in species, the cell cycle control of which is considered described in great detail. In our study, we identify a CSL homologous transcription factor, Cbf11, which is also crucially important for mitotic progression, but its exact role has not yet been determined. According to microarray-based screen for Cbf11-target genes, Cbf11 display highly pleiotropic character, regulating transcription of a wide spectrum of genes with various functions. Interestingly, the list of Cbf11-targets includes a set of lipid metabolism genes, suggesting a possible explanation for frequently occurring mitotic defects in Cbf11-defficient cells.

2 THESIS OBJECTIVES

In this study we aim to acquire a better understanding of *S. pombe* CSL homologous transcription factor, Cbf11, in the contexts of mitosis, lipid metabolism and nutrition. First of all, we want to determine, whether lipid metabolism downregulation represents the ultimate cause of mitotic failure observed in Cbf11-defficient cells. Additionally we aspire to outline general characteristics of *cbf11*-null mutant grown under different cultivation conditions. Since laboratory work with severely sick mutants, such as *cbf11* knockout, is inconvenient and often experimentally limiting, we attempt to construct the auxin-inducible Cbf11 degradation system, which, if functional, would allow us to mimic Cbf11-defficient state in a controlled manner.

3 LITERATURE REVIEW

3.1 CSL transcription factors

3.1.1 CLS proteins: brief introduction

CSL (CBF1/RBP-Jκ/Suppressor of Hairless/LAG-1) proteins are conserved transcription factors and the executive components of the Notch-signaling pathway [1,2]. Crystal structure of *Caenorhabditis elegans* CSL-homolog, LAG-1, revealed, that CSL proteins comprise of the central β-trefoil domain spanned by N-terminal and C-terminal folds, which structurally resemble the amino- and carboxy-terminal regions of RHR (Rel Homology Region) transcription factors [3] (Fig. 1).

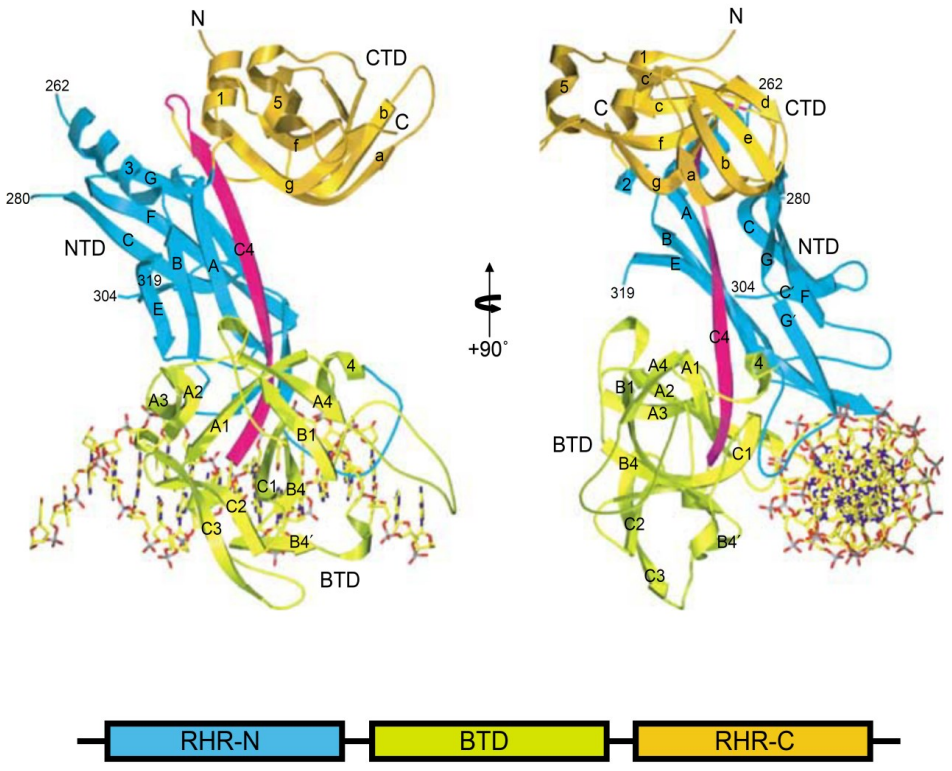

Fig. 1 – Ribbon representation of 2.85 Å crystal structure of *Caenorhabditis elegans* CSL protein (LAG-1) in a complex with DNA molecule. Structural domains: RHR-N (N-terminal domain), BTD (central β-trefoil domain), RHR-C (C-terminal domain) are indicated by different colours, as schematically illustrated. Structure is shown from two orthogonal perspectives. Figure is adapted from [3].

The Notch regulatory network, and therefore CSL function, is crucial for development [4], associated processes such as proliferation [5], apoptosis [6] and differentiation [7,8]. In the canonical Notch signaling model, the Notch receptor is activated by binding of the extracellular ligand [9]. Upon activation, the Notch receptor undergoes proteolytic cleavage, which results in liberation of the Notch intracellular domain, NICD [10]. Released NICD migrates to the nucleus and forms a complex with the CSL protein. NICD-CSL complex associates with the CSL transcriptional co-activators and promotes transcription of genes containing the CSL response element, CGTGGGAA [9,11]. Interestingly, accumulating evidence indicates that the canonical Notch pathway is not the only signaling platform involving CSLs. Notch independent CSL functions have been previously implicated in *Drosophila melanogaster* development [12–14] and recently in tumor growth and hypoxic response in breast cancer cells [15].

3.1.2 CSL proteins in Notch-deficient fungal species: *Schizosaccharomyces pombe*

Apart from higher eukaryotes, CSL homologous proteins have been identified in distinct Notch-deficient fungal species, including unicellular fission yeast, *Schizosaccharomyces pombe* [16]. *S. pombe* encodes two CSL paralogs, Cbf11 and Cbf12. Both proteins function as genuine transcription factors [17,18], recognizing canonical CSL-response element, CGTGGGAA [18]. *cbf11* and *cbf12* are non-essential genes, as yeasts depleted of one or both paralogs remain viable [17]. According to previous data of M. Prevorovsky, functions of Cbf11 and Cbf12 are not redundant, but in some cases may be allocated to the same signaling networks. Transcription of *cbf11* and *cbf12* shows markedly different profiles during the course of microbial culture growth. While *cbf11* expression is only slightly elevated from the early exponential to stationary phase of growth, *cbf12* transcription is markedly upregulated upon the stationary phase entry. Regarding the exponential growth, *cbf12* expression levels are lower in comparison with *cbf11* [17]. Cbf12-depleted fission yeasts are characterized by low surface adhesivity [17]. Interestingly, *Δcbf11* cells display exactly opposite phenotype, being solid surface hyper-adhesive and hyper-flocculating, when cultured in the liquid YES (Yeast Extract with Supplements) medium [17]. These findings imply an interesting possibility of opposing modes of Cbf11 ad Cbf12 functioning in the context of mediating the cell-surface

and cell-cell contact [17]. Apart from showing lower degree of surface adhesion, cells mutated in *cbf12* gene do not display any pronounced defects, sustaining the WT-like constitution of cellular morphology and growth [17]. Quite oppositely, Cbf11-defficient cells display broad range of morphological disorders, including aberrant cellular shapes and sizes, multi-septation, nuclear fragmentation, frequent occurrence of mitotic failure and severe growth impairment [17,19,20]. Intriguingly, *Δcbf11*-like phenotypes are developed in *cbf12*-overexpressing cells, providing another evidence of yet unclear inverse functions of both transcription factors. Consistently with cellular characteristics of *Δcbf11* cultures, colonies of Cbf11-defficient cells also display aberrant morphology and contain sectors enriched with dead cells. Additionally to the management of cellular and nuclear morphology, mitotic progression and surface interactions, Cbf11 seems to be involved in the oxidative stress responding regulatory circuits [21,22]. In comparison with WT, Cbf11-defficient cells are resistant to H_2O_2 treatment and show steady state upregulation of oxidative stress responsive genes [21,22]. Quite curiously, compared to WT cultures, *Δcbf11* populations are long-living, being capable of forming viable colonies for 2-3 times longer after the stationary phase of growth entry (unpublished data). Another complexity of Cbf11 functioning emerges from the fact that *Δcbf11*-specific defects are synthetically rescued by co-deletion of *sty1* and *pka1* genes, respectively encoding MAPK Sty1 and cAMP-dependent protein kinase catalytic subunit Pka1 [19]. Since Sty1 and Pka1 represent the core components of stress and nutrition response signaling pathways [23], Cbf11 function may be overlapping with sensing and/or integration of extracellular stimuli. Thus, based on the results of M. Prevorovsky and associates, Cbf11 transcription factor is involved in a broad range of crucially important cellular functions, which may or may not be intertwined. The function of Cbf12 is less clear, however, considering that the only defects observed in *cbf12* mutants are connected to surface adhesion, the function of Cbf12 seems to more specialized and less important at laboratory conditions. Some evidence indicate a crosstalk between Cbf11 and Cbf12 functions, but the molecular models of overlapping signaling has not yet been postulated.

3.2 Mitotic failure & lipid metabolism

3.2.1 The special case of cell division cycle mutants: CUT

The cell division cycle could be regarded as a repeating process, during which chromosomes are replicated, segregated and equally distributed among daughter cells. The faithful cell cycle progression is tightly regulated by a complex signalling network, which ensures the maintenance of genome integrity across generations. Fission yeast, *Schizosaccharomyces pombe*, has been widely used as a model for studies of cell cycle control [24]. In general, two distinct classes of mutants defective in cell cycle progression have been characterized in *S. pombe*. The cdc (cell division cycle) mutants arrest the cell cycle progression, but do not undergo catastrophic mitosis [25]. On the contrary, the cut (cell untimely torn) mutants progress through the cell cycle, but fail to divide the nucleus, which is ultimately intersected by developing septum [26,27] (Fig. 2).

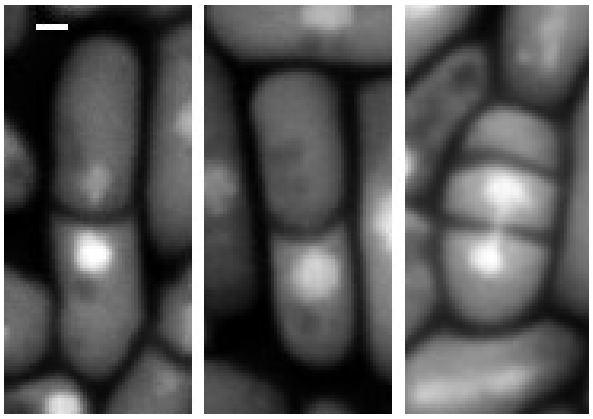

Fig. 2 – illustrative images of DAPI-stained cells with characteristic cut phenotype. DAPI-channel images are shown. Scale bar 1 µm.

Since the nuclear mass undergoing cut-mitosis is mechanically cleaved, chromosomes are grossly damaged and their segregation is not equal. Even though it has been shown that some cases of catastrophic mitosis can be coped with [28], the cut phenotype is in principle regarded as a terminal defect. Most of the cut mutants are directly involved in the anaphase promotion and segregation of chromosomes, being defective in topoisomerase II [29,30], 20S cyclosome/APC complex [31,32], 26S proteasome [33,34], securin/separase [35–37], condensin [38] and mitotic spindle [28] functions. All of these mutants fail to separate

chromosomal masses, stall in metaphase but do not inhibit cytokinesis, the execution of which is terminal. Consistently with reported defects of the metaphase/anaphase transition mutants, treatment with bortezomib, an inhibitor of 26S proteasome and an anti-cancer drug [39,40], also induces catastrophic mitosis in *S. pombe* cells [41]. Interestingly, development of cut phenotype is not exclusive for the obvious mitosis related mutants, but has been also characterized in the less understood mutants defective in lipid metabolism. Moreover, a genetic screen of the 2815-member *S. pombe* deletion library revealed 14 non-proteasomal mutants hypersensitive to bortezomib treatment. 14 newly identified SLB (synthetic lethal with bortezomib) genes are functionally connected to organization of chromatin/nucleus, vesicle transport, metabolism, PKA-signalling and metabolism of RNA, implying a complex signalling background of catastrophic mitosis commitment [41]. Regarding the main theme of this work and the recent progress in understanding of mitotic role of lipid metabolism, the phenomenon of lipid metabolism cut-mutants is reviewed in the upcoming chapters.

3.2.2 Lipid metabolism cut mutants

The first evidence indicating the importance of undisrupted lipid metabolism in the context of mitosis dates to the year of 1996, when Saitoh et al. published a study characterizing two lipid metabolism genes, *cut6* and *lsd1/fas2*, as factors necessary for proper nuclear division. Products of both genes, *cut6* (acetyl coenzyme A carboxylase) and *lsd1/fas2* (fatty acid synthase alpha subunit) represent the core components of fatty acid (FA) anabolism. Acetyl coenzyme A (Ac-CoA) carboxylase catalyzes the rate limiting step in fatty acid synthesis, using Ac-CoA as a substrate and producing malonyl-CoA [42]. Ac-CoA and 7 molecules of malonyl-CoA are utilized by fatty acid synthase, ultimately resulting in palmitate synthesis [43]. Functional impairment of Cut6 and Lsd1/Fas2 generates daughter cells with nuclei of unequal sizes or results in terminal catastrophic mitosis [44]. Both enzymes, Cut6 and Lsd1/Fas2, utilize Ac-CoA as a substrate. Thus, it is not surprising, that the impairment of Ac-CoA production results in mitotic defects of analogous character [45–47]. Yeast production of Ac-CoA depends on the pyruvate dehydrogenase complex (PDC) mediated pyruvate decarboxylation, fatty acid β-oxidation and Ac-CoA synthase reactions, of which Ac-CoA synthase is considered a major provider of cytoplasmic Ac-CoA utilizable for fatty acid

synthesis [48–50]. The molecule of CoA is synthesized from pantothenate (vitamin B_5), cysteine and ATP in the canonical 5-step reaction, mediated by enzymes: pantothenate kinase, 4'-phosphopantothenoylcysteine synthase, 4'-phosphopantothenoylcysteine decarboxylase, 4'-phosphopantetheine adenylyltransferase and dephospho-CoA kinase [51] (Fig. 3).

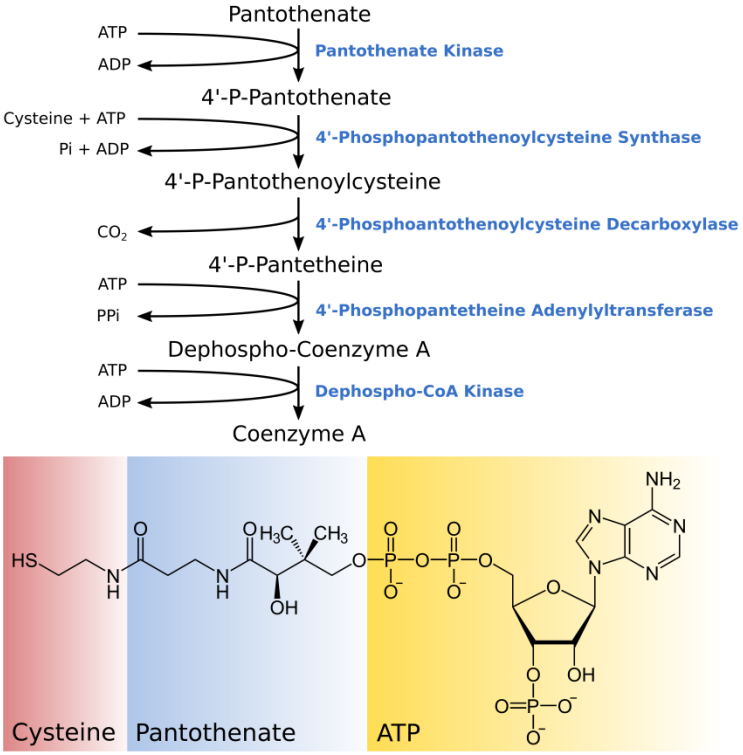

Fig. 3 – Overview of Coenzyme A synthesis. Illustration is redrawn version of image presented in [51]. The image of CoA molecule is retrieved from Wikipedia.org. Distinct contributions of cysteine, pantothenate and ATP to the final CoA structure are depicted by colour coding.

Pantothenate is acquired from the environment or de novo synthesized from the uracil precursor via metabolic pathway involving ureidopropionate and β-alanine intermediates in *S. pombe* [46]. *S. pombe* high-affinity H^+-pantothenate symporter encoding gene *liz1* has been characterized as a conditional cut mutant. *Δliz1* cells undergo catastrophic mitosis only when exposed to hydroxyurea (HU) [45,46]. HU represents the ribonucleotide reductase (RNR) inhibitor and the inducer of replication stress [52]. Several mutants defective in checkpoint signalling and DNA repair have been previously shown to undergo defective

mitosis, when exposed to HU [53–55], however, considering, that the post S-phase G_2-synchronized *Δliz1* cells fail to proceed through successful mitosis upon HU-treatment, it is not likely, that mitotic defects displayed by *Δliz1* mutant are consequential to defective DNA synthesis [46]. It is discussed, that the inhibition of RNR results in the accumulation of cytidine triphosphate (CTP) and uridine triphosphate (UTP), the higher levels of which inhibit de novo uracil synthesis in a negative feedback loop manner. Since uracil drives pantothenate synthesis, RNR function deficient *Δliz1* cells have no other means of pantothenate production. Reduction in the intracellular pantothenate levels possibly results in depletion of CoA and Ac-CoA pools and causes fatty acid anabolism malfunctioning [46]. The aberrant phenotypes of *Δliz1* cells induced by HU can be rescued by supplementing the cultivation medium with high concentration of pantothenate, uracil, ureidopropionate or β-alanin, indicating that the observed mitotic defects are indeed functionally linked to the unavailability of intracellular pantothenate [46]. Pantothenate transporter Liz1 is not the only CoA metabolism factor, the function of which has been proven to be important for successful mitosis in *S. pombe*. T. Nakamura et al. showed that the function of phosphopantothenoylcysteine synthetase (Ppc1), the enzyme catalyzing the second step in CoA synthesis (Fig. 3), is also necessary for undisrupted nuclear division [47]. Upon inactivation by thermal shock, temperature-sensitive mutants, *ppc1-537* and *ppc1-88*, undergo aberrant mitosis. *ppc1-537* mutants display decreased intracellular levels of CoA and Ac-CoA and are characterized by diminished amounts of neutral storage lipids, which indicates that inhibition of CoA synthesis directly affects cellular lipid metabolism [47]. Being long unexplained, the intriguing phenomenon of lipid metabolism cut-mutants has been recently clarified. The relevant clues, leading to deciphering the role of lipid metabolism in successful mitosis of *S. pombe* are discussed in the following text.

3.2.3 Closed mitosis and the phenomenon of nuclear expansion

While higher eukaryotes employ open mitosis, which is accompanied by nuclear envelope breakdown [56], many fungal species, such as *Schizosaccharomyces pombe* and *Saccharomyces cerevisiae*, segregate chromosomes inside the intact nuclear compartment, during so called ‘closed mitosis’ [57]. In *S. pombe*, mitotic nucleus undergoes series of

morphological changes. The initial sphere-shaped nuclear body forms spherocylinder, which is turned into a dumbbell structure. Dumbbell stage is subsequently resolved into two sphere-shaped daughter nuclei [58–60] (Fig. 4).

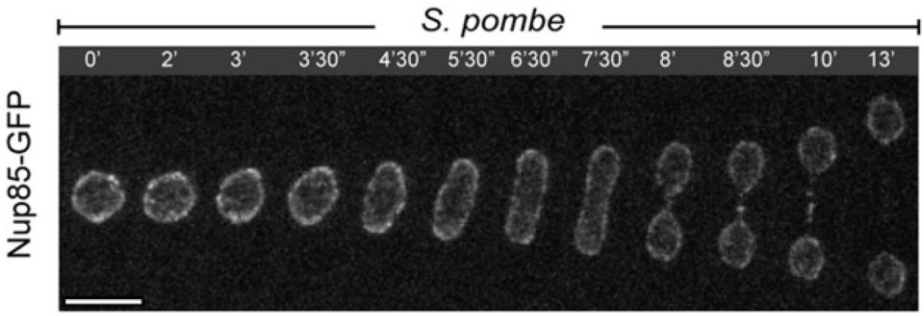

Fig. 4 – Nuclear morphology transformation during mitosis in *S. pombe*. Time lapse microscopy of mitosis-undergoing *S. pombe* cell expressing GFP-tagged nucleoporin Nup85 as a marker of nuclear membrane. Figure is adopted from [58].

Nuclear envelope (NE) transformation and chromosome segregation are driven by intranuclear mitotic spindle [59–61], which is nucleated by two opposite spindle pole bodies (SPBs), the equivalents of metazoan centrosomes. The resolution of mitotic nucleus into two daughter nuclei proceeds in less than 5 min and is accompanied by increase in NE area. The experimental results and mathematical models state, that the membrane surface of mitotic nucleus is increased by 33% ± 4% and 26%, respectively [58,61–63] in *S. pombe*. According to the biomechanical modelling of lipid bilayers, such nuclear expansion cannot be simply attributed to the membrane stretching and thus, must be accompanied by incorporation of new phospholipids [64]. It is well known, that NE area continually increases, expanding by 59% during *S. pombe* interphase [61,65], however, considering the rapidness (< 5 min) and the scale (26 / 33% ± 4%) of mitotic nuclear expansion, the increase in NE area must be explained by mechanism/s other than continual nuclear growth.

3.2.4 Nuclear membrane biogenesis during mitosis: a lipid metabolism switch

The idea of mitosis-specific nuclear membrane biogenesis is supported by the fact, that closed mitosis-employing budding yeasts accumulate abnormal nuclear membrane structures (flares), when blocked in mitosis, but not when arrested in the S or G_2 phases [66]. Interestingly, nuclear flares are also observed in the pheromone-arrested G_1 cells. Since

pheromone-activated sexual cycle is (similarly to closed mitosis) characterized by dynamic nuclear rearrangements, it is possible that nucleus-directed channelling of phospholipids is regulated as a general response to the elevated need for extensive NE dynamics [66,67]. Another piece of evidence suggesting mobilisation and NE-directed incorporation of phospholipids during closed mitosis emerges from the studies of regulatory circuits of phosphatidic acid (PA) metabolism. Except de-novo synthesis, formation of PA is secured by three enzymatic reactions: acylation of lyso-PA, phosphorylation of diacylglycerol (DAG) and phospholipase D-mediated phospholipid (PL) hydrolysis [68]. PA is utilized for production of structural phospholipids or storage triacylglycerols (TAGs). Dephosphorylation of PA to DAG, a substrate for TAG synthesis, is catalyzed by PA phosphatase (lipin) [69]. Lipin could thus be regarded as a decision point, at which it is decided whether cell favours production of structural or storage lipids (Fig. 5). Most of the knowledge covering the signalling network involving lipin emerges from the studies conducted on budding yeast, *S. cerevisiae*. The activity of budding yeast lipin Smp2p/Pah1p is regulated by phosphorylation. Membrane-bound phosphatase complex Nem1p-Spo7p localizes to the ER and NE [70] and activates Smp2p/Pah1p, which dephosphorylates PA and drives TAG synthesis [69,71,72]. Negative regulation of Smp2p/Pah1p is secured by several kinases including Cdc28p (CDK1), Pho85p-Pho80p, PKA, TORC1 and CKII [73–77]. Deletion of *SMP2/PAH1* or either one of the genes encoding the Nem1p-Spo7p complex subunits results in development of aberrantly shaped nuclei with extensive protrusions [70,71]. Consistently, the same results are achieved by overexpressing diacylglycerol kinase (*DGK1*), which functions antagonistically to *SMP2/PAH1* [78]. Nuclear defects of *smp2/pah1* and *nem1-spo7* mutants are rescued by disruption of phospholipid synthesis, indicating that the formation of NE membrane protrusions is dependent on incorporation of newly synthesized phospholipids [71]. *S. pombe* cells carrying the null alleles of *nem1*, *spo7* or *ned1* (the lipin homolog) display similar phenotypes. *Δnem1*, *Δspo7* and *Δned1* mutants are characterized by elongated occasionally constricted nuclei and overdeveloped ER membranes [62,79]. In both, *S. cerevisiae* and *S. pombe*, lipin is phosphorylated and thus inhibited by CDK1 kinase at the onset of M-phase [62,71]. It has been shown, that CDK1-mediated Ned1 phosphorylation plays a critical role in successful

mitosis. Makarova et al. showed that the *S. pombe* haploid mutants carrying the non-phosphorylatable *ned1* allele are not viable, undergoing catastrophic mitosis in the first cell division after spore germination. Thus, the elevated rate of phospholipid synthesis is necessary for nuclear division in *S. pombe* [62].

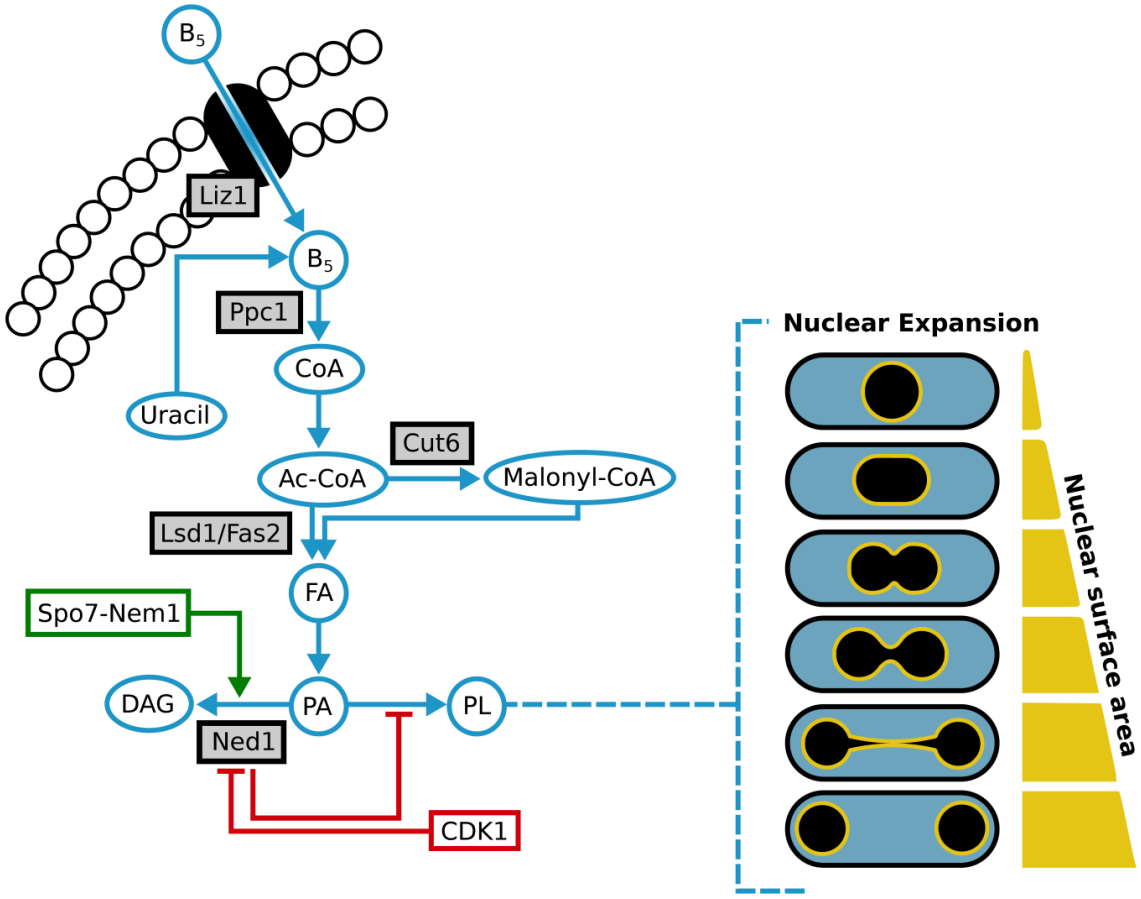

Fig. 5 – Schematic overview of lipid metabolism pathways affecting progression through closed mitosis in *Schizosaccharomyces pombe*. Several nodes of lipid metabolism pathways including Liz1, Ppc1, Lsd1/Fas2, Cut6 and Ned1 have been characterized as factors critical for successful mitosis in *S. pombe*. All factors are discussed in the text. Abbreviations: B_5 – vitamin B_5 (Pantothenate), CoA – Coenzyme A, Ac-CoA – Acetyl Coenzyme A, FA – Fatty Acid, PA – Phosphatidic Acid, PL – Phospholipid, DAG – Diacylglycerol, Liz1 – Pantothenate transporter, Ppc1 – Phosphopantothenoylcysteine synthetase, Lsd1/Fas2 – Fatty acid synthase alpha subunit, Cut6 – Ac-CoA carboxylase, Ned1 – Phosphatidic acid phosphatase, Spo7-Nem1 – Ned1 phosphatase, CDK1 – cyclin dependent kinase 1.

3.2.5 Closed & semi-open mitosis: implications of nuclear expansion

Finally, it has been determined, that nuclear expansion strictly depends on undisrupted fatty acid anabolism and is required for successful progression through mitosis in *S. pombe*. *S. pombe* cells exposed to the fatty acid synthase inhibitors, cerulenin and Cutin-1, are unable to expand nuclear membrane and ultimately undergo catastrophic mitosis or produce daughter cells with unequally sized nuclei [58,63]. Strikingly, this does not apply for *Schizosaccharomyces japonicus*, a close *S. pombe* relative. *S. japonicus* undergoes semi-open mitosis, which is not accompanied by nuclear expansion and is unaffected by cerulenin treatment [58]. It has been proven, that the CDK1-mediated mitotic phosphorylation of lipin, Ned1, is absent in *S. japonicus*, and semi-open mitosis does not negatively respond to the constant Ned1 activation [62]. Unlike closed mitosis, semi-open mitosis is accompanied by NE rupture at the point of late anaphase. NE rupture occurs independently of physical forces generated by mitotic spindle, thus, it is possible that *S. japonicus* cells breach nuclear membrane in a regulated manner independent of spindle elongation [58,80], achieving relief of spatial and geometrical constraints created by the intact nuclear membrane. To reach the same goal, *S. pombe* expands nuclear membrane by incorporating new phospholipids. Satisfactory supply of phospholipids during mitosis is dependent on functional lipid anabolism apparatus, making *S. pombe* cells highly sensitive to different kinds of lipid metabolism impairments, including genetic mutations and chemical treatments.

4 MATERIALS & METHODS

4.1 Fission yeast cultures

4.1.1 List of fission yeast strains used in this study

ID	Genotype	Source
1659	*h- cdc10-M17 ade6+pADH15.skp1:AtTIR1:2NLS:9myc mcm4:2HA:aid:ura4+ ura4-D18*	B. Grallert Institute for Cancer Research, Oslo
JB32	*h+s*	Laboratory Stock
MP26	*h+ cbf11-3HA::natR*	Laboratory Stock
MP44	*h+ Δcbf11::kanR*	Laboratory Stock
MP203	*h- cdc10-M17*	Laboratory Stock
MP326	*h- leu1 ura4 gar2:mCherry:kanR*	Laboratory Stock
MP342	*h- ura4-D18 leu1-32 ade6-M21? Pcut6MUT*	Laboratory Stock
MP344	*h+ Δcbf11::natR gar2:GFP-kanR*	Laboratory Stock
MP369	*h- ura4-D18 leu1-32 ade6-M21? Δcbf11::kanR Pcut6MUT*	Laboratory Stock
MP392	*h- ura4-D18 leu1-32 Pcut6MUT Δvht1::ura4+ can1?*	Laboratory Stock
MP420	*h- ura4-D18 leu1-32 Pcut6MUT Δvht1::ura4+ Δcbf11::natR can1?*	Laboratory Stock
MP520	*h+ cbf11:3HA:aid:kanR*	This Study
MP534	*h+ ura4-D18 ade6+pADH15.skp1:AtTIR1:2NLS:9myc*	This Study
MP535	*h- ura4-D18 ade6+pADH15.skp1:AtTIR1:2NLS:9myc cdc10-M17*	This Study
MP536	*h+ ura4-D18 ade6+pADH15.skp1:AtTIR1:2NLS:9myc cbf11-3HA-aid-kanR*	This Study
MP537	*h+ ura4-D18 ade6+pADH15.skp1:AtTIR1:2NLS:9myc cbf11-3HA-aid-kanR*	This Study
MP538	*h- ura4-D18 ade6+pADH15.skp1:AtTIR1:2NLS:9myc cbf11-3HA-aid-kanR*	This Study
MP539	*h+ ura4-D18 ade6+pADH15.skp1:AtTIR1:2NLS:9myc cbf11-3HA-aid-kanR*	This Study
MP545	*h+ s Δbio2::hygR*	Laboratory Stock
MP546	*h- ura4-D18 leu1-32 ade6-M21? Pcut6MUT Δbio2::hygR*	Laboratory Stock
MP550	*h+s natMX6-Padh1-3HA:cut6+*	Laboratory Stock
MP551	*h+s natMX6-Padh1-3HA:cut6+*	Laboratory Stock
MP552	*h+s natMX6-Padh1-3HA:cut6+*	Laboratory Stock
MP553	*h+ Δcbf11::kanR natMX6-Padh1-3HA:cut6+*	Laboratory Stock
MP555	*h+ Δcbf11::kanR natMX6-Padh1-3HA:cut6+*	Laboratory Stock
MP556	*h+ Δcbf11::kanR natMX6-Padh1-3HA:cut6+*	Laboratory Stock
Δvht1	*h- can1-1 leu1-32 ura4-D18 ade6-M210 Δvht1::ura4+*	Laboratory Stock

4.1.2 Cultivation and culture handling

Cells are stored at -80°C in a form of dense suspension containing 30% glycerol. Cells are freshly withdrawn from the freezer, plated on solid YES (Yeast Extract with Supplements) and incubated at 32°C for roughly 48 hours before every experiment. Cell containing plates may be further stored at 25°C, however usage of older cells is not recommended. Strains carrying temperature-sensitive mutations are incubated at 25°C for no more than 7 days. After initial incubation on solid media, small fraction of biomass is introduced into a liquid medium and cultured for 12-24 hours at desired temperature (usually 25°C or 32°C). Resulting culture is used for inoculation of a primary culture, which is kept in exponential growth by diluting, roughly every 12 hours, depending on the temperature and the genotype of cultured strain. Cells are cultured for at least 10 generations and subsequently used for the experimental purposes.

4.1.3 Cultivation media

Cultivation media are prepared according to the recipes listed in Table 1. To prepare a sterile medium, medium of choice without glucose and 20% glucose (G) (SIGMA-ALDRICH, G7021-1KG) solutions (20% G) are separately prepared and sterilized by autoclaving. After sterilization, medium is mixed with the corresponding volume of 20% G. The YES medium is prepared by dissolving Yeast Extract (Formedium, YEM03) and SP supplements (Formedium, PSU0101) in deionized water. Standard EMM medium is prepared by dissolving commercially available powder (EMM broth without dextrose, Formedium, PMD0405) in deionized water. The EMM medium without biotin (EMM w/o biotin) is prepared by mixing the single components according to the Formedium EMM recipe listed in Table 1. Solid media are prepared by adding 2% (w/v) Difco Bacto Agar. For preparation of the antibiotics containing selection media, concentrated antibiotics solution is mixed, filter sterilized and added to the sterile medium. Since antibiotics might be damaged by high temperatures, media must be cooled down before supplementation. In this study, selection for kanR cassette by geneticin (G418) is used. G418 is stored at 4°C as a filter sterilized 1000x (100 g/l) stock solution and added to the medium to final concentration 100 mg/l. G418 does not work in EMM, but can

be used in the YES or PMG (Pombe Minimal Glutamate) media [81]. In this study the YES+G418 medium is used.

Table 1 – Cultivation media recipes

EMM & derivatives	EMM	EMM w/o biotin	Solid EMM
Glucose	2%	2%	2%
Phthalic acid K+	3 g/l	3 g/l	3 g/l
Na_2HPO_4	2.2 g/l	2.2 g/l	2.2 g/l
NH_4Cl	5 g/l	5 g/l	5 g/l
$MgCl_2.6H_2O$	1.05 g/l	1.05 g/l	1.05 g/l
$CaCl_2.2H_2O$	14.7 mg/l	14.7 mg/l	14.7 mg/l
KCl	1 g/l	1 g/l	1 g/l
Na_2SO_4	40 mg/l	40 mg/l	40 mg/l
Pantothenic acid	1 mg/l	1 mg/l	1 mg/l
Nicotinic acid	10 mg/l	10 mg/l	10 mg/l
Inositol	10 mg/l	10 mg/l	10 mg/l
Biotin	1 mg/l	N/A	1 mg/l
H_3BO_3	0.5 mg/l	0.5 mg/l	0.5 mg/l
$MnSO_4.H_2O$	0.4 mg/l	0.4 mg/l	0.4 mg/l
$ZnSO_4.7H_2O$	0.4 mg/l	0.4 mg/l	0.4 mg/l
$FeCl_3.6H_2O$	0.2 mg/l	0.2 mg/l	0.2 mg/l
$Na_2MoO_4.2H_2O$	0.04 mg/l	0.04 mg/l	0.04 mg/l
KI	0.1 mg/l	0.1 mg/l	0.1 mg/l
$CuSO_4.5H_2O$	0.04 mg/l	0.04 mg/l	0.04 mg/l
Citric acid	1 mg/l	1 mg/l	1 mg/l
Difco Bacto Agar (w/v)	N/A	N/A	2%

YES & derivatives	YES	Solid YES	Solid YES+G418
Glucose (w/v)	3%	3%	3%
Yeast Extract (w/v)	0.5%	0.5%	0.5%
SP supplements	0.25 g/l	0.25 g/l	0.25 g/l
Difco Bacto Agar (w/v)	N/A	2%	2%
G418	N/A	N/A	100 mg/l

Malt Extract (ME)	Solid ME
Bacto-Malt Extract (w/v)	3%
Difco Bacto Agar (w/v)	2%

4.1.4 Preparation of glycerol stocks

Glycerol stocks are prepared every time a new strain is constructed. Cells are cultured to saturation (usually no more than 2 days). 600 µl aliquot is collected and mixed with sterile 60% glycerol solution. Resulting 30% glycerol cell suspension is stored at -80°C. The 60% sterile glycerol solution is prepared by diluting 100% glycerol with deionized water and subsequent autoclaving.

4.1.5 Medium shift experiments

Exponentially growing cells of OD ≈ 0.2-0.3 (1 ml of OD = 0.5, 4 x 10^6 cells) are prepared in the EMM medium. Culture fraction of desired volume is collected and centrifuged (1000 rcf, 3 min, 25°C). Supernatant is poured off and cell pellet resuspended in the same volume of a fresh medium of choice. Resuspention medium should be pre-heated to the cultivation temperature. It is not easy to sediment cells grown in the EMM medium, therefore clear pellet is not always observed. In such a case, most of the cells are spread on the wall of centrifugation tube. If this happens, it is important to discard supernatant as quickly as possible. Cells resuspended in the fresh medium are introduced into a clean flask and incubated at desired temperature. OD measurements and sample collections are conducted in desired time intervals starting at t = 0 (the time point right after the medium shift). Alternatively, the initial culture is subjected to the OD measurements and sample collections before the shift, as a control for potential changes resulting from handling during the medium shift. Note, that 0.6 ml and 1 ml aliquots are needed for OD measurement and microscopy sample collection, therefore, it is important to use a culture of sufficient volume.

4.1.6 Crossing and sporulation

Cells of different mating types (h+ and h-) are mixed and plated on the nitrogen poor Malt Extract solid medium plate. 2-5 days after plating, presence of spores and ascii is checked. If there are spores, cell biomass is collected and suspended in 300 µl of 100-fold diluted, filter-sterilized β-glucuronidase solution (Sigma-Aldrich, G7017). Resulting cell suspension is incubated over night at 37°C. β-glucuronidase treatment ensures the elimination of diploid and unsporulated haploid cells. Acquired spores are plated on desired selection solid medium plate.

4.1.7 Estimation of doubling time (DT)

Cells are pre-cultured in the YES medium. Aliquots corresponding to 0.15 ODs (1 ml of OD = 0.15) are collected by centrifugation at low centrifugal force (1000 rcf, 3 min, 25°C). Supernatant is removed. Cell pellets are washed and re-suspended in 1.5 ml of medium of choice. 1.4 ml aliquots are loaded into the 12-well plate, which is then introduced into VarioSkan Flash (Thermo Scientific) automatic spectro-photometer. 12-well plate is incubated at 32°C with a background shaking mode (180 rpm). Optical density (λ = 595 nm) is measured every 10 min. To calculate doubling time (DT), acquired data are transformed into the $\log_2$-scale and plotted (Fig. 6). Regression line spanning the linear region of the curve is constructed. Regression line is defined by the equation: y = kx + q, where k and q are slope and y-axis intercept. DT can be calculated by applying the formula: DT = 1/k.

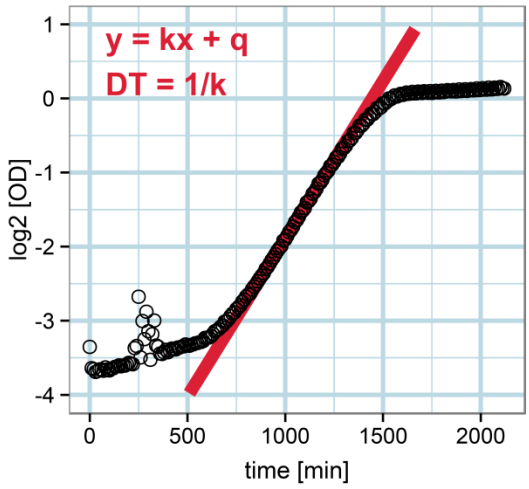

Fig. 6 – Representative growth data. Growth curve (black circles) with log-phase defined linear regression (red line). y = kx + q (the equation of linear regression), DT = 1/k (the equation determining doubling time from the slope of regression line).

4.1.8 Determination of the average k-values and hypothetical mortality of *Δcbf11* cells

The average k-values of WT and *Δcbf11* cells grown in YES are determined from the published DTs [19]. Mean DT_{WT} = 136 min, mean $DT_{\Delta cbf11}$ = 275 min. Average k-values are calculated using mathematical formula: DT = 1/k. If solved for DT = DT_{WT} (136), k = 0.00735 (k_{WT}). If solved for DT = $DT_{\Delta cbf11}$ (275), k = 0.00364 ($k_{\Delta cbf11}$) (Equation 1). The hypothetical amount of

cells dying of in every generation, which would explain the observed growth defects of *Δcbf11* mutants, is calculated using the equation: $y = 2^n$, where n = k*t (t stands for time). All calculations assume that there are no cell deaths in WT populations, and that *Δcbf11* mutants are not delayed in cell cycle progression.

Equation 1 – average k-values of WT and *Δcbf11* populations

$$\boldsymbol{DT = \frac{1}{k}} \qquad \boldsymbol{k = \frac{1}{DT}}$$

WT: $k_{WT} = \frac{1}{136}$ $k_{WT} = 0.00735$

Δcbf11: $k_{\Delta\text{cbf11}} = \frac{1}{275}$ $k_{\Delta\text{cbf11}} = 0.00364$

Equation 2 – hypothetical mortality of *Δcbf11* population

$$\boldsymbol{y = 2^n}$$

WT: $y_{wt} = 2^{0.00735*x}$ $y_{wt} = 2^{0.00735*136}$ $y_{wt} = 2$

Δcbf11: $y_{\Delta\text{cbf11}} = 2^{0.00364*x}$ $y_{\Delta\text{cbf11}} = 2^{0.00364*136}$ $y_{\Delta\text{cbf11}} = 1.409$

4.2 Microscopy and flow cytometry

4.2.1 4′,6-Diamidine-2′-phenylindole dihydrochloride (DAPI) and Aniline Blue (AB) staining

1 ml cell culture aliquot is collected and centrifuged (1000 rcf, 3 min, 25°C). Supernatant is removed and resulting pellet resuspended in 1 ml of 70% ethanol. Ethanol suspension is centrifuged (1000 rcf, 3 min, 25°C). Supernatant is removed and cell pellet resuspended in 1 ml of H_2O, for DAPI staining, or PBS, for AB staining. H_2O/PBS cell suspension is incubated at the room temperature (r.t.) for 15 min for rehydration. DAPI or AB is added to final concentrations of 1 µg/ml (DAPI) or 0.5 mg/ml (AB). Suspension is centrifuged (1000 rcf, 3 min, 25°C). Most of the supernatant is removed and cell pellet resuspended in the residual volume of supernatant. 5-10 µl of resulting cell suspensions are layered onto a microscopic

glass slide and left to dry out. Optionally, microscopic glass can be covered with lectin (Lectin from Glycine max, SIGMA-ALDRICH, L1395-5MG), which immobilizes cells by binding the surface carbohydrates. 3 µl of lectin (1 mg/ml) are spread onto one microscopic glass slide. Specimen is imaged using Olympus Cell-R microscopic device. Images are manually analyzed using ImageJ software [82]. DAPI is stored at 4°C as a 100x solution (100 µg/ml in deionized H_2O). AB is stored at 4°C as a 50x solution (25 mg/ml in deionized H_2O). Aniline blue staining procedure was adapted from [83].

4.2.2 Nile red staining

1 ml aliquot of exponentially growing culture is collected and incubated with Nile Red (10 µM, Sigma-Aldrich N3013) for 10 min at room temperature. Cell suspension is centrifuged (1000 rcf, 3 min, 25°C). Most of the supernatant is removed and cell pellet is resuspended in the residual volume. 5-10 µl of resulting cell suspension is layered onto a lectin-covered microscopic glass slide. A cover slip with a 2.5 µl drop of the YES medium is then placed onto a specimen. Specimen is imaged using Olympus Cell-R microscopic device. Microscopic setup: GFP filter, 1000 ms exposition, 50 gain, 12.03% light intensity. Z-stacked images are captured and transformed into maximum projections using ImageJ software [82]. Nile red is stored at -80°C as a 100x solution (1 mM in DMSO). Repeated freeze-thaw cycles should be avoided. Nile red staining procedure was adapted from [84].

4.2.3 DNA content analysis

10^7 exponentially growing cells are collected and centrifuged (733 rcf, 5 min, 25°C). Supernatant is removed and resulting pellet resuspended in 1 ml of 70% ethanol. 300 µl aliquot of ethanol suspension is introduced into 15 ml centrifugation tube containing 3 ml of 50 mM sodium citrate. Mixture is centrifuged (733 rcf, 5 min, 25°C) and supernatant removed. Pellet is resuspended in 0.5 ml of 50 mM sodium citrate containing 0.1 mg/ml RNase A, and incubated at 37°C over night. RNase A-treated cell suspension is mixed with 0.5 ml of 50 mM sodium citrated containing 8 ug/ml propidium iodide (PI). Final PI concentration is therefore 4 µg/ml. PI-stained cells are sonicated for 2 min in water bath. DNA content is analyzed with BC Cytoflex device and Cytexpert software (Beckman Coulter). PI staining

protocol was adapted from [85]. Gating strategy and characteristic DNA content profile are illustrated in Fig. 7.

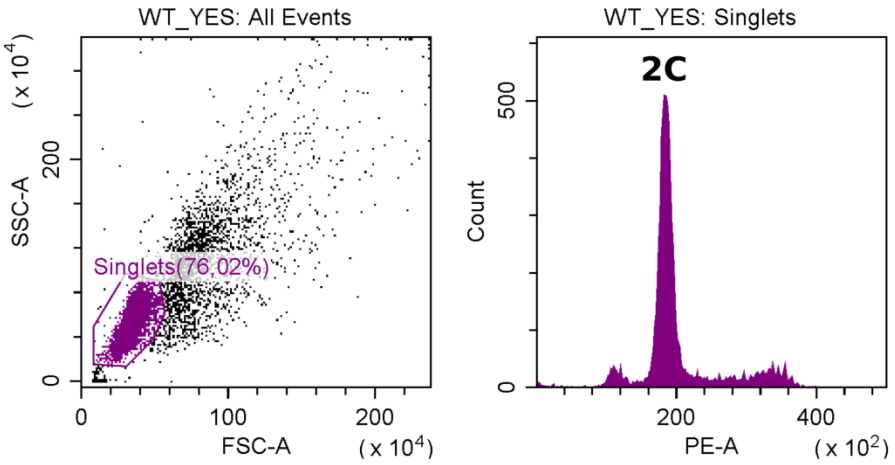

Fig. 7 – Illustrative images of the gating strategy and DNA content distribution. Images show representative flow cytometry output for WT cells grown in the YES medium. Singlets (events corresponding to single cells) are selected as a coherent subpopulation with smallest sizes. Gating is performed based on forward scatter area (FSC-A) and side scatter area (SSC-A). DNA content histogram (right panel) contains three peaks. 2C DNA content peak is characteristic for G_2 cells. Subpopulation with DNA content higher than 2C contains undivided, but already replicating cells or cell dublets. Subpopulation with DNA content lower than 2C represents S-phase cells or cellular debris. Due to the character of S. Pombe cell cycle, subpopulation of G_1 cells is absent. Graphics is made with Cytexpert software (Beckman Coulter).

4.3 Cell cycle synchronization

4.3.1 Synchronization by Cdc10-M17 temperature-driven block/release

Transcription factor Cdc10 positively regulates G_1/S transition [86]. Temperature sensitive allele, *cdc10-M17*, allows us to thermally inactivate Cdc10-M17 function and block cell cycle progression at G_1/S boundary. G_1/S-block induced by thermal inactivation of Cdc10-M17 can be reverted by thermal shift to 25°C. Culture grown at 25°C is transferred into the incubator preheated to 36°C. Cells are kept at 36°C for 4 h. After 4 h at 36°C, the culture is introduced into the 25°C water bath and cooled down (1-5 min incubation, depending on the culture volume). After cooling down, culture is transferred into 25°C incubator. 1 ml aliquots are

collected every 30 min, starting at t = 0 min. Cdc10-M17 thermal block/release synchronization protocol is derived from [81].

4.3.2 Synchronization by Hydroxyurea (HU) block/release

HU represents the inhibitor of ribonucleotide reductase, the enzyme responsible for production of deoxyribonucleotides (dNTPs). dNTPs are necessary for DNA synthesis and their depletion blocks S-phase progression. HU can thus be used for synchronization in S-phase. Exponentially growing culture is prepared as described in the cultivation and culture handling section. 1 M HU solution is prepared and filter-sterilized (always fresh). 600 µl of 1 M HU solution are added to the 49.4 ml cell culture, so the final HU concentration reaches 12 mM. HU-treated culture is incubated at 32°C for 4 h. After 4 h, culture is transferred into the 50 ml centrifugal tube and centrifuged (500 rcf, 5 min, 25°C). Supernatant is poured off and the resulting pellet washed with one volume of HU-free medium. Washing is performed twice. After the second wash, cells are resuspended in 50 ml of HU-free medium. Resulting HU-free cell suspension is transferred into a clean flask and incubated at 32°C. 1 ml aliquots are collected every 30 min, starting at t = 0 min. HU block/release protocol is derived from [81].

4.3.3 Synchronization by lactose gradient centrifugation

Cell size correlates with the actual cell-cycle phase in fission yeast. Unlike mammalian cells, due to the phase shift of karyokinesis and cytokinesis, the smallest cells are characteristic for the early G_2-phase in *Schizosaccharomyces pombe*. Using the gradient centrifugation technique, it is possible to select the subpopulation of the smallest cells and enrich the culture with the cells in early G_2. Two 10-40% lactose gradients (45 ml and 10 ml) are prepared. For preparation of lactose gradients, 10% and 40% lactose solutions are mixed. In both cases, lactose is dissolved in the cultivation medium. For the absolute dissolution, heating in the microwave oven is necessary. When properly dissolved, both lactose solutions (10% and 40%) are cooled down to 25°C in the water bath. For preparation of the larger gradient (45 ml), 50 ml centrifugation tube and the gradient maker are arranged in such a way, that 50 ml tube is situated under the gradient maker (Fig. 8). At this point, gradient maker safety valve is in the closed position, and the rubber tube connected to the gradient

maker drain leads into the 50 ml tube. 5 ml of 40% lactose solution are added to the bottom of 50 ml centrifugation tube. 20 ml of 10% lactose solution are added into the gradient maker chamber A. 20 ml of 40% lactose solution are introduced into the gradient maker chamber B. Immediately after filling the chamber B, the safety valve is opened and the lactose gradient captured by 50 ml tube containing 5 ml of 40% lactose solution at the bottom. If necessary, the final volume is brought up to 45 ml with 10 % lactose solution, using a pasteur pipette. The smaller gradient (10 ml) is prepared analogously, with following differences: the smaller version of gradient maker is used, 15 ml collection tube is used, 0.5 ml of 40% lactose solution are added to the bottom of 15 ml tube, 5 ml volumes of 10% and 40% lactose solution are introduced into the gradient maker chambers A and B, respectively (Fig. 8). Lactose gradients should be stable for 1 hr. When lactose gradients are prepared, 400 ml of culture (OD = 0.55) corresponding to 10^9 cells are collected and aliquoted into 8x 50 ml centrifugation tubes. All aliquots are centrifuged (1000 rcf, 3 min, 25°C). Supernatants are removed and cell pellets resuspended in the residual volumes. Resulting cell suspensions are pooled. The volume of pooled cell suspension is brought up to 5 ml with the medium. Using a pasteur pipette, 5 ml cell suspension is layered onto the 45 ml lactose gradient. 50 ml centrifugation tube containing the lactose gradient with layered cell suspension at the top is centrifuged (200-300 rcf, 3 min, 25°C). It is important to balance the rotor. Weighting of both, the adapters and the tubes is recommended. After centrifugation, clear gradient distribution of cell suspension should be seen. Using 5 ml pipette with the blunted 5 ml tips (the pointy end of the tip is cut off), 6 ml upper fraction of cell suspension gradient is collected and centrifuged (1000 rcf, 3 min, 25°C). Supernatant is removed and cell pellet resuspended in 1 ml of medium. Resulting 1 ml cell suspension is layered onto the second (10 ml) lactose gradient and centrifuged (200-300 rcf, 3 min, 25°C). After centrifugation a distinct cell containing band should be seen in the middle of the gradient. Using 1 ml pipette and the 1 ml tips with cut off ends, four 0.5 ml aliquots of the upper cell fraction are collected and transferred into 4 separate 1.5 ml tubes. Cells contained in the 0.5 ml aliquots are checked by microscopy. Aliquots containing uniform populations of small cells without septa are pooled. Pooled cell suspension is centrifuged (1000 rcf, 3 min, 25°C). Lactose containing supernatant

is removed. Pellet is resuspended in the fresh medium. Resulting cell suspension is used for inoculation of a new 20 ml culture. 1 ml aliquots are collected and fixed with 70% ethanol every 30 min, starting at t = 0 min. Synchronization by lactose gradient centrifugation protocol is derived from the protocol provided by B. Grallert, Institute for Cancer Research, Oslo.

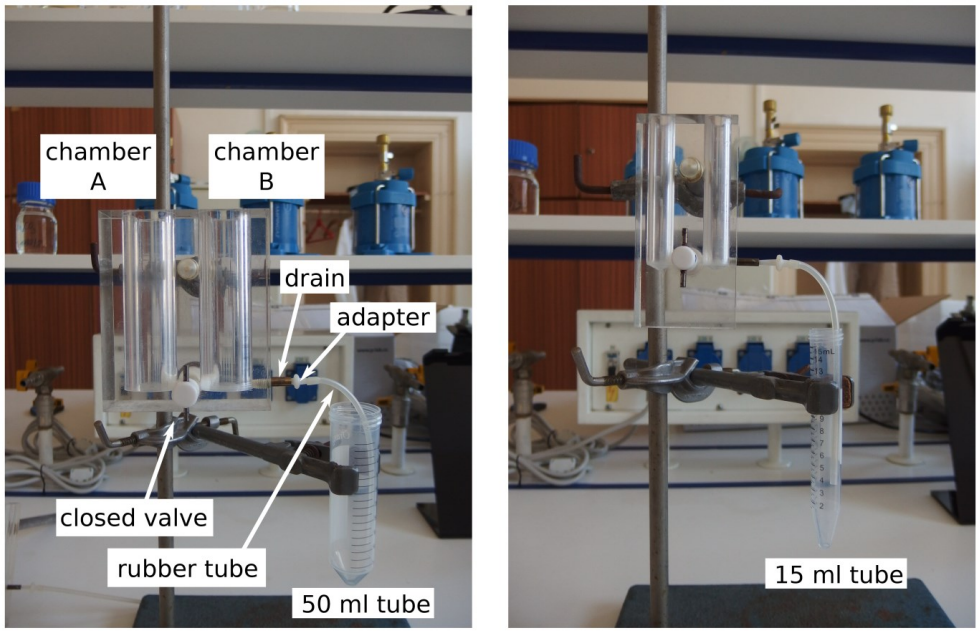

Gradient maker aparatus [45 ml] Gradient maker aparatus [10 ml]

Fig. 8 – Photodocumentation of gradient maker apparatus. Left panel – the setup for 45 ml lactose gradient preparation. Right panel - the setup for 10 ml lactose gradient preparation. Since apparatuses are analogous, only the right panel is annotated.

4.4 DNA manipulation techniques

4.4.1 Primers used in this study

Table 2 enlists the primers used for construction and genotyping of *cbf11:3HA:aid:kanR* allele. Table 3 enlists the primers for RT-qPCR based analysis of *cut6*, *vht1*, *bio2* and *cdc22* relative mRNA levels. Primers for construction and genotyping of *cbf11:3HA:aid:kanR* allele are designed by B. Grallert, Institute for Cancer Research, Oslo. Primers for qPCR analysis are designed by M. Oravcova. Sequencing primer for *cbf11:3HA:aid:kanR* genotyping is designed by R. Zach.

Table 2 – list of primers for construction and genotyping of *cbf11:3HA:aid:kanR* allele

Locus	ID	Sequence (5'-3')	Application(s)	Orientation	Source
cbf11 CDS	N1	GAGGCTATATTGCCCATAG	*cbf11:3HA:aid:kanR* integration genotyping	Forward	B. Grallert
cbf11 3'UTR	N2	AGTTGAAGGAATTTGCTATAGT	*cbf11:3HA:aid:kanR* integration genotyping	Reverse	B. Grallert
cbf11 3'UTR	N3	ACGGTCCACATAATATATGATC	*cbf11:3HA:aid:kanR* amplification Gibson assembly: fragment 4 amplification	Reverse	B. Grallert
cbf11 CDS	N4	ACGGTTACTGATTATCCATATAT	*cbf11:3HA:aid:kanR* amplification Gibson assembly: fragment 1 amplification	Forward	B. Grallert
kanR/*cbf11 3'UTR*	N5	TTAAACGAGCTCGAATTCATGCATCATGATTAATTTTACG	Gibson assembly: fragment 4 amplification	Forward	B. Grallert
cbf11 3'UTR/kanR	N6	TAAAATTAATCATGATGCATGAATTCGAGCTCGTTT	Gibson assembly: fragment 3 amplification	Reverse	B. Grallert
HA/insert/aid	N7	GATTACGCTGCTCAGTGCGCTGCTATGGGCAGTGTCGAGC	Gibson assembly: fragment 2 amplification	Forward	B. Grallert
aid/insert/HA	N8	GCTCGACACTGCCCATAGCAGCGCACTGAGCAGCGTAATC	Gibson assembly: fragment 1 amplification	Reverse	B. Grallert
aid/kanR	N9	AGTGCAAGAGCAGAGCTTGATGTTTAGCTTGCCTCG	Gibson assembly: fragment 3 amplification	Forward	B. Grallert
kanR/aid	N10	GGGACGAGGCAAGCTAAACATCAAGCTCTGCT	Gibson assembly: fragment 2 amplification	Reverse	B. Grallert
cbf11 CDS	Aid_seq	TAG AAT GGG AAG CTG TTG G	*cbf11:3HA:aid:kanR* sequencing primer	Forward	R. Zach

Table 3 – list of primers for qPCR analysis

Locus	ID	Sequence (5'-3')	Coordinates	Orientation	Efficiency (cDNA)	Amplicon size (bp)	Source
bio2 CDS	Map144	ATCTTCCCGCTACAATACC	III:177190-177208	Forward	2.011	96	M. Oravcova
	Map145	GTGCTTCCTTTAGCCTTTG	III:177267-177285	Reverse			M. Oravcova
vht1 CDS	Map148	GTCGCTTAGCTCGTTTATTC	I:4959921-4959940	Forward	2.021	129	M. Oravcova
	Map149	CGCTTACCAACATTCATCTC	I:4959811-4959831	Reverse			M. Oravcova
cut6 CDS	Map152	TTCTTCTCCAGGCTCTTATC	I:1250980-1251000	Forward	2.034	82	M. Oravcova
	Map153	CAATCCACCATCAGTCAAAG	I:1250918-1250938	Reverse			M. Oravcova
cdc22 CDS	Map154	CGAGCAATGGACCTTCTT	I:4228331-4228349	Forward	1.994	104	M. Oravcova
	Map155	CACGGTTCTCCTTCTCATAC	I:4228415-4228435	Reverse			M. Oravcova
act1 CDS	MP137	TCCTCATGCTATCATGCGTCTT	II:1476741-1476765	Forward	1.95	78	Ref. [87]
	MP138	CCACGCTCCATGAGAATCTTC	II:1476686-1476708	Reverse			Ref. [87]

4.4.2 Plasmids used in this study

In this study, pSL60 plasmid (Fig. 9) is used as a template for PCR-amplification of auxin inducible degron (aid) and kanamycin resistance (kanR) cassette, from which complete kanR sequence is not available. pSL60 plasmid is provided by B. Grallert, Institute for Cancer Research, Oslo.

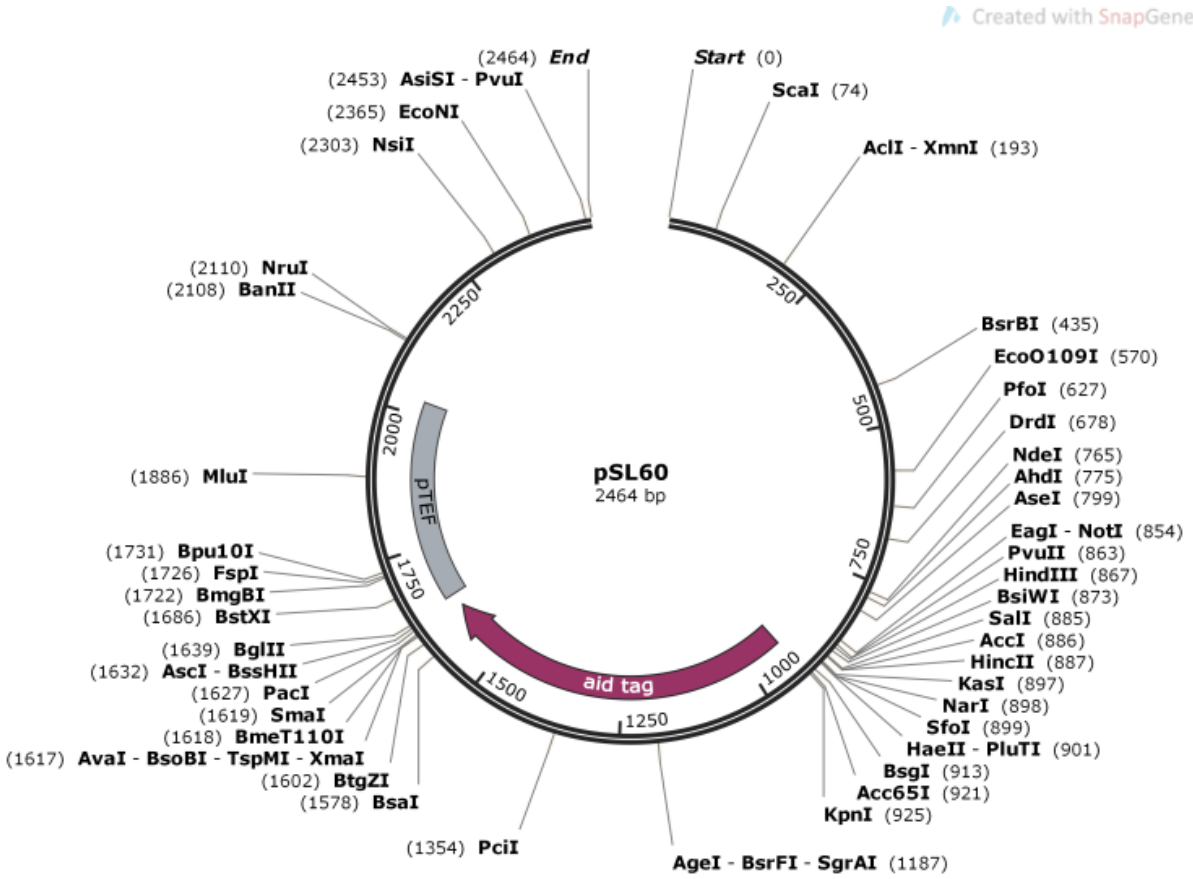

Fig. 9 – Map of the sequenced region of pSL60 plasmid. Auxin inducible degron cassette is indicated as aid tag (purple arrow). Promoter of kanR is marked as pTEF (gray box). The complete sequence of pSL60 is not provided. Illustration was created with SnapGene software (from GSL Biotech; available at snapgene.com).

4.4.3 Sequencing

In this study, sequencing is used for genotyping of *cbf11:3HA:aid:kanR* construct. Sequencing is done by GATC BIOTECH Company. To prepare samples for sequencing, DNA is isolated by genomic miniprep (Chapter 4.4.6). Isolated DNA is used as a template for PCR amplification using primers N1 and N2 situated upstream and downstream of the *cbf11:3HA:aid:kanR* integration site. PCR product is checked by capillary electrophoresis ('Qiagen QIAxcel' system). PCR fragment is cleaned, using QIAquick® PCR Purification kit (Cat No./ID: 28104). Concentration of purified PCR product is assessed by NanoDrop device (Thermo Scientific). Concentration of analyzed PCR fragment should be 10-50 ng/µl. 20 µl aliquot is transferred

into a clean 1.5 ml screw cap tube. Such sample is ready for sequencing and can be stored at -20°C. Sequencing primer is designed according to sequencing provider instructions. The length of the primer should be 17-19 bp. The sequencing primer melting temperature should be between 52°C and 58°C. 17-mer should contain 10 GC pairs. 18-mer should contain 8-9 GC pairs. 19-mer should contain 7-9 GC pairs. G or C should be at the 3' end. No more than 3 G/C should be present at the 3' end. Stretches of 4 or more identical nucleotides should be avoided. Analysis of melting temperature, self dimerization and formation of secondary structures is conducted by IDT OligoAnalyzer 3.1 tool, https://eu.idtdna.com/calc/analyzer.

4.4.4 Lithium acetate based method for transformation of S. pombe

10 ml of exponentially growing culture of OD = 0.5 are collected and centrifuged (1000 rcf, 3 min, 25°C). Supernatant is removed and cell pellet washed by one volume of sterile deionized water. Washed cell pellet is resuspended in 1 ml of deionized water and transferred into a sterile 1.5 ml tube. Cell suspension is centrifuged again (1000 rcf, 3 min, 25°C). Supernatant is removed and cell pellet washed with 1 ml of LiAc/TE solution and subsequently resuspended in 100 µl of LiAc/TE. 2 µl of denatured ssDNA (salmon sperm DNA, 10 mg/ml, SIGMA-ALDRICH) and 10 µl of transforming DNA are added to the 100 µl cell suspension. For denaturation, ssDNA is boiled for 10 min and cooled on ice. Resulting suspension is mixed with 260 µl of 40% PEG/LiAC/TE solution and incubated at 30°C for 60 min. Adequate mixing is ensured by short vortexing. Incubation time can be extended up to 3 hrs. After incubation, 43 µl of DMSO are added. Resulting suspension is incubated at 42°C for 5 min and then left to cool down to 25°C. After cooling down, cell suspension is centrifuged (1000 rcf, 3 min, 25°C). Majority of the supernatant is removed and cell pellet is resuspended in the residual volume. Resulting cell suspension is inoculated into 10 ml of liquid YES, and cultured at desired temperature for at least 2 hrs. Cells from 10 ml YES culture are collected by centrifugation (1000 rcf, 3 min, 25°C). Supernatant is poured off and cell pellet resuspended in the residual volume. Resulting cell suspension is spread onto a selection agar medium plate and incubated at desired temperature until single colonies appear. Single colonies are isolated by re-plating onto a new plate and subjected to further genotyping.

Reagents

10x LiAc (pH 7.5)

LiAc	1 M

pH is adjusted with acetic acid, buffer is sterilized by autoclaving

10x TE (pH 7.5)

Tris-HCl	0.1 M
EDTA (pH 8.0)	10 mM

pH is adjusted with HCl, buffer is sterilized by autoclaving

LiAc/TE (prepared fresh), 10 ml

10x LiAc	1 ml
10x TE	1 ml
H_2O	8 ml

40% PEG/LiAc/TE (prepared fresh), 1 ml

50 % PEG	960 ul
10x LiAc	120 ul
10x TE	120 ul

4.4.5 Extraction of genomic DNA with LiAc-SDS

The initial material is represented by cell biomass from a single colony or a 100-200 µl aliquot of exponentially growing cell culture. If cell suspension is used as an input, cells are centrifuged (1000 rcf, 3 min, 25°C) and supernatant is discarded. Cell pellet or cells from a colony are suspended in 100 µl of 0.2 M LiAc solution containing 1% SDS and incubated at 70°C for 5 min. 300 µl of 96% ethanol are added. Resulting suspension is mixed by vortexing and centrifuged (15 000 rcf, 3 min, 25°C). Supernatant is removed and cell pellet containing cell debris and DNA washed with 70% ethanol. Pellet is dissolved in 100 µl of deionized H_2O and centrifuged (15 000 rcf, 15 s, 25°C). Supernatant is transferred into a clean tube. 1-5 µl are used as a template for PCR. Protocol is adapted from [88].

Reagents

LiAc/SDS

LiAc	200 mM
SDS	1%

Ethanol

70% & 96 %

4.4.6 Genomic mini-prep for purposes of PCR

Genomic mini-prep can be used as an alternative to the genomic DNA extraction by LiAc-SDS (Chapter 4.4.5). Due to better purity of isolated DNA, mini-prep procedure is recommended when PCR templated by DNA isolated with LiAc-SDS fails. 1-2 ml aliquot of saturated culture is collected and centrifuged (1000 rcf, 5 min, 25°C). Supernatant is removed and cells are resuspended in 1 ml of citrate/phosphate/EDTA/sorbitol solution containing 2.5 mg of

zymolyase 20 T (Sunrise Science Products, cat no. NO766391). Zymolyase containing suspension is incubated at 37°C for 30-60 min. To check that cell wall is digested, 9 µl of cell suspension and 1 µl of 10% SDS are mixed and analyzed by phase-contrast microscopy. Yeasts with perforated cell walls, also known as ghosts, should be observed. If cell walls are sufficiently digested, cells are centrifuged at high speed (13 000 rcf, 10 s, 25°C). Supernatant is discarded and cell pellet resuspended in 0.5 ml of TE. 25 µl of 20% SDS are added. Resulting suspension is mixed by inverting the tube several times and incubated at 65°C for 1 hr. 175 µl of 5 M potassium acetate (pH 5.0) are added. Suspension is mixed by vigorous vortexing and kept on ice for 15 min. Suspension is centrifuged (13 000 rcf, 10 min, 4°C). Supernatant is carefully transferred into a clean tube. 0.5 ml of ice-cold isopropanol is added. Suspension is mixed and centrifuged (13 000 rcf, 10 min, 4°C). Supernatant is removed and pellet washed with 70% ethanol. Pellet is air dried and subsequently resuspended in 500 µl of deionized H_2O. 0.5-1 µl is used as a PCR template. Protocol is derived from [89].

Reagents

Citrate/Phosphate buffer (50 mM, pH 5.6)

Na_2HPO_4 (anhydrous)	7.1 g
Citric acid	11.5 g

Na_2HPO_4 and Citric acid are dissolved in 1 L of water sterilized by autoclaving

Citrate/Phosphate/EDTA/Sorbitol buffer

EDTA (pH 8)	40 mM
Sorbitol	1 M

Sorbitol and EDTA are prepared in Citrate/Phosphate buffer and filter-sterilized

5x TE buffer

Tris-HCl (pH 7.5)	50 mM
EDTA (pH 8.0)	5 mM

Buffer is sterilized by autoclaving

Potassium acetate (pH 5.0)

KAc	5 M

pH is adjusted with acetic acid, buffer is sterilized by autoclaving

4.4.7 Polymerase chain reaction – PCR

In this study, PCR is used for the genotyping and amplification of DNA fragments (1-4) required for construction of the auxin-inducible degron *cbf11* allele (*cbf11:3HA:aid:kanR*). In all cases, high fidelity phusion DNA polymerase (NEB #E0553S/L) is used. PCR reagents are stored at -20°C. PCR reaction is mixed as described in Table 4. Before use, every reagent is

thawed, vortexed and centrifuged. When worked with, all PCR components are kept on ice. Genomic DNA isolated by mini-prep or LiAc-SDS protocols is used as a template. It is important that no more than 250 ng of genomic DNA are introduced, as larger amounts of templating DNA inhibit PCR reaction. When mixed, PCR reaction is vortexed, centrifuged and introduced into the PCR-cycler machine. Three amplification programs are employed (Table 5): PCR_A (for amplification of fragments 1, 3 and 4), PCR_B (for amplification of fragment 2) and PCR_C (for genotyping of *cbf11-aid* transformants).

Table 4 – PCR reaction mixture: NEB high fidelity polymerase (NEB # E0553S/L)

Reagent	20 µl reaction	50 µl reaction	Final concentration
5x HF buffer	4 µl	10 µl	1x [1.5 mM Mg2+]
10 mM dNTP	0.4 µl	1 µl	200 µM
10 µM forward primer	1 µl	2.5 µl	0.5 µM
10 µM reverse primer	1 µl	2.5 µl	0.5 µM
Template (Genomic DNA, plasmid DNA)	1 µl	2.5 µl	< 250 ng
NEB Phusion high fidelity polymerase	0.2 µl	0.5 µl	1.0 units / 50 µl reaction
H_2O	12.4 µl	32.5 µl	

Table 5 – PCR programs

PCR_A		PCR_B		PCR_C	
1. 98°C	(30 s)	1. 98°C	(30 s)	1. 98°C	(30 s)
2. 98°C	(10 s)	2. 98°C	(10 s)	2. 98°C	(10 s)
3. 55°C	(30 s)	3. 45°C	(30 s)	3. 55°C	(20 s)
4. 72°C	(20 s)	4. 72°C	(20 s)	4. 72°C	(90 s)
5. Go to 2.	(29x)	5. Go to 2.	(34x)	5. Go to 2.	(29 x)
6. 72°C	(5 min)	6. 72°C	(5 min)	6. 72°C	(10 min)
7. END		7. END		7. END	

4.4.8 DNA agarose gel electrophoresis and capillary electrophoresis

In this study, the agarose gel electrophoresis is used for the qualitative analysis of DNA fragments during *cbf11:3HA:aid:kanR* allele construction. 0.8% agarose (different percentage

may be used, depending on the sizes of analyzed DNA fragments) is prepared in TAE (Tris base, Acetic acid, EDTA) buffer. Proper dissolution is achieved by heating in the microwave oven. Liquid agarose is cooled down and poured into the agarose gel preparation apparatus. When solidified, the agarose gel is introduced into the electrophoretic apparatus and covered in TAE. DNA samples are mixed with 6x orange loading dye (ThermoFisher Scientific, R0631) and loaded into the wells in the gel. Alongside DNA samples, DNA ladder (marker) is loaded. In this study, 1 kb ladder (New England BioLabs, #N3232S) is used. Electrophoretic apparatus is connected to the electric power source. Voltage is set up on constant 60 V (voltage depends on the application and sizes of the analyzed DNA fragments and thus may be adjusted). When separation is completed, agarose gel is bathed in 1x Gel Red (Biotum, cat no: 41003-1, 10 000x) solution for 1 hrs (if necessary, incubation time can be extended). The Gel Red-stained agarose gel is UV-illuminated and imaged. Alternatively to the agarose gel electrophoresis, capillary electrophoresis employing 'Qiagen QIAxcel' capillary system is used. To perform the capillary electrophoresis analysis, PCR tubes containing DNA samples (minimum 10 µl) are introduced into the 'Qiagen QIAxcel' system. 100 bp – 2.5 kb QX size marker (100 ng/µl, QIAGEN #929559) is used as a reference size control.

Reagents

TAE [pH 8.5]

Tris	40 mM
Acetic acid	20 mM
EDTA	2 mM

4.4.9 Gibson assembly

In this study, Gibson assembly (NEB #E2611S) is used for construction of *cbf11:3HA:aid:kanR* allele. Gibson assembly procedure joins DNA fragments with overlapping ends by utilizing 3 enzymatic reactions in a single tube. These include: 5' exonuclease, DNA polymerase and DNA ligase. 5' exonuclease degrades 5' ends of DNA fragments. 3' single strand overhangs anneal and are elongated by DNA polymerase. DNA nicks are sealed by DNA ligase. The initial step in Gibson assembly cloning is amplification of DNA fragments, which are meant to be assembled. For PCR amplification, high fidelity polymerase and primers with 5' overhangs

corresponding to sequences of neighbouring fragments are used. Amplified DNA molecules thus contain overlapping ends as illustrated in Fig. 10. PCR products are cleaned up and subjected to determination of DNA concentration. In this study, QIAquick PCR Purification Kit (QIAGEN, Cat No./ID: 28104) and NanoDrop device (Thermo Scientific) are used for purification and determination of DNA concentration, respectively. Gibson assembly reaction mixtures are prepared according to Table 6. Reactions are incubated at 50°C for 60 min. After incubation, samples are put on ice or stored at -20°C. Gibson assembly output can be used for PCR amplification or direct transformation. In one Gibson assembly reaction, 2-6 DNA fragments may be assembled. In this study, assembly of 4 fragments is performed.

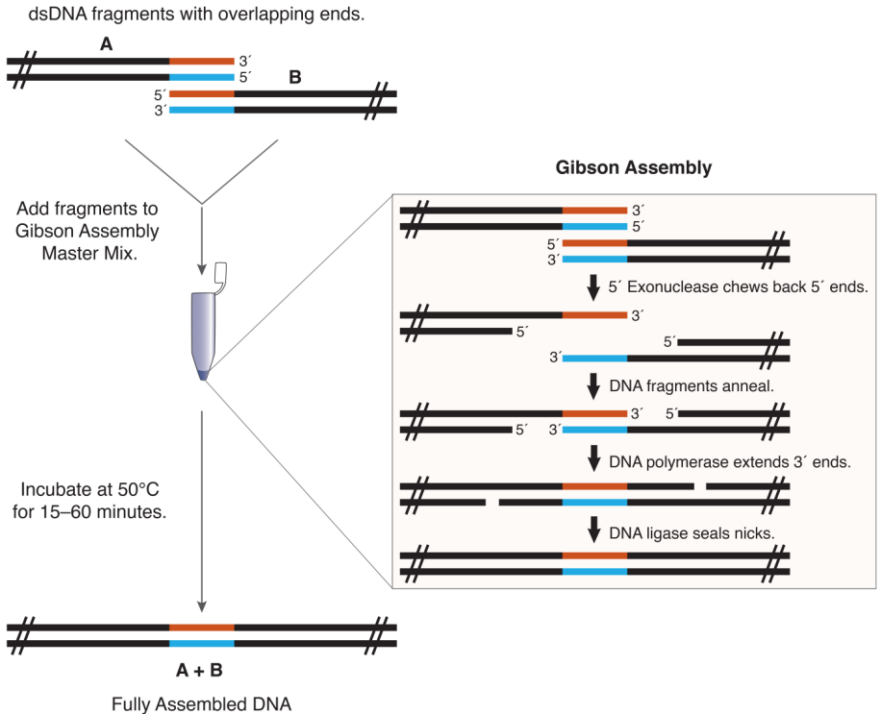

Fig. 10 – Schematic overview of the Gibson assembly principle. Adapted from the instruction manual for Gibson assembly master mix (New England BioLabs, #E2611S).

Table 6 – Gibson assembly reaction mix

Reaction component	4 fragments assembly
Total amount of fragments	0.2 - 1 pmol
Gibson assembly master mix (2x)	10 µl
H_2O	up to 20 µl
Total volume	20 µl

4.4.10 Isolation of total RNA

Total RNA isolation is performed using commercially available kit (MasterPure^{TM} Yeast RNA Purification Kit, Epicentre Biotechnologies). 1 ml aliquot of exponentially growing cells is collected and centrifuged (1000 rcf, 3 min, 25°C). Supernatant is discarded and cell pellet snap-frozen in liquid N_2. At this stage, sample can be stored at -80°C for at least a month. Cell pellet is thawed on ice and resuspended in 300 µl of 'Extraction reagent for RNA' containing 1 µl of proteinase K (50 µg/µl). Sample is briefly vortexed and incubated at 70°C for 15 min. While incubated, sample is vortexed every 5 min. After incubation, sample is kept on ice for 5 min. Next, 175 µl of 'MPC Protein Precipitation Reagent' are added. At this point, precipitated material is observed. Sample is centrifuged (20 000 rcf, 10 min, 4°C) and supernatant is transferred into a clean 1.5 ml tube. Supernatant is mixed with 500 µl of ice-cold isopropanol by inverting the tube 40 times. Precipitated RNA is sedimented by centrifugation (20 000 rcf, 10 min, 4°C). Using a pipette, isopropanol is discarded. Pellet is dissolved in 200 µl of DNase solution (175 µl of RNase-free deionized H_2O, 20 µl of 10x DNase buffer and 5 µl of RNase-free DNase – 1 U/µl). Dissolving should be done by pipetting. DNase containing mixture is incubated at 37°C for 20 min. After incubation, 200 µl of 2x 'T and C Lysis Solution' are added and mixed by vortexing for 5 s. Afterwards, 200 µl of 'MPC Protein Precipitation Reagent' are added. At this point, precipitated material is observed. Sample is vortexed for 10 s and incubated on ice for 5 min. Sample is centrifuged (20 000 rcf, 10 min, 4°C) and supernatant is transferred into a clean 1.5 ml tube. Supernatant is mixed with 500 µl of isopropanol by inverting the tube 40 times. Precipitated RNA is sedimented by centrifugation (20 000 rcf, 10 min, 4°C). Supernatant is removed and resulting RNA pellet is washed twice with 70% ethanol. Resulting RNA pellet is dissolved in 35 µl of RNase-free MP H_2O containing 1 µl of 40 U/µl RiboLock RNase Inhibitor (Biogen, EO0382). Quality and concentration of isolated RNA is analysed by NanoDrop (Thermo Scientific). Isolated RNA can be stored at -80°C. When working with RNA, it is important to follow the standard rules for RNA manipulation. If not bought RNase-free, all plastic, including tips and tubes, are three times autoclaved. If not bought RNase-free, deionized H_2O is treated with diethyl pyrocarbonate (DEPC), an RNase inactivating agent. To prepare 1 L of DEPC-H_2O, 1 ml of DEPC (SIGMA-ALDRICH) is added to 1 L of deionized H_2O, incubated o/n and sterilized by

autoclaving. RNA samples should be always handled with gloves. It is recommended to wear a laboratory coat. No more than 12 samples should be handled at a time.

4.4.11 Reverse transcription (RT)

Reverse transcription is performed using a commercially available kit 'RevertAid First Strand cDNA Synthesis Kit' (Fermentas K1622). Components of the reaction are thawed on ice, vortexed and briefly centrifuged. Two pre-mixes are prepared as described in Table 7. When mixing, all reagents are kept on ice. Premix 1 is incubated at 65°C for 5 min, centrifuged and cooled on ice. 12.5 µl of Premix 1 and 7.5 µl of Premix 2 are mixed. No-RT control reaction is also mixed and processed analogously to the experimental samples. No-RT reaction does not contain reverse transcriptase and controls for potential false positive outputs resulting from contamination by genomic DNA. All reactions are mixed by pipetting and briefly centrifuged. Sedimented mixtures are incubated at 25°C for 5 min and subsequently at 42°C for 60 min. RT-reaction is terminated by shifting to 70°C for 5 min. cDNA samples can be stored at -80°C.

Table 7 – RT-reaction premixes

Premix 1	For 1 reaction	Premix 2	For 1 reaction
Template: total RNA	0.1-5 µg	5x Reaction buffer	4 µl
Random hexanucleotides (100 µM)	1 µl	RiboLockTM RNase Inhibitor (40 u/ µl)	0.5 µl
RNase-free H_2O	up to 12.5 µl	dNTP Mix (10 mM)	2 µl
Final volume	12.5 µl	RevertAidTM M-MuLV Reverse Transriptase (200 u/µl)	1 µl
		Final volume	7.5 µl

4.4.12 Quantitative PCR (qPCR)

In this study, qPCR is used for the analysis of relative mRNA levels of *cut6*, *vht1*, *bio2* and *cdc22*. qPCR is performed, using the 'MESA GREEN qPCR MasterMix Plus for SYBR® Assay NO ROX' kit (Eurogentec). Reaction pre-mix is prepared by mixing SYBR-green master mix with solutions of primers, as described in Table 8. Solution of cDNA is 100-fold diluted with deionized H_2O. Both, primers-containing pre-mix and diluted cDNA are introduced into a 384-well plate. A single well of 384-well plate is loaded with 5.6 µl of primers-containing pre-mix and 4.4 µl of diluted cDNA. Every unique reaction (defined by the combination of specific primers and template) is loaded in triplicates. For every analyzed pair of primers a non-

template control (NTC) reaction and no-RT control reaction are prepared. NTC reaction does not contain a cDNA template, but 4.4 µl of deionized H_2O. No-RT reaction contains 4.4 µl of 100-fold diluted no-RT sample. To ensure a proper mixing of all components, loaded 384-well plate is vortexed and centrifuged (1500 rcf, 3 min, 25°C). 384-well plate is then introduced into the light cycler (LightCycler® 480 II, Roche Applied Science) and incubated according to the RT-qPCR program. When the RT-qPCR program is finished, melting curves of all PCR products are checked. All reactions using the same set of primers should display tan identical melting peak. Reactions displaying deviations in melting analyses should be excluded from further calculations. C_p-values are checked for all triplicates. Any reaction of a triplicate displaying > 10% deviation should be excluded from further calculations. The average of C_p-values is calculated for every triplicate. The relative mRNA values are estimated, using the equation 3. In the experiments determining the cell cycle oscillatory expression of *cut6*, *vht1* and *bio2* genes, *cdc22* works as positive control for cell cycle oscillatory expression. *act1* (actin) is used as a normalization control.

Table 8 – qPCR reaction mixture

SYBR green premix	5 µl
Forward primer (10 µM)	0.3 µl
Reverse primer (10 µM)	0.3 µl
100-fold diluted cDNA	4.4 µl

RT-qPCR program

1. 95°C (5 min)
2. 95°C (5 s)
3. 60°C (30 s)
4. 72°C (20 s)
5. Measure fluorescence
6. Go to 2. (39x)
7. 95°C (5 min)
8. 50°C (1 min)
9. Increase temperature by (1°C/min) continually measure fluorescence
10. END

$$mRNA_{rel} = \frac{E^{-Cp}(Test)}{E^{-Cp}(Reference)}$$

Equation 3: E – amplification efficiency of specific primer pair, C_p – a crossing point, a point at which the fluorescence signal crosses a noise-line, (Test) – values corresponding to the gene of interest, e.g. *cut6*, *vht1*, *bio2*, *cdc22*, (Reference) – value corresponding to the normalization control, e.g. *act1*.

4.5 Protein manipulation techniques

4.5.1 TCA protein extracts

In this study, denatured TCA protein extracts are used for genotyping of the *ade6+pADH15.skp1:AtTIR1:2NLS:9myc* and *cbf11:3HA:aid:kanR* constructs. Roughly 10-15 ml of exponentially growing cells are collected and centrifuged (1000 rcf, 3 min, 25°C). Supernatant is removed and cells resuspended in 1 ml of STOP buffer. 1 ml cell suspension is transferred into a clean 2 ml screw cap tube and centrifuged (1000 rcf, 3 min, 25°C). Supernatant is discarded and cell pellet snap-frozen in liquid N_2. At this stage, cells can be stored at -80°C. The frozen sample is thawed on ice and subsequently suspended in 20% trichloracetic acid (TCA). Cells are centrifuged (1000 rcf, 3 min, 4°C) and supernatant is removed. To neutralize remnants of TCA, cell pellet is washed once with 1 ml of 1 M Tris (pH not adjusted). Resulting pellet is resuspended in 100 µl of 2x Sample Buffer (Laemmli buffer) and boiled (95°C) for 2 min. Roughly 100 µl of glass beads are added and tube is boiled (95°C) for 2 more minutes. Cells are broken with FastPrep (MP Biomedicals) using 4x 15 s, 6.5 m/s program. Alternatively, one 60 s cycle can be used. Samples are boiled for another 2 min and briefly centrifuged. Tube is pierced at the bottom with a hot needle and placed onto a 1.5 ml tube without a cap. Resulting 'tube set up' is placed in a 50 ml tube and centrifuged (1000 rcf, 5 min, 4°C). The upper (glass beads containing) 1.5 ml tube is discarded. Supernatant from the lower tube is transferred into a clean 1.5 tube. In order to remove residual cell debris, sample is centrifuged (15 000 rcf, 5 min, 4°C) and supernatant is transferred into a clean 1.5 ml tube. Before protein separation by SDS-Page, sample is boiled (95°C) and centrifuged.

Reagents

2.5x SDS Sample buffer (Laemmli buffer) without DTT (recipe for 40 ml)

Tris-HCl (pH 7.5)	0.125 M	(1M Tris-HCl, 5ml)
SDS	5% (w/v)	(10 % SDS, 20ml)
Glycerol	25 % (v/v)	(99 % Glycerol, 10 ml)
Bromophenol Blue	0.25 % (w/v)	(100 mg Bromphenol Blue)
H_2O		up to 40 ml

Sterilized by filtration.

2x SDS Sample buffer (Laemmli buffer) with 0.2 M DTT
Prepared by mixing 2.5x SDS Sample buffer and 1M DTT in 4:1 ratio, always prepared fresh.

Stop buffer

NaF	50 mM
NaN_3	1 mM
Hepes K+ (pH 7.0)	25 mM
NaCl	150 mM

20% TCA

1 M Tris (pH not adjusted)

4.5.2 SDS-Polyacrylamide gel electrophoresis (SDS-Page) & Western Blot

In this study, SDS-Page is used for genotyping of strains carrying the *cbf11:3HA:aid:kanR* and *skp1:AtTIR1:2NLS:9myc* alleles. For SDS-Page, commercially available pre-cast polyacrylamide gels are used (4–15% Criterion™ TGX™ Precast Midi Protein Gel, 18 well, 30 µl #5671084; 4–15% Criterion™ TGX™ Precast Midi Protein Gel, 26 well, 15 µl #5671085). Pre-cast gel is introduced into the vertical electrophoretic apparatus (Bio-Rad) and covered by electrophoretic (running) buffer. 10 µl of a boiled (95°C, 10 min) protein sample dissolved in Laemmli buffer are loaded into a single well in the gel. Alongside the protein samples, 5 µl of protein size marker are loaded. In this study Page Ruler (PageRuler™ Prestained Protein Ladder, 10 to 180 kDa #26616, ThermoFisher Scientific) and Dual colour precision plus (Precision Plus Protein™ Dual Color Standards, 500 µl #1610374, Bio-Rad) protein standards are used. The electrophoretic apparatus containing loaded gel and running buffer is connected to the electric power source set up to constant 200 V. The electric power source is switched on and left running until the bromophenol blue band reaches the gel base. Gel containing separated proteins is equilibrated by soaking in the transfer buffer. PVDF membrane and filter papers are equilibrated in the same manner. Note, that highly hydrophopic PVDF membrane must be rinsed with 70% ethanol before introducing to the aqueous solution. Equilibration takes about 15 min. After equilibration, the blotting 'sandwich' is put together. To make the 'blotting sandwich' filter paper, PVDF membrane, gel and filter paper are placed onto each other (listed from the bottom to the top). Assembled sandwich is introduced into the Trans-Blot® SD Semi-Dry Transfer Cell system (Bio-Rad).

Proteins are transferred to the PVDF membrane by 15 V for 30 min. When the blotting procedure is finished, membrane is washed with distilled H_2O and stained with Ponceau solution (SIGMA-ALDRICH, P7170-1L) to check the successful protein transfer. Ponceau stain is washed off with distilled H_2O for 1 hrs. PVDF membrane is introduced into a 50 ml tube, in such a way, that it is stuck to the wall with the proteins-containing face being exposed and the protein-less face being in direct contact with the wall. If necessary, PVDF membrane is cut and two 50 ml tubes are used. 5 ml of blocking solution (VWR, cat no: RPN2125, 0.25 g in 5 ml TBSt) are introduced into the PVDF membrane containing 50 ml tube. 50 ml tube is placed on the roller mixer. Membrane is blocked for 1 hr while constantly rotating. After 1 hr, blocking solution is poured off and membrane is washed three times with TBSt for 15 min and 2x 5 min. After washing, PVDF membrane is incubated with TBSt solution containing primary antibody. 5 ml are used for one 50 ml tube. Incubation time depends on the actual antibody, but standardly, over night incubation at 4°C is used. When the incubation with a primary antibody is over, PVDF membrane is washed three times with TBSt for 15 min and 2x 5 min. After washing, PVDF membrane is incubated with TBSt containing AP-linked secondary antibody. AP stands for alkaline phosphatase. 5 ml are used for one 50 ml tube. Incubation with secondary antibody takes 1-2 hrs. After incubation, PVDF membrane is washed three times with TBSt for 15 min and 2x 5 min. When washed, PVDF membrane is placed onto a clean glass plate and covered with ECF substrate (GE healthcare, cat. No. RPN3685), the fluorescent properties of which are activated by AP-mediated dephosphorylation. ECF-incubation time depends on detected protein and primary antibody and must be empirically adjusted. ECF substrate is cleared off by drying the PVDF membrane with a filter paper. Dried PVDF membrane is introduced into a transilluminator and imaged. Antibodies used in this study are enlisted in Table 9.

Reagents

10x Running buffer with SDS [2 L]	
Glycine	288 g
Tris base	60.4 g
SDS	20 g
H_2O	up to 2 L

10x TBS [1 L]	
NaCl	80 g
1M Tris-HCl [pH 7.5]	200 ml
H_2O	up to 1 L

Transfer buffer [1 L]

Tris base	2.9 g
10 % SDS (w/v)	10 ml
Glycine	14.4 g
Methanol/Ethanol	200 ml
H_2O	up to 1 L

1x Running buffer with SDS [1 L]

10x Running buffer with SDS	100 ml
H_2O	900 ml

1x TBS [1 L]

10x TBS	100 ml
H_2O	900 ml

TBSt

1x TBS + 0.1 % Tween 20

Table 9 – List of used antibodies

Antibody description	Manufacturer	Working dilution
Mouse monoclonal [9E10] to c-Myc - ChIP Grade	Abcam #ab32	1:1000 in TBSt
Anti-mouse IgG, AP-linked	Signaling Technology #7056	1:5000 in TBSt
Anti-rabbit IgG, AP-linked Antibody	Signaling Technology #7054	1:5000 in TBSt
Anti-HA.11 Epitope Tag Antibody [16B12]	Covance #MMS-101P-500	1:1000 in TBSt
HA-Tag (262K) Mouse mAb	Signaling Technology #2362	1:1000 in TBSt
HA-probe Antibody (F-7)	Santa Cruz #sc-7392	1:1000 in TBSt
Anti-HA tag antibody [16B12]	Abcam #ab130275	1:1000 in TBSt
Anti-HA tag antibody [HA.C5]	Abcam #ab18181	1:1000 in TBSt
Anti-HA tag antibody - ChIP Grade	Abcam #ab9110	1:4000 in TBSt
HA-probe (Y-11): sc-805	Santa Cruz #sc-805	1:1000 in TBSt

5 RESULTS

5.1 Morphological aberration characteristic for *Δcbf11* mutants

Cbf11-deficient *S. pombe* cells display a broad range of defects in cellular and nuclear morphology [17]. Population of *Δcbf11* mutant is enriched with misshaped cells of larger sizes and multiple developed septa (Fig. 11 B). Nuclear aberrancies include the presence of diffused nuclei (Fig. 11 C), extra micronuclei (Fig. 11 D), chromatin bridges (Fig. 11 E) and nuclei intersected by developed septa (Fig. 11 F), a phenotype also known as cut (cell untimely torn) in *S. pombe.* Even though, these phenotypes represent serious defects, not much is known about the function of Cbf11.

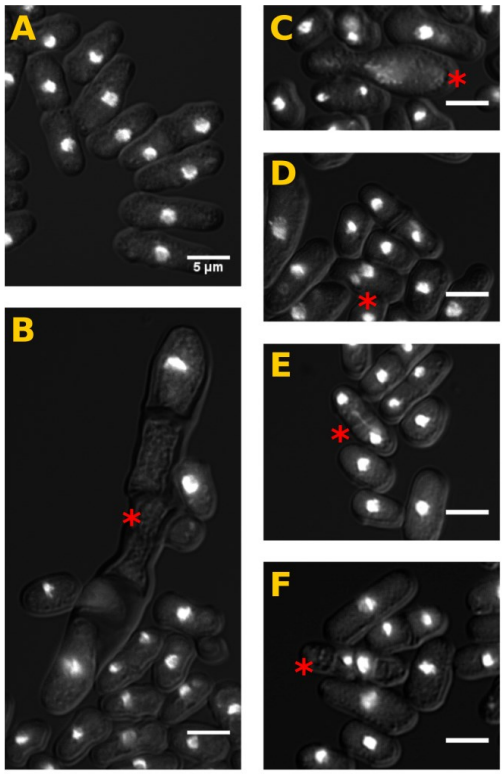

Fig. 11 – Demonstration of morphological defects observed in *Δcbf11* mutants. Exponentially growing cells were fixed with 70% ethanol and stained with DAPI (1 µg/ml). Overlay images of DIC and DAPI channels are shown. **[A]** WT cells with normal cell morphology. Images designated as **[B – F]** represent characteristic *Δcbf11* phenotypes. **[B]** – aberrant cell morphology with multiple septa, **[C]** – diffuse nucleus, **[D]** – micronucleus, **[E]** – chromatin bridge, **[F]** – nucleus intersected by septum (Cut: cell untimely torn). Defective cells are indicated by red asterisk. For better clarity, contrast and brightness were adjusted using the ImageJ software [82]. Scale bar 5 µm.

Considering the pleiotropic character of phenotypes observed in *Δcbf11* mutant, it would be almost impossible to cover all of them in a single project. Since mitosis represents a highly relevant topic with broad range of scientific implications, we decided to narrow down the area of interest with primary focus on investigation of cut phenotype.

5.2 Cbf11: a novel transcriptional regulator of lipid metabolism

To acquire a more in depth understanding of Cbf11 biology, we wanted to uncover the molecular mechanisms responsible for the aberrant mitosis in Cbf11-defficient cells and postulate a model describing mitosis-contextual function of Cbf11. Employing microarray analysis, M. Prevorovsky identified a set of lipid metabolism genes, which expression is downregulated upon *cbf11* deletion [19]. Since several studies implicate that undisrupted lipid metabolism is required for successful mitosis in *S. pombe* (Chapter 3.2), we speculated that impairment of lipid metabolism could represent the ultimate cause of cut phenotype in *Δcbf11* mutant.

5.2.1 Lipid metabolism is defective in *Δcbf11* mutant

To test whether lipid metabolism is altered in *Δcbf11* cells, we examined the state of intracellular lipid droplets, the lower level of which has been previously shown to be consequential to lipid metabolism downregulation [47]. We stained the live WT and *Δcbf11* cells with nile red (9-diethylamino-5H-benzo[a]phenoxazine-5-one), a hydrophobic fluorescence dye localizing to lipid droplets [84,90], revealing that the amount of storage lipids is indeed decreased in *Δcbf11* mutant [Fig. 12 A-B]. A significant fraction of *Δcbf11* cells did not show any nile red signal, implying truly severe lipid metabolism downregulation [19]. The important observation was that *Δcbf11* mutant showed dramatic decrement in the lipid droplets content when grown in the YES medium, but not when cultured in EMM [Fig. 12 C], indicating the environmental modulation of lipid metabolism.

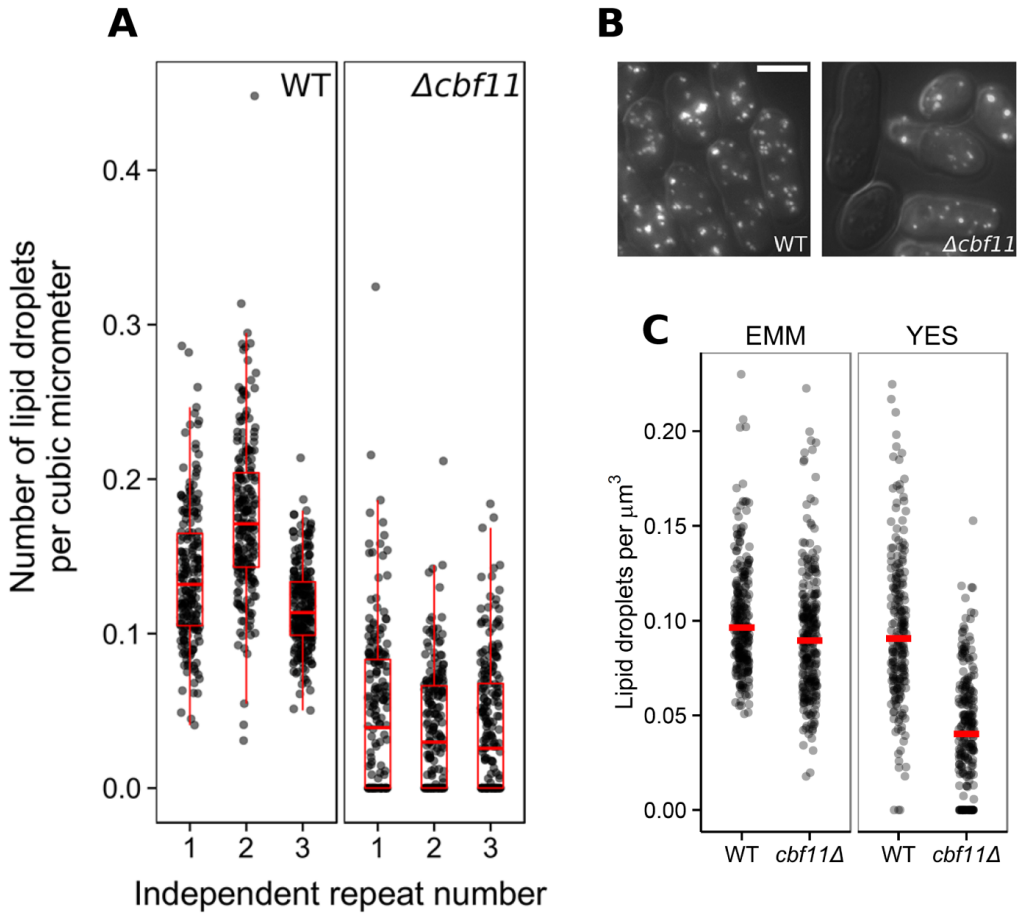

Fig. 12 – The amount of the storage lipids is affected in *Δcbf11* mutants. [A] Quantification of the number of lipid droplets in WT and *Δcbf11* cells cultured in YES. Exponentially growing live cells were stained with 10 µM nile red and imaged by fluorescence microscopy. Maximum projections of Z-stack images were analyzed. The number of lipid droplets per cell was counted for every cell and normalized to the cylindrical approximation of cellular volume. At least 200 cells per sample were scored. Data for three independent repeats are shown. Every dot represents a single cell. Dot plots are overlaid with corresponding box plots. Population of *Δcbf11* cells display decreased number of lipid droplets per cell. No nile red signal was observed in 40.4% ± 2.5% of *Δcbf11* cells. **[B]** Representative images of the live WT and *Δcbf11* cells stained with nile red. GFP filter (excitation, 475 nm) was used for visualization of nile red signal. Overlay images of DIC and GFP channels are shown. Scale bar 5 µm. **[C]** Analysis of the lipid droplets content analogous to [A] of WT and *Δcbf11* cells grown in EMM or YES. Red bars represent median values. EMM causes rescue of the lower lipid droplets number observed in *Δcbf11* cells grown in YES. Results from one experiment are shown. Results [A-B] were published in [19].

5.2.2 Impairment of Ac-CoA carboxylase: the cause of mitotic failure in *Δcbf11* mutant

Lipid metabolism factors the expression of which was evaluated as decreased in *Δcbf11* cells included three functionally connected genes *cut6*, *vht1* and *bio2* [19], respectively encoding acetyl coenzyme A carboxylase, biotin transporter and biotin synthase. Biotin-dependent Cut6 catalyzes the rate limiting step in fatty acid (FA) synthesis and its function is required for mitotic progression in *S. pombe* [44]. In *S. pombe*, sufficient supply of biotin is ensured by cooperative action of the only two biotin metabolism proteins Vht1 and Bio2. While Bio2 synthesizes biotin from its precursor dethiobiotin [91], Vht1 mediates high affinity H^+-driven symport, gathering biotin or dethiobiotin from the environment [92]. M. Prevorovsky and M. Oravcova proved that Cbf11 binds to the *cut6*, *vht1* and *bio2* promoters, acting as a positive transcriptional regulator. We hypothesized, that the sole or combinatorial deregulation of *cut6*, *vht1* and *bio2* expressions results in insufficient FA production and unsuccessful progression through mitosis. To test whether the sole deregulation of *cut6* transcription causes catastrophic mitosis, M. Prevorovsky constructed the strain carrying mutated version of *cut6* promoter (*Pcut6MUT*), in which CSL response element, GTGGGAA, is mutated to CTCGAGA sequence, making it unrecognisable by Cbf11 (Fig. 13).

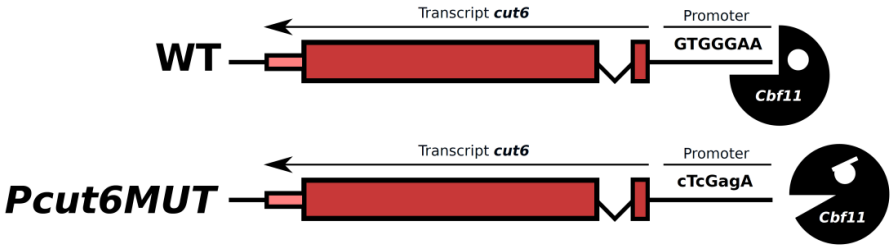

Fig. 13 – Cartoon illustration of *cut6* allele carrying promoter mutation in Cbf11-binding site. Mutated bases are indicated by lowercase letters. *Pcut6MUT* strain was constructed by M. Prevorovsky.

The RT-qPCR analysis proved that the level of *cut6* mRNA is reduced to 50% of the WT value in *Pcut6MUT* strain, which perfectly mimics the state of *cut6* mRNA in *Δcbf11* cells [20]. However, neither the growth nor mitosis was defective in *Pcut6MUT* populations (Fig. 14 A-

B). We also did not observe any genetic interactions between *Δcbf11* and *Pcut6MUT* mutations (Fig. 14 B). Similarly to *Pcut6MUT* mutant, cells carrying single deletion of *vht1* or *bio2* did not show any increase in the cut phenotype occurrence (Fig. 14 B). Though, it must be noted, that single *Δvht1* mutant displayed a serious growth defect (Data not shown). Since the sole downregulation of *cut6* expression and single deletions of *vht1* and *bio2* had no apparent effect on mitotic progression, we tested genetic interactions between *Pcut6MUT* and null-alleles of *vht1* and *bio2*. While *Δbio2 Pcut6MUT* double mutants did not show significant increase in the cut phenotype occurrence compared to WT, cells carrying combination of *Δvht1* and *Pcut6MUT* mutations were undergoing catastrophic mitosis at notably elevated frequencies (Fig. 14 B). Thus, the occurrence of mitotic catastrophe in *Δcbf11* mutant could be theoretically explained by transcriptional deregulation of *cut6* and *vht1*. We hypothesize that *Δcbf11* cells contain fewer Cut6 molecules, of which not all are biotinylated, resulting in reduction of Cut6 mediated malonyl-CoA production, inadequate FA synthesis and defective mitosis. This theory is supported by the fact that phenotypes observed in *Δcbf11* cells were rescued by overexpression of *cut6* (Fig. 14 B). Interestingly, the cut phenotype incidence was significantly higher in *Δcbf11 Δvht1 Pcut6MUT* triple mutant compared to *Δvht1 Pcut6MUT* double mutant (Fig. 14 B), indicating that *cut6* is not the only cut-related factor regulated by Cbf11.

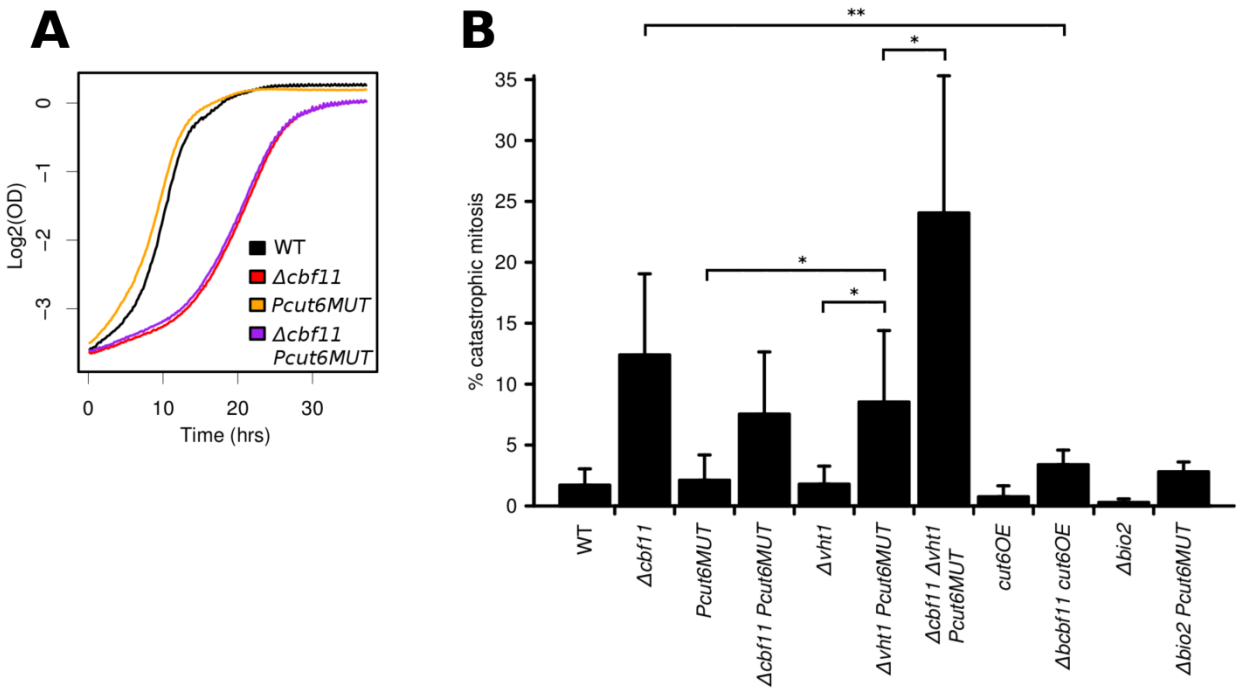

Fig. 14 – Mitotic catastrophe observed in *Δcbf11* cells possibly results from transcriptional downregulation of *cut6* and *vht1* genes. [A] Representative growth curves of WT, *Δcbf11*, *Pcut6MUT* and *Δcbf11 Pcut6MUT* strains. *Pcut6MUT* mutation does not cause any growth defects in either WT or *Δcbf11* genetic background. **[B]** The occurrence of mitotic catastrophes in mutants of Cbf11-regulated lipid metabolism genes. Exponentially growing cells fixed with 70% ethanol were stained with DAPI (1 µg/ml) and analyzed by fluorescent microscopy. At least 200 cells per sample were scored. Results from three or more independent repeats are shown. Error bars represent positive standard deviation values. The asterisks represent the significance values (*p ≤ 0.05, **p ≤ 0.01), calculated by one-sided unpaired t-test. Results presented in [B] were acquired by R. Zach and M. Prevorovsky. Graphics for [A-B] was done by M. Prevorovsky. Results [A-B] were published in [20].

5.2.3 Cellular response to biotin depletion

Since our data indicated that the limited biotin supply combined with downregulation of *cut6* transcription promotes catastrophic mitosis, we hypothesized, that the YES medium contains biotin levels, which are insufficient for growth of Cbf11-defficient cells. Considering this theory, we were curious about the impact of biotin-free environment on cellular physiology. The ultimate question was, whether biotin depletion causes defective mitosis in WT cells. To test, whether the sole biotin unavailability affects mitosis in WT yeasts, we introduced the

exponentially growing WT cells into the biotin-containing (1 mg/l) or biotin-free (0 mg/l) EMM medium and assessed the following parameters: growth capacity, cell size, nuclear morphology and DNA content. The EMM medium was used due to its synthetic character, which allowed us to prepare a biotin-free variant. The experiment was performed as a time course, during which all four parameters were determined in 5 hrs intervals for the total of 20 hrs. Since 20 hrs-long period is enough for cells to enter stationary phase of growth, to keep cells exponentially growing, cultures were diluted at every point of sample collection. The biotin-free cultures were progressively ceasing growth and displayed reduction in cell length (Fig. 15 A-B). The observed growth retardation, however, could not be attributed to the elevated frequency of catastrophic mitoses, as biotin-deprived cells retained normal nuclear morphology (Fig. 15 C). Considering the apparent downscaling of proliferation, we concluded that biotin unavailability induced the cell cycle exit. *S. pombe* cells are able to enter G_0 from both, G_1 and G_2, depending on environmental conditions [93]. To determine, whether biotin depletion-induced cell cycle exit was cell cycle phase specific, we performed flow cytometry based analysis of DNA content. While the early cell populations (5, 10 hrs after initiation of biotin starvation) contained mostly G_2 cells (2C DNA peak), the later cell populations (15, 20 hrs after initiation of biotin starvation) consisted of a mixture of G_1 (1C DNA peak) and G_2 cells (Fig. 15 D). Thus, biotin deprivation did not cause any mitotic abnormalities, but rather inhibited proliferation by inducing cell cycle exit in G_1 or G_2.

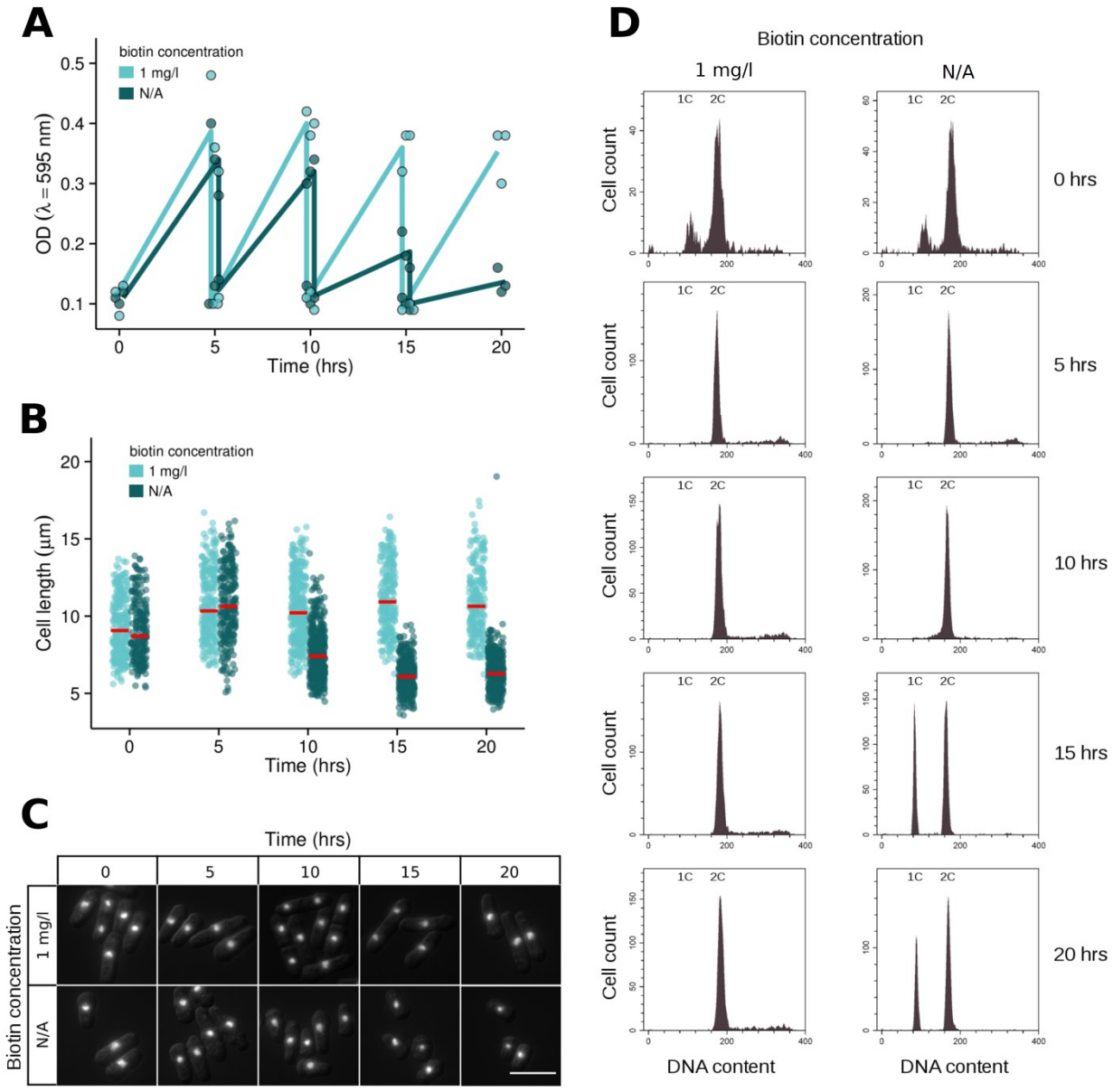

Fig. 15 – Biotin depletion causes the cell cycle exit but not catastrophic mitosis. Exponentially growing WT cells were transferred from YES into the EMM medium w/ (1 mg/l) or w/o (0 mg/l) biotin. To ensure the exponential growth throughout the whole 20 hrs-long experiment, cultures were diluted in 5 hrs intervals. **[A]** Growth capacities of WT cells cultured in the biotin-containing and biotin-free media were assessed as a sequence of 5 hrs interval OD measurements. Points represent the OD values from three independent experiments. Lines represent the mean values of 3 independent experiments. OD was measured just before and immediately after every dilution. Biotin deprivation resulted in progressive growth cessation. **[B-C]** Cell size changes and nuclear morphology status were analyzed throughout the biotin starvation time course. Cells were fixed with 70% ethanol,

stained with DAPI (1 µg/ml) and imaged. DIC images were used for cell length measurements. Measurements were done using the ImageJ software [82]. Biotin-starvation resulted in reduction of cell size but not mitotic failure. In [B], data corresponding to three independent repeats were pooled and plotted. Red lines indicate the median values. At least 200 cells per sample were analyzed. In [C], representative images of one independent experiment are shown. Bar 10 µm. **[D]** Cells were fixed with 70% ethanol and stained with propidium iodide (PI). DNA content was analyzed by flow cytometry. Biotin starved populations showed two distinct peaks of PI signal, corresponding to the subpopulations with 1C and 2C DNA content. Note, that DNA content profile is strikingly different at t = 0 hrs. The reason for this is that cell cycle progression and therefore DNA content distribution vary between the fission yeast populations cultured in YES and EMM. At least 1000 singlet cells per sample were scored. Two out of three independent experiments shown in [A-C] were analyzed. Results from one repeat are presented.

5.2.4 The question of periodicity: the expression of *cut6*, *vht1*, *bio2*

Since the impairment of Cut6 and Vht1 affects successful mitotic progression, we hypothesized that *cut6* and *vht1* transcription might show cell cycle periodic character potentially dependent on Cbf11 function. To test this hypothesis, we analyzed the relative mRNA levels of *cut6*, *vht1* and functionally connected *bio2* in different cell cycle stages. Indeed, the earlier work of M. Oravcova showed that the mRNA levels of *cut6*, *vht1* and *bio2* (quantified by RT-qPCR) oscillate during the cell cycle and this oscillation is Cbf11-dependent [20]. In that particular work, M. Oravcova employed the Cdc25-22 block/release synchronization technique, which allows synchronization in late G_2 by thermal inactivation and subsequent reactivation of temperature sensitive Cdc25 phosphatase (the positive regulator of G_2/M transition) [94]. Cdc25-22 block/release provides a high degree of synchrony, but comes together with heat shock and extensive cell cycle deregulation. Since heat shock and non-physiological cell cycle progression potentially influence the experimental output, the relevance of obtained results is always questionable. To rule out, that fluctuations in transcription of *cut6*, *vht1* and *bio2* observed by M. Oravcova are artefactual, we performed complementary experiments, using only WT cells and three synchronization protocols other than Cdc25-22 block/release. Namely, we employed the Cdc10-M17 block/release, hydroxyurea block/release and lactose gradient synchronizations

(Chapter 4.3). Following synchronization, we collected samples every 30 min, starting at t = 0 min, which corresponded to the time point of cell cycle release. Cell samples were collected in duplicates, being fixed with 70% ethanol or snap-frozen in liquid nitrogen. 70% ethanol fixed cells were stained with aniline blue and used for estimation of septation index (SI), which corresponds to the percentage of cells with developed septa within the population and indicates the level of synchrony and cell cycle progression. Note, that fission yeast cytokinesis and karyokinesis are slightly out of sync, and cells initiate DNA replication before cytokinesis takes place. Thus, the peak of septation index can be regarded as a point of S-phase entry [95]. Snap-frozen samples were used for total RNA isolation and subsequent RT-qPCR analysis of the *cut6*, *vht1*, *bio2* and *cdc22* relative mRNA levels. We assessed the expression of *cdc22* as a positive control of cell-cycle oscillatory expression, as *cdc22* encodes ribonucleotide reductase large subunit, transcription of which is activated at the onset of S-phase [96]. From all three synchronization approaches, only Cdc10-M17 block/release provided results somewhat similar to those of M. Oravcova, showing distinct *cut6* and *vht1* expression peaks around 90 min after cell cycle release (Fig. 16 A). The mRNA levels obtained from the experiments employing hydroxyurea block/release and lactose gradient centrifugation displayed profiles unique for both protocols and were highly inconsistent with data obtained from the Cdc10-M17 and Cdc25-22 block/release experiments (Fig. 16 B-C). Thus, it is likely that transcription of *cut6*, *vht1* and *bio2* is not cell cycle regulated and the upregulation of expression at the mRNA level displayed after release from Cdc25-22 and Cdc10-M17 thermal blocks represents a cellular response to stimuli, which are unrelated to cell cycle progression.

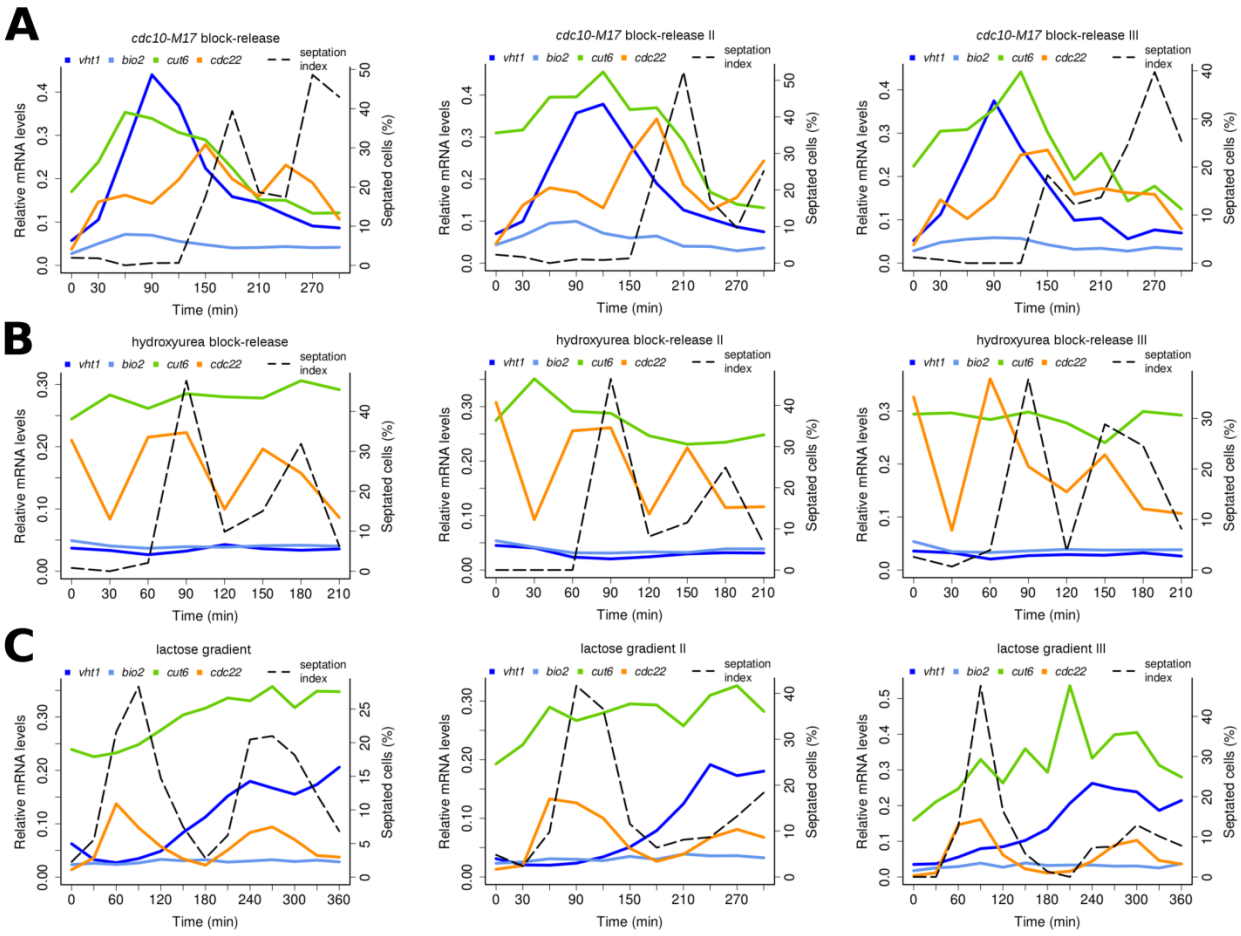

Fig. 16 – Lipid metabolism genes *cut6*, *vht1* and *bio2* do not show cell cycle contextual periodic transcription. [A] WT cells carrying the temperature sensitive allele *cdc10-M17* were synchronized in G_1-phase by thermal block (36°C) for 4 hours and released into cell cycle by thermal down-shift to 25°C. **[B]** WT cells were synchronized in S-phase by hydroxyurea (HU) treatment for 4 hours and released into cell cycle by HU wash off. **[C]** WT cells were synchronized in early G_2-phase by lactose gradient centrifugation, using two consecutive 10%-40% gradients. **[A-C]** Relative mRNA level profiles of *cut6*, *vht1*, *bio2* and *cdc22* were analyzed by RT-qPCR in the cell cycle context of WT cells synchronized in G_1, S and early G_2 phases. Three independent experiments for every synchronization technique are presented. Septation index (SI) indicates the cell cycle progression and the level of synchrony. SI values and mRNA levels were estimated at indicated time points (every 30 min). SI was calculated as a percentage of cells with developed septa. For the estimation of septation index, at least 100 cells per sample were scored. Data were acquired by R. Zach. Graphics was done by M. Prevorovsky. Results were published in [20].

5.3 *Δcbf11* mutant: conditional nature of phenotypes

5.3.1 Mitotic defects & growth retardation are environment-responsive in *Δcbf11* mutant

Considering morphological nature of *Δcbf11* mutant, it is not surprising, that *Δcbf11* populations are also characterized by growth retardation. While the average doubling time (DT) of WT cells grown in the YES (Yeast Extract with Supplements) medium is approximately 135 min, *Δcbf11* mutant grown in YES doubles only once per 275 min. Curiously, the pronounced growth defect of *Δcbf11* cultures shows a notable conditional character. When compared with WT values, the increase in DT is severe when *Δcbf11* cells are grown in the YES medium, but is considerably lower when cultured in the EMM (Edinburgh Minimal Medium) medium (Fig. 17 A-B). We wanted to elucidate, whether there is a correlation between partial rescue of growth capacity and susceptibility for mitotic failure. Indeed, we found that positive effect of EMM does not only increase the growth rate, but also diminishes the occurrence of cut phenotype in *Δcbf11* populations (Fig. 17 C). Interestingly, the same phenomenon has been previously observed with regard to the amount of storage lipids in *Δcbf11* cells (Fig. 12 C). The observed conditional nature of *Δcbf11* mutant can be explained by two alternative hypotheses. First, the YES medium, but not EMM, contains a chemical factor(s), which is/are poisonous for fission yeasts depleted of Cbf11. Second, the EMM medium contains component(s), which cause the rescue of *Δcbf11* mutant phenotypes. Alternatively, observed conditionality could also result from combination of both hypothetical causes. To determine which possibility properly describes our system, we mixed the YES and EMM media in different ratios and measured doubling times (DTs) of WT and *Δcbf11* cultures. If *Δcbf11* mutant grown in the mixed medium showed DT values comparable to those characteristic for EMM-cultured *Δcbf11* cells, it would be likely that observed differences in growth rate are consequential to a growth defect suppressing factor(s) included in EMM, rather than a poisonous compound(s) present in YES. Inversely, if *Δcbf11* mutant grown in the mix medium displayed DT analogous to that of the YES-cultured *Δcbf11* cultures, it would imply the existence of a deleterious compound present in the YES medium. DTs of *Δcbf11* cultures were reduced in the mix media with the EMM:YES ratios of 1:1 and 1:3, indicating that the phenotypic rescue is induced by the exposure to a yet unknown EMM

component(s) (Fig. 17 B). To get a more in depth insight into the responsiveness to cultivation medium, we determined the rate at which *Δcbf11* cells acquire defective phenotypes when exposed to the YES-based environment. We performed the experiment in which we transferred the exponentially growing WT and *Δcbf11* cells from EMM to the YES medium. To be sure cells did not cease the growth as a response to environmental stress or handling, we monitored growth during the whole experiment by measuring optical density (OD). As indicated in Fig. 17 D, neither WT nor *Δcbf11* cultures entered the lag-phase of growth. Remarkably, *Δcbf11* mutants started to accumulate cut defects immediately after the EMM to YES transition (Fig. 17 E-F), implicating that the very first post-transition mitotic events are defective in *Δcbf11* cells, when exposed to YES.

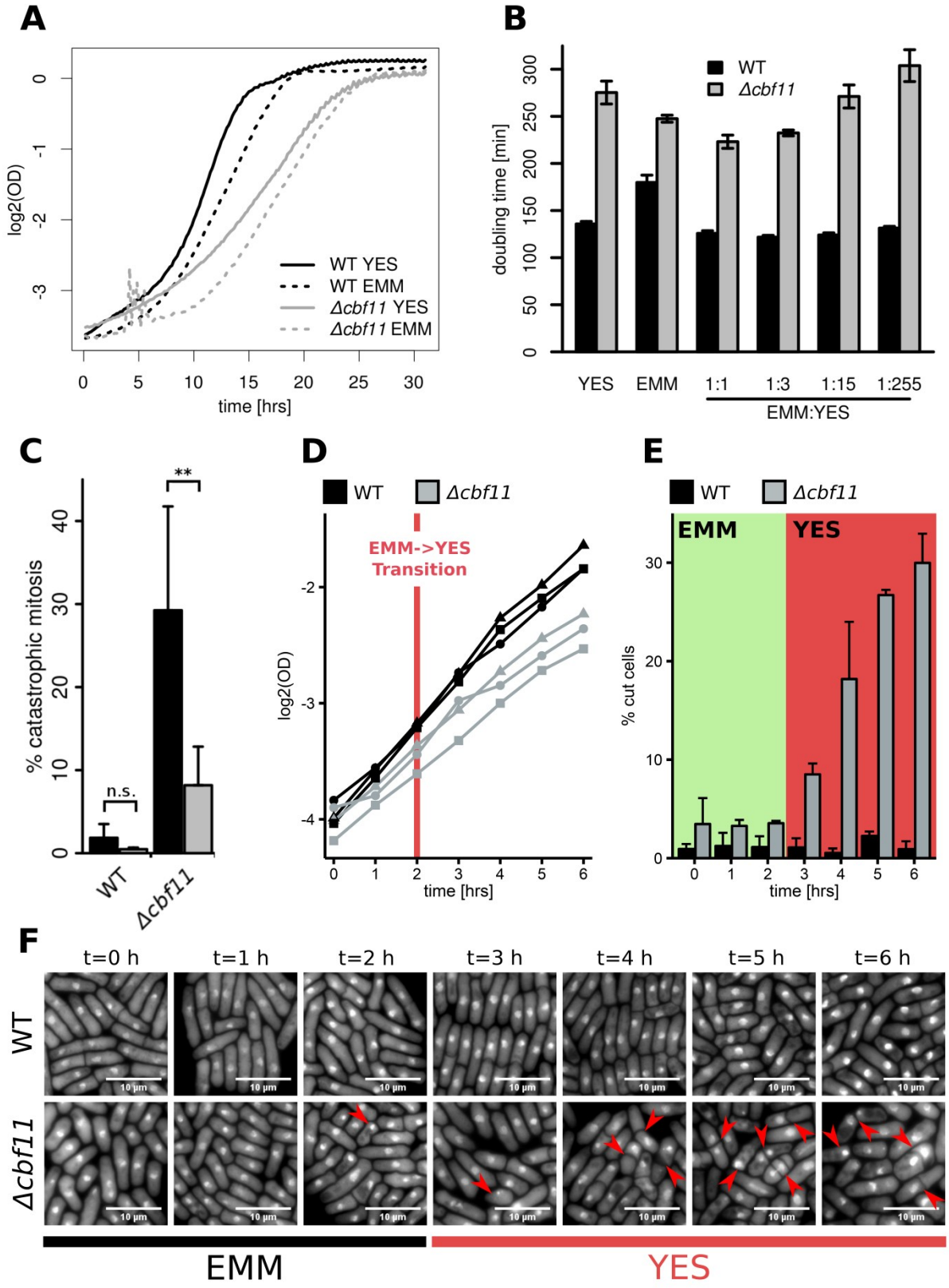
A
log2(OD)
time [hrs]
WT YES
WT EMM
Δcbf11 YES
Δcbf11 EMM
B
doubling time [min]
WT
Δcbf11
YES
EMM
1:1
1:3
1:15
1:255
EMM:YES
C
% catastrophic mitosis
n.s.
**
WT
Δcbf11
D
WT
Δcbf11
EMM->YES
Transition
log2(OD)
time [hrs]
E
WT
Δcbf11
EMM
YES
% cut cells
time [hrs]
F
t=0 h
t=1 h
t=2 h
t=3 h
t=4 h
t=5 h
t=6 h
WT
Δcbf11
10 μm
EMM
YES

Fig. 17 – Morphological and growth defects observed in *Δcbf11* mutants are conditional. **[A]** Growth curves of WT and *Δcbf11* cultures grown in YES or EMM. Results from a single representative experiment are shown. OD stands for optical density. **[B]** Doubling times of WT and *Δcbf11* cultures grown in YES, EMM and the variations of EMM:YES mix media. Mean values ± standard deviations from three independent experiments are shown. The EMM component(s) partially suppresses the growth defects, which are observed in *Δcbf11* mutants grown in YES. **[C]** Microscopy based quantification of the cut phenotype occurrence in WT and *Δcbf11* cultures grown in YES or EMM. Exponentially growing cells were fixed with 70% ethanol and stained with DAPI (1 µg/ml). The percentage of cut occurrence was estimated by manual counting. At least 200 cells per sample were scored. Mean values ± standard deviations from six independent experiments are shown. Significance was calculated using one-sided paired t-test (**p < 0.01), n.s. – nonsignificant. Cultivation in EMM markedly suppresses the occurrence of cut defects in *Δcbf11* mutants. **[D]** Growth curves of WT and *Δcbf11* cultures during EMM to YES transition experiments. Data from three independent experiments are shown. Different point shapes (circles, squares, triangles) discriminate the data corresponding to different independent repeats. The vertical line indicates the time point at which the EMM medium was changed for YES. No retardation of growth (lag) was observed. **[E]** Microscopy based quantification of the cut phenotype occurrence in WT and *Δcbf11* cultures from the panel [D]. Cells were collected and fixed with 70% ethanol at every time point indicated in [D]. DAPI-stained cells were imaged by fluorescence microscopy. The percentage of cut occurrence was estimated by manual counting. At least 200 cells per sample were scored. Mean values + standard deviations from three independent experiments are shown. The occurrence of cut phenotype in *Δcbf11* cultures dramatically rises after the EMM medium is changed for YES. **[F]** Representative images of DAPI-stained WT and *Δcbf11* cells from the experiment [D-E] at distinct time points. Red arrowheads indicate cells, which underwent catastrophic mitosis. Scale bars 10 µm. The experiment presented in the panel [C] and the graphics for panels [A-C] were done by M. Prevorovsky. Results [A-C] were published in [19,20].

5.3.2 Growth retardation: catastrophic mitosis or cell cycle delay?

Considering defective nature and propensity to undergo catastrophic mitosis, we hypothesized that growth retardation of *Δcbf11* populations could be attributed to a certain degree of mortality in every generation, checkpoint-mediated cell cycle delay, slow cell cycle progression or combination of factors. To test the hypothesis that the slower growth of *Δcbf11* mutants is a consequence of high mortality, we used a mathematical approach. Since

the cut phenotype is considered a terminal phenotype, we aspired to determine the percentage of cells, which would have to die off in every generation to explain the difference between average DTs of WT and *Δcbf11* cultures and compare the acquired hypothetical value with the real microscopic results. As described in Chapter 4.1.8, using the average DT values (DT_{WT} = 136 min, $DT_{\Delta cbf11}$ = 275 min), we determined the average slopes of logarithmic phases of growth for WT and *Δcbf11* cultures (k_{WT} = 0.00735, $k_{\Delta cbf11}$ = 0.00364), which can be used for modelling of hypothetical exponential growth curves. For illustration, exponential curves defined by WT and *Δcbf11* k values are plotted (Fig. 18 A). By substituting k and t variables for $k_{\Delta cbf11}$ and DT_{WT} in the exponential growth characterizing equation ($y = 2^{k*t}$), we assessed that *Δcbf11* population achieves only ≈ 140.9% of initial biomass in the time course during which WT culture doubles. Therefore, *Δcbf11* population could be theoretically regarded as WT population, in which ≈ 30% of cells die and ≈ 70% of cells divide every DT_{WT}. Such a situation is defined by equation: $y = 1.409^{0.00735*t}$. This result is highly consistent with our data (Fig. 17 C), which show the mean value of cut phenotype occurrence equal to 29.25% in YES-grown *Δcbf11* cells. Considering the cut phenotype a 100% terminal defect, this situation can be described by equation: $y = 1.415^{0.00735*t}$. For purposes of graphical comparison, exponential curves defined by $y = 1.407^{0.00735*t}$ and $y = 1.415^{0.00735*t}$ together with WT-characteristic curve are plotted (Fig. 18 B). Even though we found a strong agreement between the model and real data, over-simplifying premises upon which we have built our calculations might be misleading. A major problematic aspect resides in the fact, that experiments determining growth parameters and the cut phenotype occurrence were conducted separately. Considering a high variability in frequencies of mitotic failure events characteristic for *Δcbf11* cultures (Fig. 17 C), correlations between growth and cut regarding data may be disputable. Additionally, it has been shown that some cells remain viable even after undergoing cut mitosis [28]. Unfortunately, we do not have any data regarding this matter and thus, mathematical model cannot be corrected.

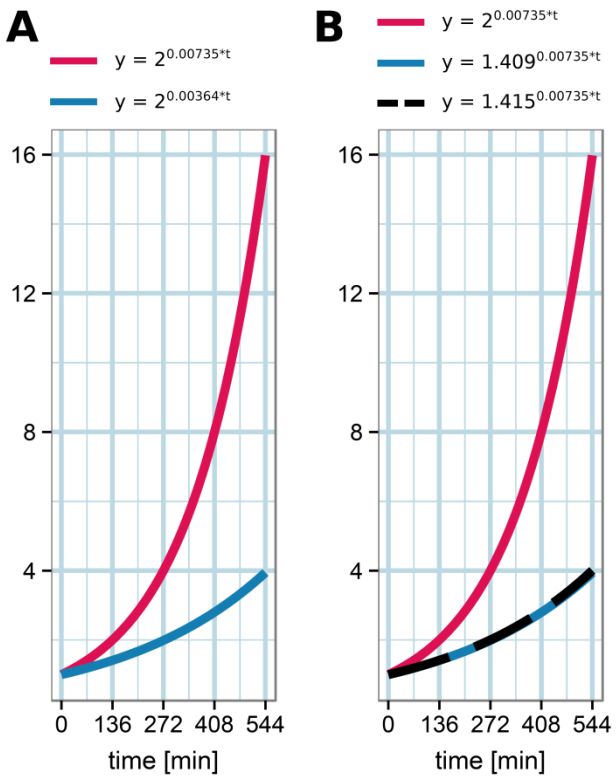

Fig. 18 – Mathematical models of fission yeast growth. [A] Exponential growth models of WT and *Δcbf11* cultures. Red line – exponential growth of WT ($y = 2^{0.00735*t}$). Blue line –exponential growth of *Δcbf11* mutant ($y = 2^{0.00364*t}$). **[B]** Exponential growth models of WT with 0% (red line), 30% and (blue line) and 29.25% (black dashed line) mortality. Note, that blue lines in [A] and [B] are identical, implying, that the growth defects characteristic for *Δcbf11* mutants could be theoretically explained by 30% mortality. Mathematically acquired insight into the growth retardation of *Δcbf11* cells corresponds to microscopic data, which are modelled by $y = 1.415^{0.00735*t}$ (black dashed line).

As mentioned before, slow growth could be also attributed to checkpoint-mediated cell cycle delay or slow cell cycle progression. To test whether cell cycle length is altered in *Δcbf11* mutant we performed a pair of time-lapse microscopy experiments, hoping to be able to measure the actual time needed for completion of cell cycle in WT and *Δcbf11* cells. To do this, we used the mixed cultures of WT and *Δcbf11* strains, each of which carried a different fluorescent variant of nucleolar protein Gar2 (Gar2-mCherry for WT and Gar2-GFP for *Δcbf11*). Thus, we could culture cells together in one microscopic chamber, ensuring the same growth conditions for both strains and at the same time being able to distinguish between the cells of particular genotype (WT or *Δcbf11*). Since *S. pombe* cells are not surface adhesive, we could not use the liquid medium based cultures. Alternatively, we covered the cells with a thin agar based solid YES medium slice, ensuring nourishment and keeping cells immobile. Unfortunately, we were unable to properly humidify the microscopic chamber, which resulted in agar slice drying and shrinking. As a consequence of the agar shrinkage, cells were rapidly moving and exiting the focal area, making image sequences unquantifiable. Another observation we made, was that *gar2:GFP Δcbf11* cells did not display any of the

previously described phenotypes, raising doubts about validity of the strain genotype. The laboratory stock *gar2:GFP Δcbf11* strain has thus been designated for revalidation. The genotyping, however, has not yet been performed. Since live cell imaging experiments were unsuccessful due to above described technical complications, we could not support or disprove the hypothesis that the cell cycle is delayed in *Δcbf11* cells. The images (t = 0 min) of mixed cultures are presented in Fig. 19 A-B.

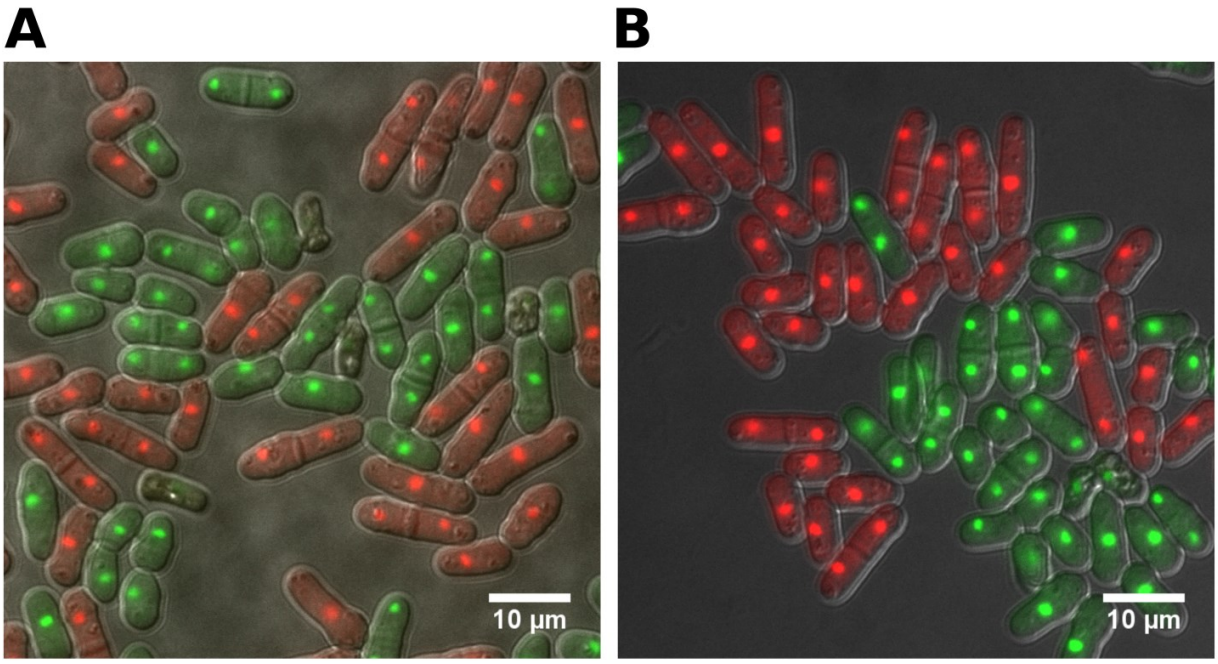

Fig. 19 – Live cell imaging of WT and *Δcbf11* cells. [A-B] Images taken at t = 0 of two independent time lapse imaging time-courses, illustrating the mixed cultures of WT and *Δcbf11* cells expressing the fluorescent nucleolar protein (Gar2-mCherry for WT and Gar2-GFP for *Δcbf11)*. Images are overlays of bright field, BF [A] or differential interference contrast, DIC [B], mCherry and GFP channels. Scale bar 10 µm.

5.3.3 Cultivation media and their components: cell cycle context

Since growth retardation and the occurrence of cut phenotype observed in *Δcbf11* populations grown in YES is considerably diminished when exposed to the components of EMM medium, we aspired to identify the exact component(s) responsible for this phenotypic rescue. If successful, such determination might possibly unravel the cut-related signalling

pathways involving Cbf11. The idea was to supplement the complex YES medium with the EMM components in concentrations listed in the EMM recipe and asses seriousness of growth and mitotic defects. Apart from the carbon source, which is glucose, EMM contains 19 other chemical substances, which form three larger groups: minerals, vitamins and trace elements. To narrow down the list of tested compounds, we prepared three variants of the YES medium, each of which was supplemented by one of the three complex EMM compounds (minerals, vitamins and trace elements). As indicated in Fig. 20 A-C, only the mineral supplementation of YES resulted in elevation *Δcbf11* culture growth rate. Mineral component of EMM had no apparent effect on growth rate of WT cultures (Fig. 20 A-C) and (Fig. 21 A-B). The list of EMM minerals includes 7 compounds: potassium phthalate (phthalic acid K+), disodium hydrogen phosphate (Na_2HPO_4), ammonium chloride (NH_4Cl), magnesium chloride ($MgCl_2$), calcium chloride ($CaCl_2$), potassium chloride (KCl) and sodium sulfate (Na_2SO_4) in concentrations provided by Formedium, http://www.formedium.com/. Note, that the mineral component of EMM contains non-mineral chemical substances, such as phthalate and NH_4Cl. The reason for using the term 'mineral component' is strictly practical, as it is used by Formedium Company in the same way we use it. To test the possibility that a single compound is responsible for growth rate acceleration of *Δcbf11* populations, we prepared the YES media supplemented with single EMM mineral components and assessed doubling times. Curiously, for unknown reasons, neither WT nor *Δcbf11* cells grew in YES + Na_2HPO_4. Results acquired for other tested media displayed high degree of variability among three independent experiments and did not support the idea of a single 'growth defect suppressor' (Fig. 21 B). Additionally to testing the growth parameters, we also determined the percentage of cells undergoing catastrophic mitosis in WT and *Δcbf11* cultures grown in the YES media supplemented with the complex and single EMM mineral components. Remarkably, we found, that the minerals supplementation indeed diminishes the occurrence of mitotic failure and this rescue seems to be dependent on the addition of ammonium chloride (Fig. 21 C). It must be noted, that we observed a high degree of variability among three independent repeats, however, the data regarding the positive effect of NH_4Cl were highly consistent and therefore credible.

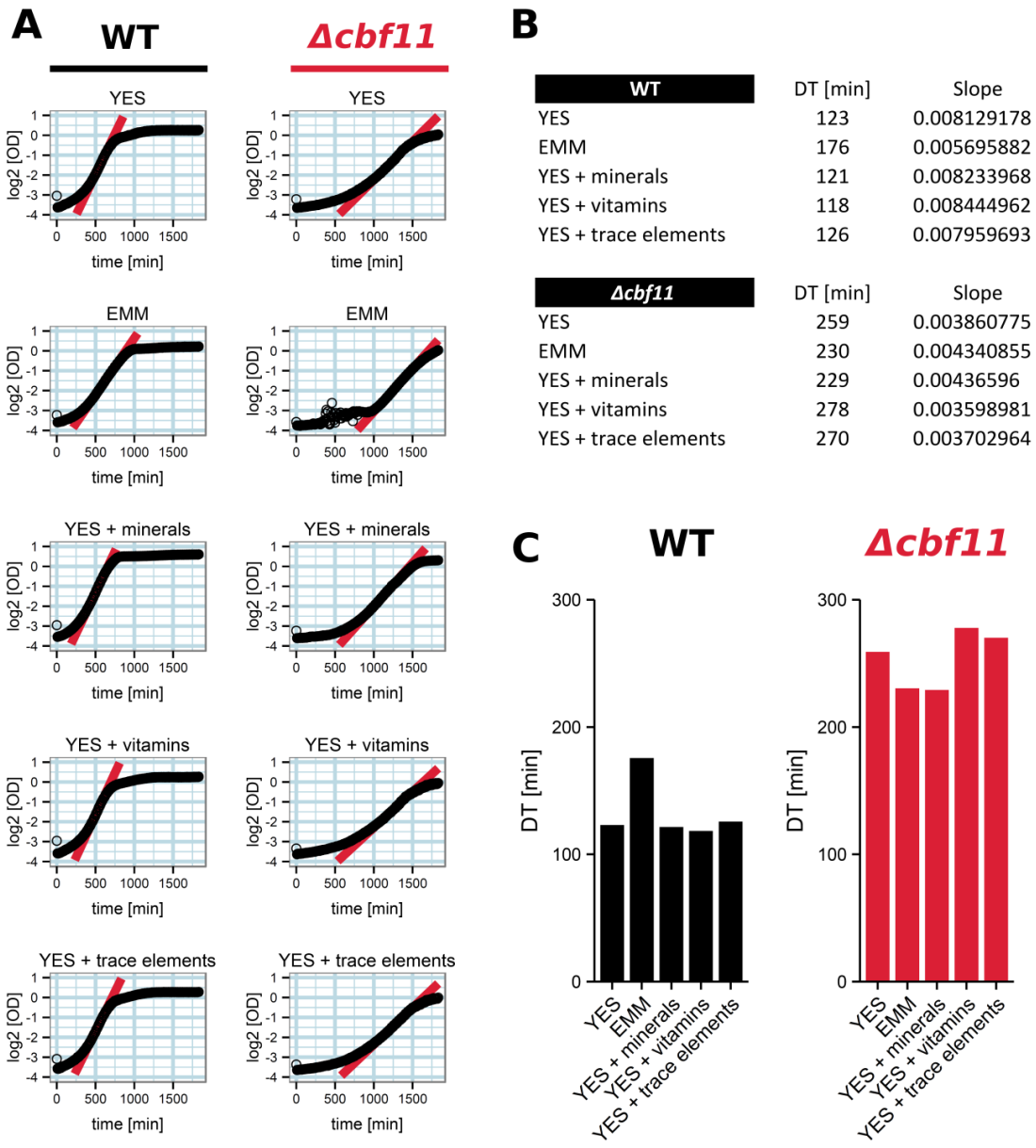

WT	DT [min]	Slope
YES	123	0.008129178
EMM	176	0.005695882
YES + minerals	121	0.008233968
YES + vitamins	118	0.008444962
YES + trace elements	126	0.007959693

Δcbf11	DT [min]	Slope
YES	259	0.003860775
EMM	230	0.004340855
YES + minerals	229	0.00436596
YES + vitamins	278	0.003598981
YES + trace elements	270	0.003702964

Fig. 20 – The complex mineral component of EMM medium is solely responsible for growth acceleration of *Δcbf11* cultures. [A] Growth curves of WT and *Δcbf11* populations grown in YES, EMM and YES supplemented with the EMM complex components (minerals, vitamins and trace elements). Red lines represent the linear regressions of log-phases of growth. **[B]** The table enlisting the slopes of log-phase linear regressions and doubling times (DT) calculated as DT = 1/Slope. **[C]** Bar plots of calculated DTs of WT and *Δcbf11* cultures grown in the listed media. The growth defect observed in Cbf11-depleted cells grown in YES is partially suppressed by addition of the EMM-contained minerals, but not vitamins nor trace elements. Experiment was performed once.

Previously, we postulated the hypothesis that the propensity of *Δcbf11* cells to undergo catastrophic mitosis is at least partially consequential to transcriptional downregulation of acetyl coenzyme A carboxylase (*cut6*) and biotin transporter (*vht1*). Since Vht1 functions as a high affinity H^+ symporter with the maximal operational efficiency at pH = 4 [97], we speculated, that differences in pH might be relevant for functionality of partially impaired biotin-Cut6 system in Cbf11-defficient cells. Indeed, we discovered a significant difference between the pH values of YES and EMM (pH_{YES} = 6.45 pH_{EMM} = 4.69) (Fig. 21 D). The more acidic character of EMM, however, does not seem to be attributed to NH_4Cl as YES supplemented with NH_4Cl display only minor decrease in pH. According to our pH measurements, two factors (base: Na_2HPO_4 and acid: phthalic acid) are major contributors to the final pH of EMM. YES supplemented with Na_2HPO_4 displays increased pH (Fig. 21 D), which might theoretically explain the observation, that fission yeasts fail to grow in the YES + Na_2HPO_4 medium. The addition of potassium phthalate to the YES medium dramatically decreases pH value (Fig. 21 D). Interestingly, we found that WT cells grown in the YES + phthalic acid K+ medium are longer compared to those cultured in non-supplemented YES (Fig. 22). This cell size increment is analogous to that observed in the EMM-grown yeasts (Fig. 22). Potassium hydrogen phthalate was introduced into the EMM medium by P. Nurse to suppress flocculation of problematic strains [98,99]. As phthalate represents the acidifying agent (Fig. 21 D), it is possible, that fission yeast cell size is somehow determined by the environmental pH. However, molecular bases of phthalate effect on *S. pombe* cells are unclear, therefore other potential impacts cannot be ruled out. Since phthalate does not seem to be the factor influencing successful mitotic progression and this study does not focus on cellular responses to the environmental pH status, the issue has not been further investigated.

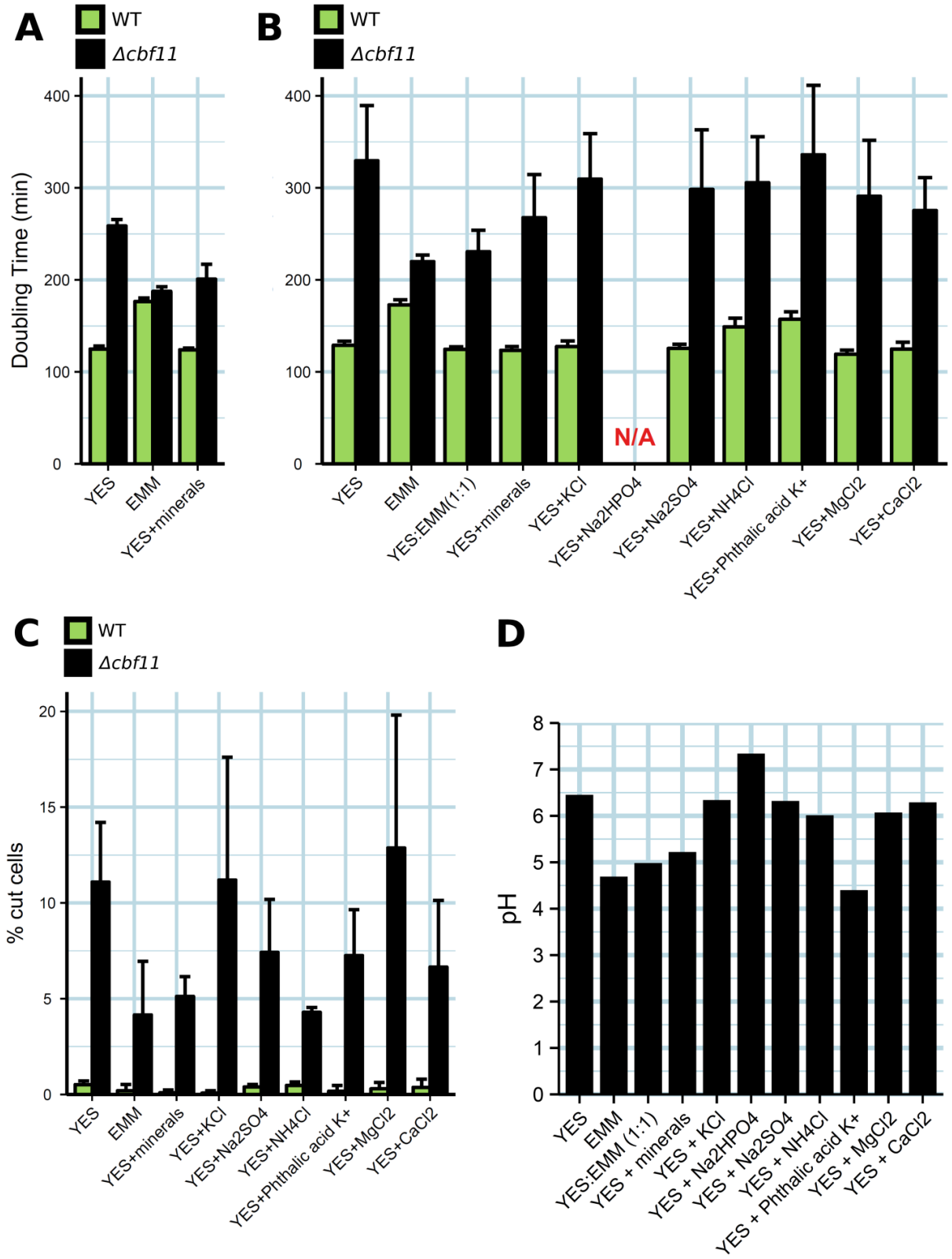

Fig. 21 – Mineral component of EMM partially rescues the growth retardation and decreases the occurrence of cut phenotype in *Δcbf11* cells. [A-B] Doubling times (DT) of WT

and *Δcbf11* cells grown in YES, EMM and the YES media supplemented with mineral EMM components. DTs were calculated from the slopes of logarithmic growth phases. Mean values of three independent experiments are shown. Error bars represent positive standard deviations. The supplementation of YES with the complex mineral EMM component containing KCl, Na_2HPO_4, Na_2SO_4, NH_4Cl, Phthalic acid K+, $MgCl_2$ and $CaCl_2$ notably improved the growth defect of *Δcbf11* populations grown in YES. The positive effect of minerals probably cannot be attributed to a single mineral component. DTs of WT and *Δcbf11* populations grown in YES + Na_2HPO_4 were not assessed (N/A) as growth of both strains was terminated by the addition of Na_2HPO_4. **[C]** The cut phenotype occurrence of WT and *Δcbf11* cells grown in YES, EMM and the YES media supplemented with the mineral EMM components. Cells fixed with 70% ethanol were stained with DAPI (1 μg/ml) and imaged. Mean values of three independent experiments are shown. Error bars represent positive standard deviations. At least 200 cells per sample were scored. The cut phenotype occurrence in *Δcbf11* cells grown in YES was dramatically rescued by addition of the complex EMM mineral component (KCl, Na_2HPO_4, Na_2SO_4, NH_4Cl, Phthalic acid K+, $MgCl_2$ and $CaCl_2$) or NH_4Cl alone. **[D]** pH values of all tested media. The EMM, YES:EMM (1:1) and YES + minerals display more acidic character compare to YES. The acidic nature of the EMM, YES:EMM (1:1) and YES + minerals media is not attributed to the NH_4Cl, but phthalic acid K+, the addition of which dramatically decreases pH value of YES. The YES medium supplemented with Na_2HPO_4 display increased pH.

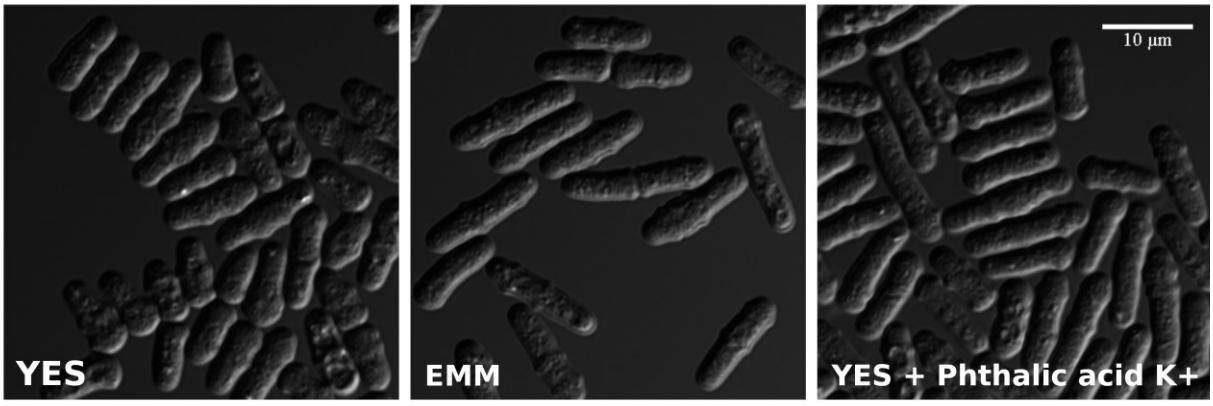

Fig. 22 – Phthalate is solely responsible for larger cell sizes of fission yeasts grown in the EMM medium. Representative DIC-images of WT cells fixed with 70% ethanol. Yeasts grown in EMM or YES supplemented with phthalate are longer compared to cells cultured in YES. The phenomenon of increased cell sizes was not observed in any other tested YES-based media (YES variants containing the single EMM components: KCl, Na_2HPO_4, Na_2SO_4, NH_4Cl, $MgCl_2$ and $CaCl_2$) and therefore is solely attributed to phthalate.

5.4 Construction of conditional *cbf11* mutant

5.4.1 Auxin-inducible Cbf11 degron: principle

Since *Δcbf11* mutants display a broad range of potentially interconnected defects, in some cases it might be almost impossible to distinguish between the primary and secondary phenotypes. To address this problem, we decided to construct a conditional *cbf11* mutant, which would allow us to rapidly induce Cbf11 depletion and determine the cascade of appearing phenotypes. Conditional mutant would also help us to control the occurrence of suppressor mutations, which potentially accumulate in cultures of severely sick mutants, such as *Δcbf11*. We chose a system derived from plants, which utilizes a plant hormone auxin to target proteins for degradation. In plants, auxin binds to the transport inhibitor response 1 (TIR1) protein of the SCF^{TIR1} E3 ubiquitin ligase complex and facilitates its docking to the Aux/IAA transcription repressors, which are subsequently poly-ubiqitinated and thus marked for proteasome-mediated degradation [100]. SCF (Skp1, Cullin and F-box protein) E3 ubiquitin ligases are highly conserved across species, creating a possibility for employment of auxin-inducible SCF^{TIR1} degradation system in non-plant organisms. The general idea is to introduce the TIR1 gene and tag the protein of interest with the auxin inducible degron (aid) motive. In such a system, exposure to auxin specifically induces degradation of aid-tagged protein, as illustrated in Fig. 23. The auxin inducible SCF^{TIR1} module has been also implemented in *S. pombe* [101]. Since the expression of fused Skp1-TIR1 protein increases the efficiency of the system [101], we aimed to construct the strain carrying the Skp1-TIR1 fusion and the *cbf11* allele C-terminally tagged with the HA and aid domains (Fig. 24).

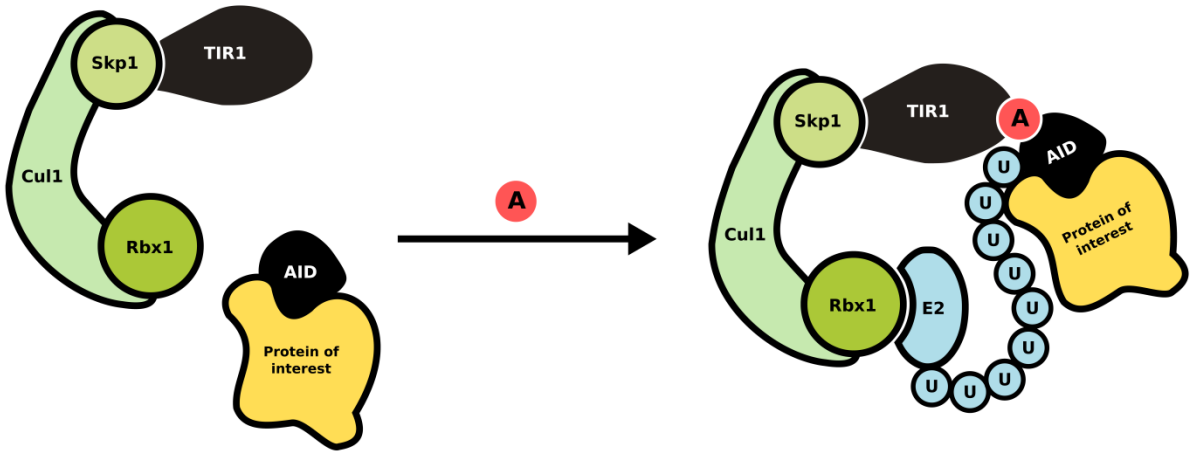

Fig. 23 – Schematic illustration of auxin inducible protein degradation system. Illustrated are: SCF^{TIR1} complex and aid-tagged protein. SCF^{TIR1} is composed of Cul1 scaffold protein, Rbx1 ring box protein, Skp1 adapter and TIR1 F-box protein. Rbx1 ensures binding of ubiquitin-conjugated E2 enzyme. Skp1 mediates TIR1 association. TIR1 recognises target proteins. Upon exposure to auxin, TIR1 binds to auxin inducible degron motive, which is subsequently poly-ubiquitinated and destined for proteasome-mediated degradation. AID – auxin inducible degron, A – auxin, U - ubiquitin. Image layout is adapted from [102].

5.4.2 Auxin-inducible Cbf11 degron: construction

As the initial step we aimed to construct a fragment containing the sequence of the 3'end of *cbf11* coding region, 3 HA tag copies, aid domain, kanamycin resistance cassette and the very 5'end of *cbf11* 3'UTR region. As the end regions of this fragment are complementary to the sequences at the boundary between *cbf11* coding sequence and 3'UTR, constructed sequence could be integrated into the genome by homology recombination. For construction, we amplified 4 DNA fragments: 1) 3'*cbf11*CDS-3HA, 2) aid, 3) kanR and 4) 5'end of *cbf11* 3'UTR (Fig. 24). Since we wanted to join fragments 1-4 together using the Gibson assembly reaction, all fragments contained 5' end extensions complementary to the ends of neighbouring fragments, as described in Chapter 4.4.9.

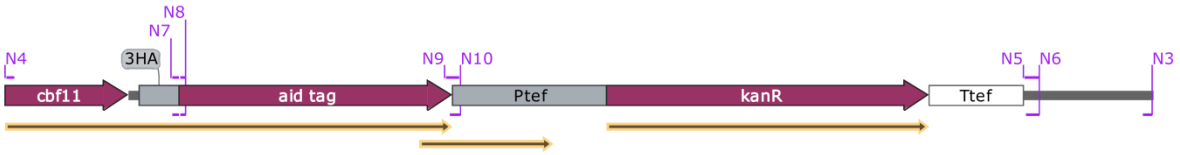

Fig. 24 – Graphical illustration of *cbf11-3HA-aid-kanR* construct. Fragment 1 is defined by N4/N8 primer pair and encodes 3' end region of *cbf11* coding sequence followed by 3 consecutive HA tags. Fragment 2 is defined by N7/N10 primer pair and encodes auxin-inducible degron (aid) tag. Fragment 3 is defined by N9/N6 primer pair and encodes kanamycin resistance cassette (kanR). Fragment 4 is defined by N5/N3 primer pair and encodes 3' non-coding region of *cbf11* mRNA situated just upstream of termination codon. The yellow arrows indicate translated regions. Whole construct size is 2870 bp. Illustration was created with SnapGene software (from GSL Biotech; available at snapgene.com).

The first fragment was amplified by PCR, using primers N4 & N8 and the genomic DNA isolated from the MP26 strain as a template. The second fragment was amplified by PCR, using primers N7 & N8 and the pSL60 plasmid DNA as a template. The third fragment was amplified by PCR, using primers N9 & N6 and the pSL60 plasmid DNA as a template. The fourth fragment was amplified by PCR, using primers N5 & N3 and the genomic DNA isolated from JB32 strain as a template. The expected sizes of fragments (1-4) were 457 bp, 731 bp, 1487 bp and 318 bp, respectively. Products of all four PCR amplifications were checked by capillary electrophoresis (Fig. 25).

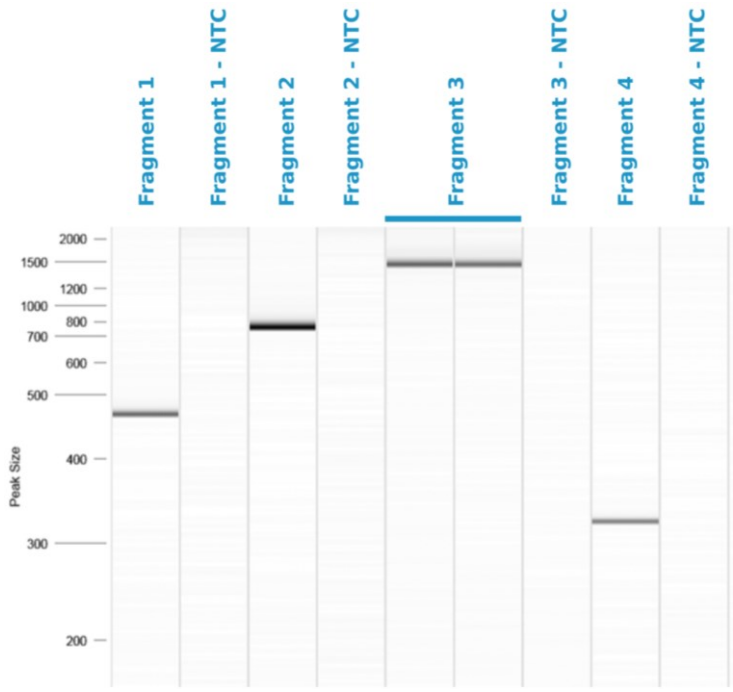

Fig. 25 – The output of high-resolution capillary electrophoresis: fragments 1-4. PCR fragments of 3'end of *cbf11* CDS region fused with 3 HA tags, auxin inducible degron, kanamycin resistance cassette and 5'end of *cbf11* 3'UTR region (Fragments 1-4) were subjected to capillary electrophoresis. Sizes of fragments 1-4 corresponded to the expected lengths: 457 bp, 731 bp, 1487 bp and 318 bp, respectively. NTC stands for none template control. Fragment 3 was loaded in duplicates. Qiagen QIAxcel capillary system was used for analysis.

Fragments 1-4 were subsequently joined together in 4 separate Gibson assembly reactions, using different amounts of the Gibson assembly master mix. The reason to use such a reaction set up was to test the performance of Gibson assembly kit at different dilutions. Gibson assembly products were checked by capillary electrophoresis, however no bands were detected. This could be due to the low efficiency of assembly, technical issues with the Qiagen QIAxcel capillary system or Gibson assembly reaction failure. 2 µl of every reaction were used as a template for PCR-amplification with primers N3 & N4, expecting the 2870 bp product. The PCR products were analyzed by standard agarose gel electrophoresis. Two out of four reactions displayed a DNA band of a relative size just below 3 kbp, which would correspond to the expected length of the construct (2870 bp). Bands of lower relative sizes were also detected, but these probably represented original unassembled fragments of

Gibson reaction. It must be noted that signals of observed bands were very weak, indicating the low efficiency of Gibson reaction or PCR amplification (Fig. 26 A). Reactions containing ≈ 3 kb bands were pooled and used for transformation of WT *S. pombe* strain (JB32). Transformants were selected for kanamycin resistance. Selected single colonies were tested for the incorporation of *cbf11:3HA:aid:kanR* by PCR with primers N1 & N2 situated downstream and upstream of the construct integration site. 10 out of 10 tested clones showed a distinct band of the relative size ≈ 3 kb. The isolate 10 also displayed the 'WT' sized band, indicating a mixed initial culture containing transformed and non-transformed cells (Fig. 26 B).

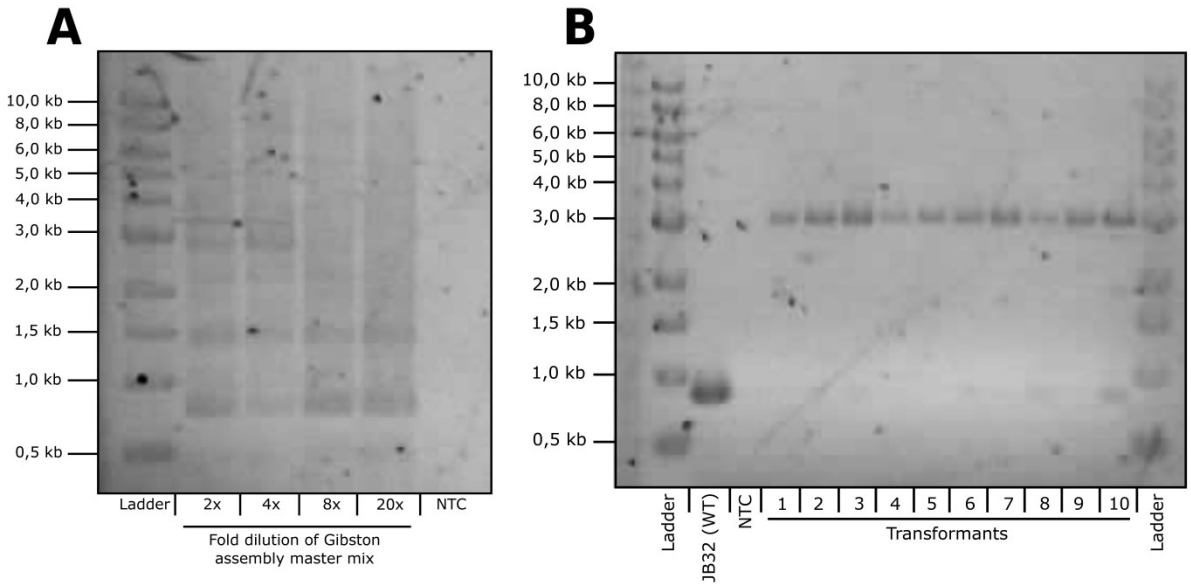

Fig. 26 – The output of agarose gel electrophoresis: Gibson assembly product. [A] Fragments 1-4 were joined in Gibson assembly reaction. 4 assembly reactions with different dilutions of Gibson assembly master mix were prepared. Two PCR reactions displayed product of the relative size ≈ 3 kb, which corresponds to the expected length of 2870 bp. **[B]** Genomic DNA of selected clones transformed by PCR product from [A], was used as a template for PCR amplification, using primers N1 & N2. PCR products were visualized by agarose gel electrophoresis. 10 out of 10 colonies showed the expected ≈ 3 kb band. The isolate 10 was probably mixed culture as bands of two sizes were displayed. NTC stands for no template control. JB32 represents non-transformed WT control. [A-B] The agarose gels were stained with gel red.

5.4.3 Auxin-inducible Cbf11 degron: introduction of *skp1:TIR1* fusion and final genotyping

Clone 'one' was stored as a glycerol stock (strain MP520). Strains MP520 and 1659 (Fig. 27) were crossed, sporulated and subsequently plated on three types of selection plates: EMM, YES+G418 and YES. The aim was to select the clones of four genotypes enlisted in Table 10. Strains of genotypes designated as 1) and 2) carry *skp1:TIR1* fusion allele and were meant as controls for future experiments. Additionally to *skp1:TIR1*, Strain 2) carries temperature-sensitive *cdc10-M17* allele, which allows synchronization in G_1. Strains marked as 3) and 4) are analogous to 1) and 2), but carry *cbf11:3HA:aid* allele, which, when combined with *skp1:TIR1*, should allow auxin-induced proteasomal degradation of Cbf11:3HA:aid protein.

Table 10 - List of selected genotypes

1)	*h? ura4-D18 ade6+pADH15.skp1:AtTIR1:2NLS:9myc*
2)	*h? ura4-D18 ade6+pADH15.skp1:AtTIR1:2NLS:9myc cdc10-M17*
3)	*h? ura4-D18 ade6+pADH15.skp1:AtTIR1:2NLS:9myc cbf11:3HA:aid:kanR*
4)	*h? ura4-D18 ade6+pADH15.skp1:AtTIR1:2NLS:9myc cbf11:3HA:aid:kanR cdc10-M17*

The uracil deficient EMM plates were incubated at 25°C and selecting for the *mcm4:2HA:aid:ura4+* construct (present in the parental strain "1659"), which was unwanted in the clones of desired genotypes. The YES+G418 plates were incubated at 25°C and worked as a discriminatory selection for the *cbf11:3HA:aid:kanR* construct. YES plates were incubated at 36° and discriminated between temperature-sensitive (*cdc10-M17*) and insensitive ($cdc10^{+}$) clones. Crossing and selection procedure are illustrated in (Fig. 27).

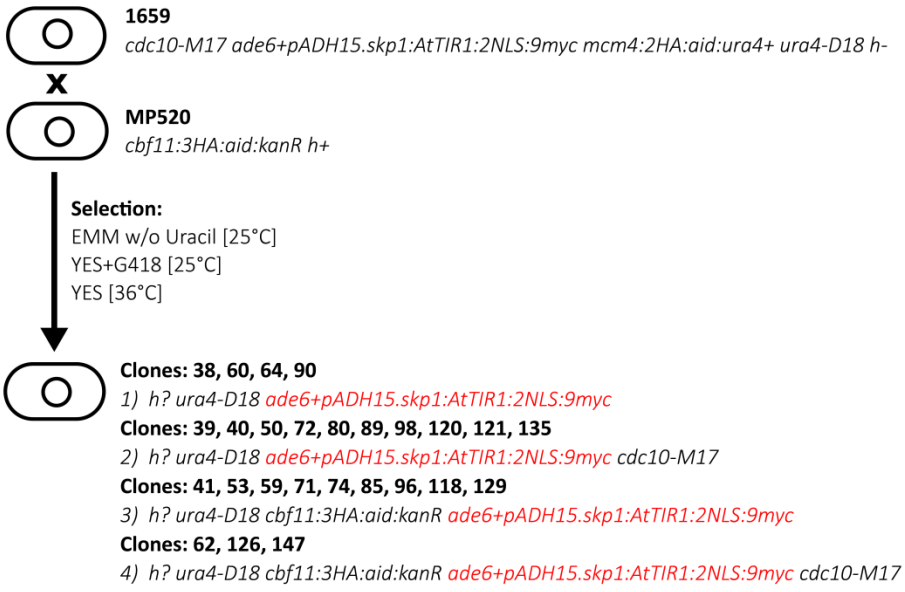

Fig. 27 – Schematic illustration of the crossing and selection process with the aim to acquire the clones of genotypes 1-4. Strains 1659 and MP520 were crossed and sporulated. Single colonies of germinated cells were isolated and incubated at selective conditions as described in the main text. 4, 10, 9 and 3 clones of the genotypes respectively potentially corresponding to the genetic variants 1-4 were selected and subjected to genotyping of *ade6+pADH15.skp1:AtTIR1:2NLS:9myc* construct.

Clones potentially corresponding to the desired genotypes (1-4) were selected and subjected to further validation of the *ade6+pADH15.skp1:AtTIR1:2NLS:9myc* construct by western blotting with the use of anti-myc primary antibody. Clones: 38, 41, 50, 60, 71, 74, 96, 120, 129 and 147 were myc-tag positive (Fig. 28 A). Due to uncertainties about the sample layout in experiment presented in Fig. 28 A, clones: 120, 129 and 147 were subjected to double checking of *ade6+pADH15.skp1:AtTIR1:2NLS:9myc*. The myc-positivity of isolates: 38, 60, 64 and 90 were also evaluated, as they were not included in previous myc-tag verification. Consistently with previous results, clones: 120, 129 and 147 were myc-positive. Single colonies: 38 and 60 also displayed clear myc signal (Fig. 28 B). To be absolutely sure about the results from Fig. 28 A, clones: 41, 71, 74 and 96 were also re-validated for myc-positivity. All four clones displayed clear myc-specific signal, indicating the presence of *ade6+pADH15.skp1:AtTIR1:2NLS:9myc* construct (Fig. 28 C). All myc-positive clones were re-genotyped for the uracil auxotrophy. Clones: 129 and 147 showed positive growths on EMM w/o uracil, therefore were prototrophic. Since prototrophic character meant the possibility

of carrying the undesirable *mcm4:2HA:aid:ura4+* allele, clones: 129 and 147 were removed from further validation process.

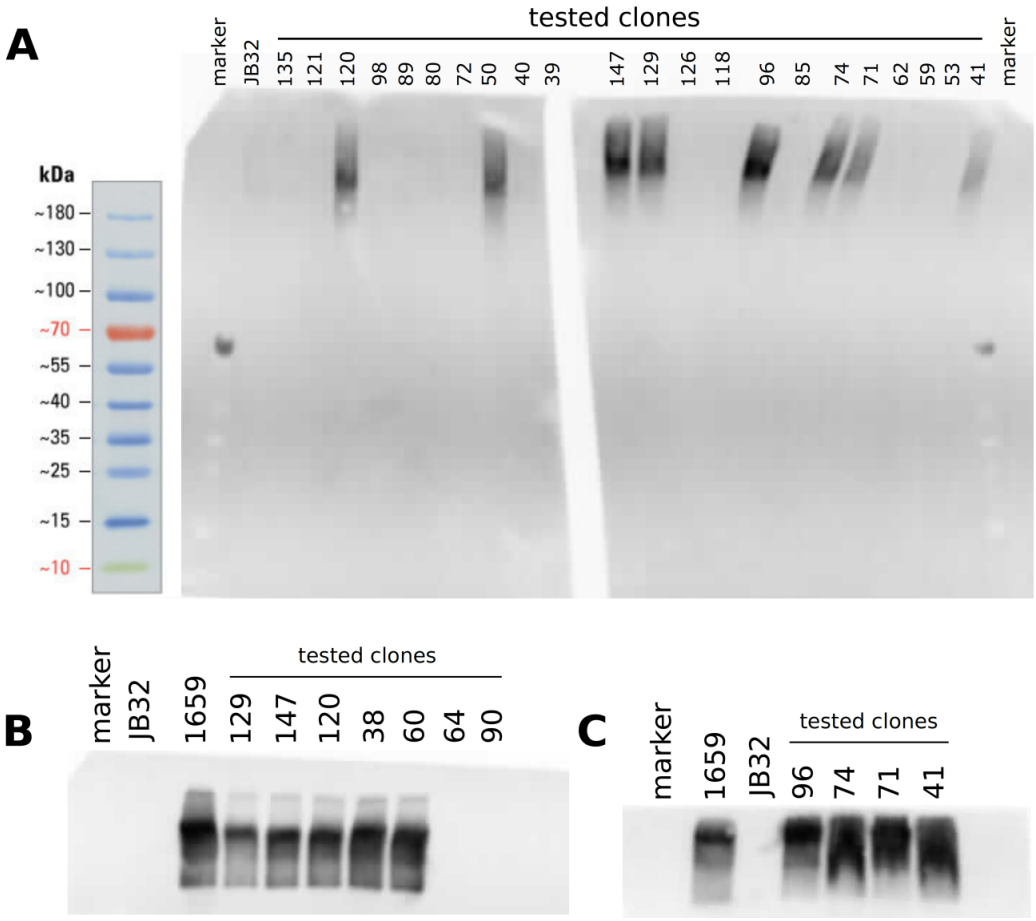

Fig. 28 – Genotyping of the *ade6+pADH15.skp1:AtTIR1:2NLS:9myc* construct. Proteins were isolated and separated by SDS-Page. Proteins were transferred to PVDF membrane using semi dry blotting technique. Membranes were blocked and probed with anti-myc primary and AP-linked secondary antibodies. Skp1-AtTIR1-2NLS-9myc was detected by treating the membrane with fluorescence AP substrate (ECF). JB32 – negative WT control. 1659 – positive Skp1-AtTIR1-2NLS-9myc carrying control. To check successful gel-membrane transfer, blots were stained with ponceau solution before probing. **[A]** Initial screen for clones positive for Skp1-AtTIR1-2NLS-9myc. **[B]** Re-verification of isolates: 120, 129, 147 and genotyping of clones: 38, 60, 64 and 90, which were not included in [A]. **[C]** Re-validation of clones: 41, 71, 74 and 96.

The rest of the clones (38, 41, 60, 71, 74 and 120) were subjected to re-validation for uracil auxotrophy, temperature-sensitivity and positivity for *cbf11:3HA:aid:kanR*. Cells were spotted and cultivated on 3 selection plates: YES [36°C], YES+G418 [25°C] and EMM [25°C]. The YES plate incubated at 25°C was used as a positive control of growth. Additionally to cultivation on YES+G418 plates, positivity/negativity for *cbf11:3HA:aid:kanR* was also determined by PCR using primers N1 and N2, which are situated 150 bp upstream and 78 bp downstream of the construct integration site (Fig. 29 A-B).

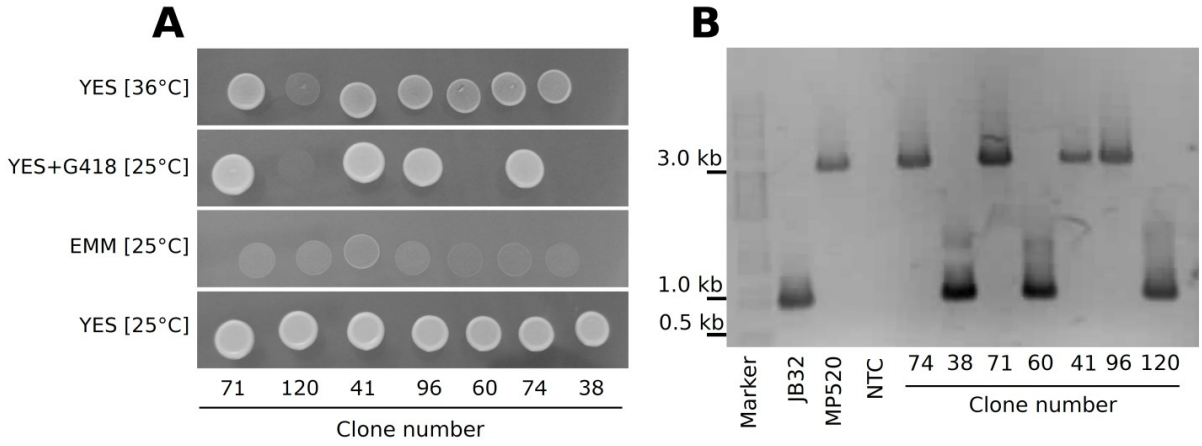

Fig. 29 – Re-genotyping of potentially valid clones. [A] Clones: 38, 41, 60, 71, 74 and 120 were grown to saturation and subsequently spotted on the 2x YES, YES+G418 and EMM plates. First YES plate was incubated at 36°C. The YES+G418 and EMM plates were incubated at 25°C. Second YES plate was incubated at 25°C and represented a positive control of growth. **[B]** Presence of *cbf11:3HA:aid:kanR* was checked by PCR using N1 & N2 primers (150 bp upstream and 78 bp downstream of the construct) and DNA isolated from the listed clones as a template. The expected size of the amplicon was 3098 bp. NTC – No Template Control, JB32 – *cbf11:3HA:aid:kanR* negative control, MP520 – *cbf11:3HA:aid:kanR* positive control.

Based on the growth and PCR results, clones of three genotypes were selected and stored as glycerol stocks: clone 38 [*h? ura4-D18 ade6+pADH15.skp1:AtTIR1:2NLS:9myc*], clone 120 [*h? ura4-D18 ade6+pADH15.skp1:AtTIR1:2NLS:9myc cdc10-M17*] and clones 41, 71, 74, 96 [*h? ura4-D18 ade6+pADH15.skp1:AtTIR1:2NLS:9myc cbf11-3HA-aid-kanR*]. Unfortunately, clone of genotype 4) was not selected and thus is not included in the list of new strains. Mating

types of all new strains were determined by crossing with h+ and h- strains. The final list of new strains is enlisted in Table 11.

Table 11 – List of new strains of genotypes 1-3)

MP534 (clone 38)	*h+ ura4-D18 ade6+pADH15.skp1:AtTIR1:2NLS:9myc*
MP535 (clone 120)	*h- ura4-D18 ade6+pADH15.skp1:AtTIR1:2NLS:9myc cdc10-M17*
MP536 (clone 41)	*h+ ura4-D18 ade6+pADH15.skp1:AtTIR1:2NLS:9myc cbf11-3HA-aid-kanR*
MP537 (clone 71)	*h+ ura4-D18 ade6+pADH15.skp1:AtTIR1:2NLS:9myc cbf11-3HA-aid-kanR*
MP538 (clone 74)	*h- ura4-D18 ade6+pADH15.skp1:AtTIR1:2NLS:9myc cbf11-3HA-aid-kanR*
MP539 (clone 96)	*h+ ura4-D18 ade6+pADH15.skp1:AtTIR1:2NLS:9myc cbf11-3HA-aid-kanR*

To check, that there are no mutations in the integrated *cbf11:3HA:aid* sequence, *cbf11:3HA:aid:kanR* locus was amplified by PCR with N1 & N2 primers and sequenced, using sequencing primer localizing 115 bp upstream of the construct. Sequenced strains included MP520, MP536, MP537 and MP538. Analysis of retrieved sequences did not reveal any mutations. Only regions with clearly distinguishable chromatogram peaks were considered, as visualized in Fig. 30. Since we used only one sequencing primer, we did not obtain the sequence of whole construct and the validity of aid sequence has remained unconfirmed (Fig. 30).

Fig. 30 – Cartoon illustration of sequencing coverage of *cbf11:3HA:aid* construct. The chromatograms of obtained sequences were analyzed by SnapGene software. Parts with clearly distinguishable peaks of fluorescence were aligned with construct sequence using Clustal Omega Multiple Sequence Alignment tool, EMBL-EBI [103]. Analyzed part did not contain any mutations. Cartoon is adapted from SnapGene exported graphics.

The last two steps in the genotyping process would be detection of Cbf11-3HA-aid protein and validation of auxin-inducible degradability. Unfortunately, so far we have not been able to detect the Cbf11-3HA-aid, using HA specific antibodies and thus this part of the project remains unfinished.

6 DISCUSSION

6.1 Combinatorial deregulation of *vht1* and *cut6* results in mitotic failure

In our study we show that Cbf11-defficient fission yeasts are slow growing and develop broad range of defects, including the special case of mitotic failure also known as cut phenotype. We determined that propensity to undergo catastrophic mitosis in *Δcbf11* cells is likely consequential to combinatorial downregulation of Cbf11-target lipid metabolism genes *cut6* and *vht1*, respectively encoding Ac-CoA carboxylase and biotin transporter. The actual link between Vht1 and Cut6 resides in the fact that biotin functions as a cofactor of carboxylation enzymes and therefore is necessary for Cut6-mediated catalysis. According to our model, *Δcbf11* cells are distinctive by fewer Cut6 molecules of which not all are biotinylated due to impaired biotin import. We hypothesize that such cellular configuration is characterized by partial impairment of Cut6 catalytic capacity and negative attenuation of fatty acid synthesis. Since adequate fatty acid synthesis is crucial for nuclear expansion and successful division in species employing closed mitosis (Reviewed in 3.2), *Δcbf11 S. pombe* cells are predisposed to mitotic failure. This theory is based on experiments employing Cbf11 non-responsive *cut6* promoter mutant (*Pcut6MUT*) and *Δvht1* strains. This might represent a problem, as the expression of *vht1* is entirely abolished in null-mutant but only attenuated in *Δcbf11* cells. Consequently, modelling of *Δcbf11* system based on usage of *Δvht1* mutant is only approximate and could theoretically lead to false positive findings. We also observed that the occurrence of cut phenotype in *Δcbf11 Δvht1 Pcut6MUT* triple mutant is significantly higher compared to *Δvht1 Pcut6MUT* double mutant, implying the existence of Cbf11-related cut factor(s) other than *cut6* and *vht1*. Another finding worth consideration is the evidence that biotin unavailability does not negatively affect mitosis in WT cells, as fission yeasts ceased proliferation and entered G_0 in response to biotin starvation without developing any apparent mitotic defects. This might be contradictory to our hypothesis, however, complete biotin withdrawal represents an extreme condition and it is questionable, whether the same result would be obtained if cells were cultured in the medium containing severely limiting but non-zero biotin concentration. Postulated model of Cbf11 function in lipid metabolism

and mitosis is illustrated in Fig. 31.

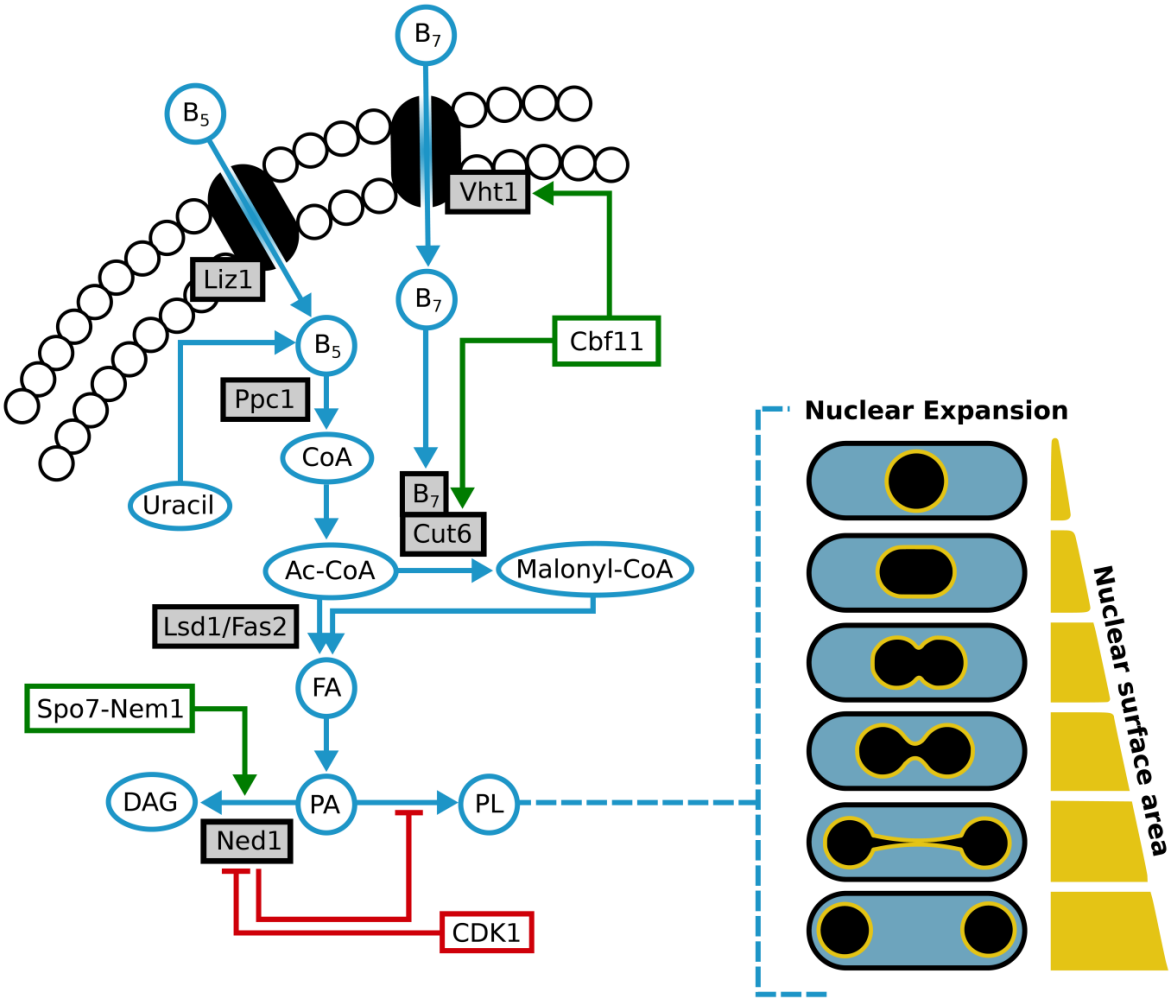

Fig. 31 – allocation of Cbf11 transcription factor in the circuits governing lipid metabolism and nuclear expansion. A scheme analogous to that presented in the introduction section, showing the role of Cbf11 in lipid metabolism in the context of nuclear expansion. Abbreviations: B_5 – vitamin B_5 (Pantothenate), B_7 – biotin, CoA – Coenzyme A, Ac-CoA – Acetyl Coenzyme A, FA – Fatty Acid, PA – Phosphatidic Acid, PL – Phospholipid, DAG – Diacylglycerol, Liz1 – Pantothenate transporter, Vht1 – biotin transporter, Ppc1 – Phosphopantothenoylcysteine synthetase, Lsd1 – Fatty acid synthase alpha subunit, Cut6 – Ac-CoA carboxylase, Ned1 – Phosphatidic acid phosphatase, Spo7-Nem1 – Ned1 phosphatase, CDK1 – cyclin dependent kinase 1.

6.2 Periodic expression of *cut6*, *vht1* and *bio2*

Since factors involved in management of cell cycle progression are often periodically expressed [104], M. Oravcova tested whether *cut6*, *vht1* and *bio2* show Cbf11-dependent cell cycle phase oscillatory pattern of transcription. Using commonly employed Cdc25-22 block/release synchronization protocol, M. Oravcova showed that *cut6*, *vht1* and *bio2* display Cbf11-dependent oscillatory expression, peaking at the point of S-phase. To validate the relevancy of observed fluctuations in transcription, we performed analogous experiments using only WT cells and three other methods of synchronization, including Cdc10-M17 block/release, HU block/release and lactose gradient centrifugation. To our surprise, we discovered high variability in expression profiles among different synchronization approaches. The only results comparable with data of M. Oravcova emerged from the experiments employing Cdc10-M17 block/release procedure, displaying apparent upregulation of *cut6* and *vht1* transcription ≈ 90 min after release from thermal block. Considering strikingly different mRNA profiles of Cbf11 targets obtained from synchronizations by HU block/release and lactose gradient centrifugation, we hypothesize that transcriptional oscillations observed in *cdc10-M17* and *cdc25-22* synchronous cultures are unrelated to cell cycle progression and represent a response to yet undetermined stimuli accompanying Cdc25-22 and Cdc10-M17 block/release synchronization procedures. Since protocols, Cdc25-22 block/release and Cdc10-M17 block/release, employ incubation at elevated temperature (36°C), we speculate that pronounced upregulation of *cut6* and *vht1* represents a part of cellular response to heat shock, possibly triggered in the Cbf11-dependent manner. Another fact worth considering is that G_2-blocked *cdc25-22* cells are characterized by considerably larger nuclei [63]. It is possible, that maintenance of nuclear envelopes of such nuclei is more demanding for supply of structural phospholipids, to which cells respond by upregulating certain lipid metabolism factors, again, possibly dependently on Cbf11 activity. Even though we likely ruled out the cell cycle periodic character of *cut6*, *vht1* and *bio2* transcription, it is still possible that the expression oscillates at the level of translation. Indeed, recent study based on *S. cerevisiae* shows that fatty acid anabolism enzymes *ACC1* (acetyl coenzyme A carboxylase, *cut6* homolog), *FAS1* (fatty acid synthase β-subunit) and *FAS2* (fatty acid synthase α-subunit) are periodically expressed, being most

efficiently translated at the G_2/M boundary [105]. Authors of this work show that periodic translation of ACC1 is dependent on short upstream ORF (uORF). Such a uORF is not present in either of *cut6*, *vht1* and *bio2*, however, experiments regarding periodic translation of lipid metabolism factors in *S. pombe* have not yet been carried out, leaving hypothetical question of analogously acting regulation in fission yeast unanswered.

6.3 Conditionality of *Δcbf11* mutant

The aberrant characteristics of *Δcbf11* mutant, including storage lipid diminishment, growth retardation and frequent occurrence of cut phenotype, are much more pronounced when grown in the complex YES medium compared to synthetic EMM. Curiously, similar observation regarding mitotic failure has been made for temperature sensitive mutant of Cbf11-target gene, *cut6*, the impairment of which is suspected to be responsible for mitotic defects in *Δcbf11* mutant [20]. It would be convenient to hypothesize that phenotypic rescue observed in EMM-grown *Δcbf11* cells is consequential to environmental supplementation for impaired lipid metabolism, however, we do not have any data explicitly linking the increase in amount of storage lipids and decreased propensity for catastrophic mitosis. Moreover, similarly to the cells deficient of Cbf11 and Cut6, two temperature-sensitive mutants defective in the cyclosome/APC complex subunits, *cut4-533* and *cut20-100*, are unviable when cultured at non-permissive 36°C in the YPD (Yeast Extract Peptone Dextrose) medium, but not in EMM [31,106], indicating that positive effect of EMM is not exclusive for lipid metabolism mutants, but applies for cut mutants as well. We determined that ammonium chloride, which functions as the only nitrogen source in EMM, represents the sole factor responsible for observed suppression of cut phenotype in *Δcbf11* mutant. It would be tempting to discuss that the exposure to high doses of NH_4Cl suppresses the cut phenotype in general, but we have not tested any cut mutants other than *Δcbf11* and thus we cannot rule out that this phenomenon is specific for *Δcbf11* mutant. We showed that exponentially growing Cbf11-defficient cells accumulate mitotic defects immediately after transfer from EMM to YES, indicating that propensity to undergo unsuccessful mitosis is set up at the immediate point of medium transfer and influences the outcome of very first nuclear division. This observation suggests the existence of a Cbf11-linked regulatory mechanism,

which rapidly responds to alterations in nitrogen supply and ensures successful mitotic progression in a yet unknown manner and context. The most promising candidate to look at is TOR signalling, which governs cellular response to the actual nitrogen availability [107–110].

6.4 TOR signalling as a hypothetical platform influencing susceptibility to catastrophic mitosis

While mammals signal through a single TOR-kinase (mTOR), *S. pombe* encodes two TOR-kinase family members, designated as Tor1 and Tor2, of which only Tor2 is essential for viability [108]. TOR-kinases do not function as solo signalling elements, but form multi-protein complexes. Irrespectively of the number of expressed TOR-kinases, two canonical TOR complexes, TORC1 and TORC2, have been characterized across eukaryotic species. Canonical TOR complexes are defined by unique composition. While *S. pombe* TORC1 contains Mip1 (Raptor), Wat1 (Lst8) and Tor2, TORC2 is formed by Ste20 (Rictor), Sin1 (Avo1), Wat1 (Lst8) and Tor1 [111,112]. Interestingly, TORC1 has been shown to be associated with Tor1 in *S. pombe* cells grown in the minimal EMM medium, but not in YES [113], implying differential modes of signalling at different environmental conditions. Though, it must be noted that this result is somewhat controversial, as it has not been reproduced in other studies and the work by N. Ikai et al. states the exact opposite [114]. In general, cells encounter two kinds of nitrogen supply insufficiencies, to which they must respond: nitrogen stress and nitrogen starvation. While nitrogen stress is triggered, when the only available nitrogen source is so called ‘poor’, nitrogen starvation is induced by complete nitrogen source withdrawal. In *S. pombe*, the good nitrogen sources are those, which can be easily turned into ammonium, e.g. glutamate or ammonium itself [115]. The poor nitrogen sources are represented by chemical substances, which can be converted to ammonium, but the biochemical conversion takes multiple steps and is energetically demanding. Such nitrogen sources are proline and uracil [115]. Nitrogen-starved cells ultimately cease proliferation, arrest cell cycle progression and enter sexual cycle or G_0 [107,108]. Quite differently, nitrogen stress is not accompanied by cell cycle block. Nitrogen-stressed cells accelerate mitotic commitment and continue to grow at smaller sizes [116]. It has been shown, that

nitrogen stress results in the initial inhibition of Tor1 and subsequent cascade of signalling events ultimately resulting in activation of polo kinase (Plk1), which accelerates G_2/M transition [113]. Interestingly, activation of Plk1 is dependent on modest activation of Sty1 MAPK [113], the function of which has been linked to mitotic failure in *Δcbf11* mutant [19]. In our previous study, we show that deletion of Sty1 remarkably rescues defective phenotypes observed in *Δcbf11* cells [19]. In his master thesis, P. Danek showed that, when compared with WT, YES-grown *Δcbf11* cells display higher level of Sty1 activity, even if not exposed to any apparent Sty1 activating stress [22], implying possibility of YES-induced Sty1 activation in Cbf11-defficient fission yeasts. It has been published, that artificially induced acceleration of G_2/M transition by inactivation of mitotic entry negative regulator, Wee1, negatively influences the severity of cut phenotype occurrence in cells treated with lipid metabolism impairing drug, Cutin-1 [63]. Therefore, we hypothesize that *Δcbf11* cells are hyper-sensitive to the character of nitrogen supply and the YES medium is to certain degree nitrogen poor. Thus, Cbf11-defficient, but not WT, cells cultured in the YES medium experience a certain type of nitrogen stress, possibly activating Sty1 and Plk1 kinases (due to inhibition of Tor1 kinase), which accelerate mitotic commitment and promote nuclear division failure in *Δcbf11* cells predisposed to defective mitosis due to downregulation of lipid metabolism.

6.5 Construction of inducible Cbf11 degradation system

In this study, we constructed conditional *cbf11* mutant expressing Cbf11-3HA-aid protein variant, degradation of which can be theoretically stimulated by addition of plant hormone, auxin. The *cbf11* degron strain has been validated by cultivation at selective conditions, targeted PCR and sequencing, however, detection of Cbf11-3HA-aid construct at the protein level has not been successfully conducted. For protein detection we employed standard SDS-Page followed by western blotting procedure using several HA-targeting antibodies (Chapter 4.5.2). Unfortunately, the usage of none of them provided clear band representing Cbf11:3HA:aid construct. Since population average of number of Cbf11 protein molecules per cell is relatively low, equalling 1053 in EMM [117], it is possible that our protein samples were simply not concentrated enough. To address this, Cbf11-3HA-aid detection should be carried out in concentrated or HA-immunoprecipitated protein samples. As another

alternative, we acquired the aid domain specific antibody, however, it has not yet been tested. Regarding responsiveness to auxin treatment, our pilot data indicate that cellular physiology is not altered in *cbf11* degron cells exposed to auxin (1-Napthalenacetic acid). It is though unclear, whether this observation results from malfunction of the inducible system or only partial degradation of Cbf11-3HA-aid, which is insufficient to induce development of defects characteristic for *Δcbf11* mutant.

7 CONCLUSIONS

- To a certain degree, mitotic defects characteristic for Cbf11-defficient *S. pombe* cells are likely attributed to downregulation of fatty acid synthesis due to partial impairment of Cbf11-regulated factors: biotin-dependent Ac-CoA carboxylase (Cut6) and biotin transporter (Vht1). Impairment of biotin synthase (Bio2), another Cbf11-target gene and an enzyme synthesizing biotin from its precursor dethiobiotin, does not seem to be influential for mitotic progression.

- Complete biotin withdrawal does not result in mitotic failure, but induces inhibition of proliferation.

- Studied lipid metabolism genes (*cut6*, *vht1*, *bio2*) do not display cell cycle contextual periodic transcription, but are likely responsive to the exogenous or endogenous stimuli accompanying synchronization procedures employing *cdc25-22* and *cdc10-M17* temperature-sensitive alleles.

- Conditional character of cut phenotype in Cbf11-defficient cells is likely attributed to nitrogen availability. This observation suggests a new line of investigation, emphasizing TOR signalling and regulation of mitotic commitment in the context of nitrogen stress

- According to performed genotyping, we managed to construct the auxin-inducible Cbf11 degron mutant, however, detection of Cbf11-3HA-aid fusion has not yet been successfully performed, leaving functionality of the system unanswered.

8 REFERENCES

1. Fortini ME, Artavanis-Tsakonas S. The suppressor of hairless protein participates in notch receptor signaling. Cell. 1994;79: 273–82. doi:10.1016/0092-8674(94)90196-1

2. Bailey AM, Posakony JW. Suppressor of hairless directly activates transcription of enhancer of split complex genes in response to Notch receptor activity. Genes Dev. 1995;9: 2609–22. Available: http://www.ncbi.nlm.nih.gov/pubmed/7590239

3. Kovall R a, Hendrickson W a. Crystal structure of the nuclear effector of Notch signaling, CSL, bound to DNA. EMBO J. 2004;23: 3441–51. doi:10.1038/sj.emboj.7600349

4. Louvi A, Artavanis-Tsakonas S. Notch signalling in vertebrate neural development. Nat Rev Neurosci. 2006;7: 93–102. doi:10.1038/nrn1847

5. Kwon O-J, Valdez JM, Zhang L, Zhang B, Wei X, Su Q, et al. Increased Notch signalling inhibits anoikis and stimulates proliferation of prostate luminal epithelial cells. Nat Commun. Nature Publishing Group; 2014;5: 4416. doi:10.1038/ncomms5416

6. Yu B, Song B. Notch 1 signalling inhibits cardiomyocyte apoptosis in ischaemic postconditioning. Heart Lung Circ. Australian and New Zealand Society of Cardiac and Thoracic Surgeons (ANZSCTS) and the Cardiac Society of Australia and New Zealand (CSANZ); 2014;23: 152–8. doi:10.1016/j.hlc.2013.07.004

7. Ogaki S, Shiraki N, Kume K, Kume S. Wnt and Notch signals guide embryonic stem cell differentiation into the intestinal lineages. Stem Cells. 2013;31: 1086–96. doi:10.1002/stem.1344

8. Backer RA, Helbig C, Gentek R, Kent A, Laidlaw BJ, Dominguez CX, et al. A central role for Notch in effector CD8(+) T cell differentiation. Nat Immunol. 2014;15: 1143–51. doi:10.1038/ni.3027

9. Kopan R, Ilagan MXG. The canonical Notch signaling pathway: unfolding the activation mechanism. Cell. 2009;137: 216–33. doi:10.1016/j.cell.2009.03.045

10. Schroeter EH, Kisslinger JA, Kopan R. Notch-1 signalling requires ligand-induced proteolytic release of intracellular domain. Nature. 1998;393: 382–6. doi:10.1038/30756

11. Tun T, Hamaguchi Y, Matsunami N, Furukawa T, Honjo T, Kawaichi M. Recognition sequence of a highly conserved DNA binding protein RBP-J kappa. Nucleic Acids Res. 1994;22: 965–71. Available: http://www.ncbi.nlm.nih.gov/pubmed/8152928

12. Barolo S, Walker RG, Polyanovsky a D, Freschi G, Keil T, Posakony JW. A notch-independent activity of suppressor of hairless is required for normal mechanoreceptor

physiology. Cell. 2000;103: 957–69. doi:10.1016/S0092-8674(00)00198-7

13. Koelzer S, Klein T. A Notch-independent function of Suppressor of Hairless during the development of the bristle sensory organ precursor cell of Drosophila. Development. 2003;130: 1973–88. doi:10.1242/dev.00426

14. Kaspar M, Klein T. Functional analysis of murine CBF1 during Drosophila development. Dev Dyn. 2006;235: 918–27. doi:10.1002/dvdy.20667

15. Braune E-B, Tsoi YL, Phoon YP, Landor S, Silva Cascales H, Ramsköld D, et al. Loss of CSL Unlocks a Hypoxic Response and Enhanced Tumor Growth Potential in Breast Cancer Cells. Stem cell reports. 2016;6: 643–51. doi:10.1016/j.stemcr.2016.03.004

16. Prevorovský M, Půta F, Folk P. Fungal CSL transcription factors. BMC Genomics. 2007;8: 233. doi:10.1186/1471-2164-8-233

17. Prevorovský M, Grousl T, Stanurová J, Rynes J, Nellen W, Půta F, et al. Cbf11 and Cbf12, the fission yeast CSL proteins, play opposing roles in cell adhesion and coordination of cell and nuclear division. Exp Cell Res. 2009;315: 1533–47. doi:10.1016/j.yexcr.2008.12.001

18. Oravcová M, Teska M, Půta F, Folk P, Převorovský M. Fission yeast CSL proteins function as transcription factors. PLoS One. 2013;8: e59435. doi:10.1371/journal.pone.0059435

19. Převorovský M, Oravcová M, Tvarůžková J, Zach R, Folk P, Půta F, et al. Fission Yeast CSL Transcription Factors: Mapping Their Target Genes and Biological Roles. Whitehall S, editor. PLoS One. 2015;10: e0137820. doi:10.1371/journal.pone.0137820

20. Převorovský M, Oravcová M, Zach R, Jordáková A, Bähler J, Půta F, et al. CSL protein regulates transcription of genes required to prevent catastrophic mitosis in fission yeast. Cell Cycle. 2016;15: 3082–3093. doi:10.1080/15384101.2016.1235100

21. Tvarůžková J. The role of CSL proteins in oxidative stress response of Schizosaccharomyces pombe. 2015.

22. Daněk P. Molekulární mechanismus účasti proteinů rodiny CSL v odpovědi na oxidativní stress u Schizosaccharomyces pombe. 2015.

23. Bahn Y-S, Xue C, Idnurm A, Rutherford JC, Heitman J, Cardenas ME. Sensing the environment: lessons from fungi. Nat Rev Microbiol. 2007;5: 57–69. doi:10.1038/nrmicro1578

24. Hoffman CS, Wood V, Fantes PA. An ancient yeast for young geneticists: A primer on the Schizosaccharomyces pombe model system. Genetics. 2015;201: 403–423. doi:10.1534/genetics.115.181503

25. Nurse P, Thuriaux P, Nasmyth K. Genetic control of the cell division cycle in the fission

yeast Schizosaccharomyces pombe. MGG Mol Gen Genet. 1976;146: 167–178. doi:10.1007/BF00268085

26. Hirano T, Funahashi S, Uemura T, Yanagida M. Isolation and characterization of Schizosaccharomyces pombe cutmutants that block nuclear division but not cytokinesis. EMBO J. 1986;5: 2973–9. Available: http://www.ncbi.nlm.nih.gov/pubmed/16453724

27. Samejima I, Matsumoto T, Nakaseko Y, Beach D, Yanagida M. Identification of seven new cut genes involved in Schizosaccharomyces pombe mitosis. J Cell Sci. 1993;105 (Pt 1: 135–43. Available: http://www.ncbi.nlm.nih.gov/pubmed/8395535

28. Syrovatkina V, Tran PT. Loss of kinesin-14 results in aneuploidy via kinesin-5-dependent microtubule protrusions leading to chromosome cut. Nat Commun. Nature Publishing Group; 2015;6: 7322. doi:10.1038/ncomms8322

29. Uemura T, Tanagida M. Mitotic spindle pulls but fails to separate chromosomes in type II DNA topoisomerase mutants: uncoordinated mitosis. EMBO J. 1986;5: 1003–10. Available: http://www.ncbi.nlm.nih.gov/pubmed/15957215

30. Uemura T, Ohkura H, Adachi Y, Morino K, Shiozaki K, Yanagida M. DNA topoisomerase II is required for condensation and separation of mitotic chromosomes in S. pombe. Cell. 1987;50: 917–25. doi:10.1016/0092-8674(87)90518-6

31. Yamashita YM, Nakaseko Y, Kumada K, Nakagawa T, Yanagida M. Fission yeast APC/cyclosome subunits, Cut20/Apc4 and Cut23/Apc8, in regulating metaphase-anaphase progression and cellular stress responses. Genes Cells. 1999;4: 445–63. doi:10.1046/j.1365-2443.1999.00274.x

32. Berry LD, Feoktistova A, Wright MD, Gould KL. The schizosaccharomyces pombe dim1(+) gene interacts with the anaphase-promoting complex or cyclosome (APC/C) component lid1(+) and is required for APC/C function. Mol Cell Biol. 1999;19: 2535–46. Available: http://www.pubmedcentral.nih.gov/articlerender.fcgi?artid=84046&tool=pmcentrez&rendertype=abstract

33. Gordon C, McGurk G, Dillon P, Rosen C, Hastie ND. Defective mitosis due to a mutation in the gene for a fission yeast 26S protease subunit. Nature. 1993;366: 355–7. doi:10.1038/366355a0

34. Tatebe H, Yanagida M. Cut8, essential for anaphase, controls localization of 26S proteasome, facilitating destruction of cyclin and Cut2. Curr Biol. 2000;10: 1329–38. doi:10.1016/S0960-9822(00)00773-9

35. Funabiki H, Kumada K, Yanagida M. Fission yeast Cut1 and Cut2 are essential for sister chromatid separation, concentrate along the metaphase spindle and form large complexes. EMBO J. 1996;15: 6617–28. Available:

http://www.ncbi.nlm.nih.gov/pubmed/8978688

36. Yuasa T, Hayashi T, Ikai N, Katayama T, Aoki K, Obara T, et al. An interactive gene network for securin-separase, condensin, cohesin, Dis1/Mtc1 and histones constructed by mass transformation. Genes Cells. 2004;9: 1069–82. doi:10.1111/j.1365-2443.2004.00790.x

37. Nagao K, Yanagida M. Securin can have a separase cleavage site by substitution mutations in the domain required for stabilization and inhibition of separase. Genes Cells. 2006;11: 247–60. doi:10.1111/j.1365-2443.2006.00941.x

38. Saka Y, Sutani T, Yamashita Y, Saitoh S, Takeuchi M, Nakaseko Y, et al. Fission yeast cut3 and cut14, members of a ubiquitous protein family, are required for chromosome condensation and segregation in mitosis. EMBO J. 1994;13: 4938–52. Available: http://www.ncbi.nlm.nih.gov/pubmed/7957061%5Cnhttp://www.pubmedcentral.nih.gov/articlerender.fcgi?artid=PMC395434

39. Chen S, Blank JL, Peters T, Liu XJ, Rappoli DM, Pickard MD, et al. Genome-wide siRNA screen for modulators of cell death induced by proteasome inhibitor bortezomib. Cancer Res. 2010;70: 4318–26. doi:10.1158/0008-5472.CAN-09-4428

40. Bose P, Batalo MS, Holkova B, Grant S. Bortezomib for the treatment of non-Hodgkin's lymphoma. Expert Opin Pharmacother. 2014;15: 2443–59. doi:10.1517/14656566.2014.965142

41. Takeda K, Mori A, Yanagida M. Identification of genes affecting the toxicity of anti-cancer drug bortezomib by genome-wide screening in S. pombe. PLoS One. 2011;6: e22021. doi:10.1371/journal.pone.0022021

42. Waite M, Wakil SJ. Studies on the mechanism of fatty acid synthesis. XII. Acetyl coenzyme A carboxylase. J Biol Chem. 1962;237: 2750–2757.

43. Chirala SS, Wakil SJ. Structure and function of animal fatty acid synthase. Lipids. 2004;39: 1045–53. doi:10.1007/s11745-004-1329-9

44. Saitoh S, Takahashi K, Nabeshima K, Yamashita Y, Nakaseko Y, Hirata a, et al. Aberrant mitosis in fission yeast mutants defective in fatty acid synthetase and acetyl CoA carboxylase. J Cell Biol. 1996;134: 949–61. Available: http://www.pubmedcentral.nih.gov/articlerender.fcgi?artid=2120970&tool=pmcentrez&rendertype=abstract

45. Moynihan EB, Enoch T. Liz1p, a novel fission yeast membrane protein, is required for normal cell division when ribonucleotide reductase is inhibited. Mol Biol Cell. 1999;10: 245–57. Available: http://www.ncbi.nlm.nih.gov/pubmed/9950674

46. Stolz J, Caspari T, Carr AM, Sauer N. Cell division defects of Schizosaccharomyces pombe liz1- mutants are caused by defects in pantothenate uptake. Eukaryot Cell.

2004;3: 406–12. doi:10.1128/EC.3.2.406-412.2004

47. Nakamura T, Pluskal T, Nakaseko Y, Yanagida M. Impaired coenzyme A synthesis in fission yeast causes defective mitosis, quiescence-exit failure, histone hypoacetylation and fragile DNA. Open Biol. 2012;2: 120117. doi:10.1098/rsob.120117

48. Malecki M, Bitton DA, Rodríguez-López M, Rallis C, Calavia NG, Smith GC, et al. Functional and regulatory profiling of energy metabolism in fission yeast. Genome Biol. Genome Biology; 2016;17: 240. doi:10.1186/s13059-016-1101-2

49. Strijbis K, Distel B. Intracellular acetyl unit transport in fungal carbon metabolism. Eukaryot Cell. 2010;9: 1809–15. doi:10.1128/EC.00172-10

50. Van den Berg M a, Steensma HY. ACS2, a *Saccharomyces cerevisiae* gene encoding acetyl-coenzyme A synthetase, essential for growth on glucose. Eur J Biochem. 1995;231: 704–13. Available: http://www.ncbi.nlm.nih.gov/pubmed/7649171

51. Martinez DL, Tsuchiya Y, Gout I. Coenzyme A biosynthetic machinery in mammalian cells. Biochem Soc Trans. 2014;42: 1112–7. doi:10.1042/BST20140124

52. Vesela E, Chroma K, Turi Z, Mistrik M. Common Chemical Inductors of Replication Stress: Focus on Cell-Based Studies. Biomolecules. 2017;7: 19. doi:10.3390/biom7010019

53. Francesconi S, Grenon M, Bouvier D, Baldacci G. p56(chk1) protein kinase is required for the DNA replication checkpoint at 37 degrees C in fission yeast. EMBO J. 1997;16: 1332–41. doi:10.1093/emboj/16.6.1332

54. Shikata M, Ishikawa F, Kanoh J. Tel2 is required for activation of the Mrc1-mediated replication checkpoint. J Biol Chem. 2007;282: 5346–55. doi:10.1074/jbc.M607432200

55. Hayles J, Wood V, Jeffery L, Hoe K-L, Kim D-U, Park H-O, et al. A genome-wide resource of cell cycle and cell shape genes of fission yeast. Open Biol. 2013;3: 130053. doi:10.1098/rsob.130053

56. Güttinger S, Laurell E, Kutay U. Orchestrating nuclear envelope disassembly and reassembly during mitosis. Nat Rev Mol Cell Biol. 2009;10: 178–91. doi:10.1038/nrm2641

57. Arnone JT, Walters AD, Cohen-Fix O. The dynamic nature of the nuclear envelope: lessons from closed mitosis. Nucleus. 2013;4: 261–6. doi:10.4161/nucl.25341

58. Yam C, He Y, Zhang D, Chiam K-H, Oliferenko S. Divergent strategies for controlling the nuclear membrane satisfy geometric constraints during nuclear division. Curr Biol. Elsevier Ltd; 2011;21: 1314–9. doi:10.1016/j.cub.2011.06.052

59. Castagnetti S, Božič B, Svetina S. Mechanical and molecular basis for the symmetrical division of the fission yeast nuclear envelope. Phys Chem Chem Phys. Royal Society of

Chemistry; 2015;17: 15629–36. doi:10.1039/c5cp01243k

60. Zhu Q, Zheng F, Liu AP, Qian J, Fu C, Lin Y. Shape Transformation of the Nuclear Envelope during Closed Mitosis. Biophys J. Biophysical Society; 2016;111: 2309–2316. doi:10.1016/j.bpj.2016.10.004

61. Lim H W G, Huber G, Torii Y, Hirata A, Miller J, Sazer S. Vesicle-like biomechanics governs important aspects of nuclear geometry in fission yeast. PLoS One. 2007;2: e948. doi:10.1371/journal.pone.0000948

62. Makarova M, Gu Y, Chen J-S, Beckley JR, Gould KL, Oliferenko S. Temporal Regulation of Lipin Activity Diverged to Account for Differences in Mitotic Programs. Curr Biol. 2016;26: 237–43. doi:10.1016/j.cub.2015.11.061

63. Takemoto A, Kawashima SA, Li J-J, Jeffery L, Yamatsugu K, Elemento O, et al. Nuclear envelope expansion is crucial for proper chromosomal segregation during a closed mitosis. J Cell Sci. 2016;129: 1250–9. doi:10.1242/jcs.181560

64. Rawicz W, Olbrich KC, McIntosh T, Needham D, Evans E. Effect of chain length and unsaturation on elasticity of lipid bilayers. Biophys J. Elsevier; 2000;79: 328–39. doi:10.1016/S0006-3495(00)76295-3

65. Jorgensen P, Edgington NP, Schneider BL, Rupes I, Tyers M, Futcher B. The size of the nucleus increases as yeast cells grow. Mol Biol Cell. 2007;18: 3523–32. doi:10.1091/mbc.E06-10-0973

66. Witkin KL, Chong Y, Shao S, Webster MT, Lahiri S, Walters AD, et al. The budding yeast nuclear envelope adjacent to the nucleolus serves as a membrane sink during mitotic delay. Curr Biol. Elsevier Ltd; 2012;22: 1128–1133. doi:10.1016/j.cub.2012.04.022

67. Stone EM, Heun P, Laroche T, Pillus L, Gasser SM. MAP kinase signaling induces nuclear reorganization in budding yeast. Curr Biol. 2000;10: 373–82. doi:10.1016/S0960-9822(00)00413-9

68. Raben DM, Barber CN. Phosphatidic acid and neurotransmission. Adv Biol Regul. Elsevier Ltd; 2016; 1–7. doi:10.1016/j.jbior.2016.09.004

69. Han G-S, Wu W-I, Carman GM. The Saccharomyces cerevisiae Lipin homolog is a Mg2+-dependent phosphatidate phosphatase enzyme. J Biol Chem. 2006;281: 9210–8. doi:10.1074/jbc.M600425200

70. Siniossoglou S, Santos-Rosa H, Rappsilber J, Mann M, Hurt E. A novel complex of membrane proteins required for formation of a spherical nucleus. EMBO J. 1998;17: 6449–64. doi:10.1093/emboj/17.22.6449

71. Santos-Rosa H, Leung J, Grimsey N, Peak-Chew S, Siniossoglou S. The yeast lipin Smp2 couples phospholipid biosynthesis to nuclear membrane growth. EMBO J. 2005;24: 1931–41. doi:10.1038/sj.emboj.7600672

72. O'Hara L, Han G-S, Peak-Chew S, Grimsey N, Carman GM, Siniossoglou S. Control of phospholipid synthesis by phosphorylation of the yeast lipin Pah1p/Smp2p Mg2+-dependent phosphatidate phosphatase. J Biol Chem. 2006;281: 34537–48. doi:10.1074/jbc.M606654200

73. Choi H-S, Su W-M, Morgan JM, Han G-S, Xu Z, Karanasios E, et al. Phosphorylation of phosphatidate phosphatase regulates its membrane association and physiological functions in Saccharomyces cerevisiae: identification of SER(602), THR(723), AND SER(744) as the sites phosphorylated by CDC28 (CDK1)-encoded cyclin-dependen. J Biol Chem. 2011;286: 1486–98. doi:10.1074/jbc.M110.155598

74. Choi H-S, Su W-M, Han G-S, Plote D, Xu Z, Carman GM. Pho85p-Pho80p phosphorylation of yeast Pah1p phosphatidate phosphatase regulates its activity, location, abundance, and function in lipid metabolism. J Biol Chem. 2012;287: 11290–301. doi:10.1074/jbc.M112.346023

75. Su W-M, Han G-S, Casciano J, Carman GM. Protein kinase A-mediated phosphorylation of Pah1p phosphatidate phosphatase functions in conjunction with the Pho85p-Pho80p and Cdc28p-cyclin B kinases to regulate lipid synthesis in yeast. J Biol Chem. 2012;287: 33364–76. doi:10.1074/jbc.M112.402339

76. Dubots E, Cottier S, Péli-Gulli M-P, Jaquenoud M, Bontron S, Schneiter R, et al. TORC1 regulates Pah1 phosphatidate phosphatase activity via the Nem1/Spo7 protein phosphatase complex. Arkowitz RA, editor. PLoS One. 2014;9: e104194. doi:10.1371/journal.pone.0104194

77. Hsieh L-S, Su W-M, Han G-S, Carman GM. Phosphorylation of Yeast Pah1 Phosphatidate Phosphatase by Casein Kinase II Regulates Its Function in Lipid Metabolism. J Biol Chem. 2016;291: 9974–90. doi:10.1074/jbc.M116.726588

78. Han G-S, O'Hara L, Carman GM, Siniossoglou S. An unconventional diacylglycerol kinase that regulates phospholipid synthesis and nuclear membrane growth. J Biol Chem. 2008;283: 20433–42. doi:10.1074/jbc.M802903200

79. Tange Y, Hirata A, Niwa O. An evolutionarily conserved fission yeast protein, Ned1, implicated in normal nuclear morphology and chromosome stability, interacts with Dis3, Pim1/RCC1 and an essential nucleoporin. J Cell Sci. 2002;115: 4375–85. doi:10.1242/jcs.00135

80. Aoki K, Hayashi H, Furuya K, Sato M, Takagi T, Osumi M, et al. Breakage of the nuclear envelope by an extending mitotic nucleus occurs during anaphase in Schizosaccharomyces japonicus. Genes Cells. 2011;16: 911–26. doi:10.1111/j.1365-2443.2011.01540.x

81. Sabatinos SA, Forsburg SL. Molecular genetics of Schizosaccharomyces pombe. Methods Enzymol. 2nd ed. Elsevier Inc; 2010;470: 759–95. doi:10.1016/S0076-6879(10)70032-X

82. Schneider C a, Rasband WS, Eliceiri KW. NIH Image to ImageJ: 25 years of image analysis. Nat Methods. Nature Publishing Group; 2012;9: 671–5. doi:10.1038/nmeth.2089

83. Kippert F, Lloyd D. The aniline blue fluorochrome specifically stains the septum of both live and fixed Schizosaccharomyces pombe cells. FEMS Microbiol Lett. 1995;132: 215–9. doi:0378-1097(95)00313-T [pii]

84. Rostron KA, Rolph CE, Lawrence CL. Nile red fluorescence screening facilitating neutral lipid phenotype determination in budding yeast, Saccharomyces cerevisiae, and the fission yeast Schizosaccharomyces pombe. Antonie Van Leeuwenhoek. Springer International Publishing; 2015;108: 97–106. doi:10.1007/s10482-015-0467-6

85. Sabatinos SA, Forsburg SL. Measuring DNA content by flow cytometry in fission yeast. Methods Mol Biol. 2009;521: 449–61. doi:10.1007/978-1-60327-815-7_25

86. Whitehall S, Stacey P, Dawson K, Jones N. Cell cycle-regulated transcription in fission yeast: Cdc10-Res protein interactions during the cell cycle and domains required for regulated transcription. Mol Biol Cell. 1999;10: 3705–15. Available: http://www.ncbi.nlm.nih.gov/pubmed/10564266

87. Woolcock KJ, Gaidatzis D, Punga T, Bühler M. Dicer associates with chromatin to repress genome activity in Schizosaccharomyces pombe. Nat Struct Mol Biol. Nature Publishing Group; 2011;18: 94–9. doi:10.1038/nsmb.1935

88. Lõoke M, Kristjuhan K, Kristjuhan A. Extraction of genomic DNA from yeasts for PCR-based applications. Biotechniques. 2011;50: 325–8. doi:10.2144/000113672

89. Murray JM, Watson AT, Carr AM. Extraction of Chromosomal DNA from Schizosaccharomyces pombe. Cold Spring Harb Protoc. 2016;2016: pdb.prot090985. doi:10.1101/pdb.prot090985

90. Greenspan P, Mayer EP, Fowler SD. Nile red: a selective fluorescent stain for intracellular lipid droplets. J Cell Biol. 1985;100: 965–73. Available: http://jcb.rupress.org/content/100/3/965.abstract

91. Phalip V, Lemoine Y, Jeltsch JM. Cloning of Schizosaccharomyces pombe bio2 by heterologous complementation of a Saccharomyces cerevisiae mutant. Curr Microbiol. 1999;39: 348–0350. doi:10.1007/s002849900470

92. Stolz J. Isolation and characterization of the plasma membrane biotin transporter from Schizosaccharomyces pombe. Yeast. 2003;20: 221–31. doi:10.1002/yea.959

93. Sabatinos SA, Forsburg SL. Molecular Genetics of Schizosaccharomyces pombe [Internet]. 2nd ed. Guide to Yeast Genetics: Functional Genomics, Proteomics, and Other Systems Analysis. Elsevier Inc; 2010. doi:10.1016/S0076-6879(10)70032-X

94. Hagan IM, Grallert A, Simanis V. Synchronizing Progression of Schizosaccharomyces

pombe Cells from G2 through Repeated Rounds of Mitosis and S Phase with cdc25-22 Arrest Release. Cold Spring Harb Protoc. 2016;2016: pdb.prot091264. doi:10.1101/pdb.prot091264

95. Forsburg SL, Rhind N. Basic methods for fission yeast. Yeast. 2006;23: 173–183. doi:10.1002/yea.1347

96. Gordon CB, Fantes P a. The cdc22 gene of Schizosaccharomyces pombe encodes a cell cycle-regulated transcript. EMBO J. 1986;5: 2981–5. Available: http://www.ncbi.nlm.nih.gov/pubmed/16453725

97. Stolz J. Isolation and characterization of the plasma membrane biotin transporter from Schizosaccharomyces pombe. Yeast. 2003;20: 221–31. doi:10.1002/yea.959

98. Nurse P. Genetic control of cell size at cell division in yeast. Nature. 1975;256: 547–51. doi:10.1038/256547a0

99. Petersen J, Russell P. Growth and the Environment of Schizosaccharomyces pombe. Cold Spring Harb Protoc. 2016;2016: pdb.top079764. doi:10.1101/pdb.top079764

100. Tan X, Calderon-Villalobos LIA, Sharon M, Zheng C, Robinson C V, Estelle M, et al. Mechanism of auxin perception by the TIR1 ubiquitin ligase. Nature. 2007;446: 640–5. doi:10.1038/nature05731

101. Kanke M, Nishimura K, Kanemaki M, Kakimoto T, Takahashi TS, Nakagawa T, et al. Auxin-inducible protein depletion system in fission yeast. BMC Cell Biol. BioMed Central Ltd; 2011;12: 8. doi:10.1186/1471-2121-12-8

102. Nishimura K, Kanemaki MT. Rapid Depletion of Budding Yeast Proteins via the Fusion of an Auxin-Inducible Degron (AID). Current Protocols in Cell Biology. Hoboken, NJ, USA: John Wiley & Sons, Inc.; 2014. p. 20.9.1-20.9.16. doi:10.1002/0471143030.cb2009s64

103. McWilliam H, Li W, Uludag M, Squizzato S, Park YM, Buso N, et al. Analysis Tool Web Services from the EMBL-EBI. Nucleic Acids Res. 2013;41: W597-600. doi:10.1093/nar/gkt376

104. Rustici G, Mata J, Kivinen K, Lió P, Penkett CJ, Burns G, et al. Periodic gene expression program of the fission yeast cell cycle. Nat Genet. 2004;36: 809–17. doi:10.1038/ng1377

105. Blank HM, Perez R, He C, Maitra N, Metz R, Hill J, et al. Translational control of lipogenic enzymes in the cell cycle of synchronous, growing yeast cells. EMBO J. 2017;36: 487–502. doi:10.15252/embj.201695050

106. Yamashita YM, Nakaseko Y, Samejima I, Kumada K, Yamada H, Michaelson D, et al. 20S cyclosome complex formation and proteolytic activity inhibited by the cAMP/PKA pathway. Nature. 1996;384: 276–9. doi:10.1038/384276a0

107. Kawai M, Nakashima A, Ueno M, Ushimaru T, Aiba K, Doi H, et al. Fission yeast tor1 functions in response to various stresses including nitrogen starvation, high osmolarity, and high temperature. Curr Genet. 2001;39: 166–74. doi:10.1007/s002940100198

108. Weisman R, Choder M. The fission yeast TOR homolog, tor1+, is required for the response to starvation and other stresses via a conserved serine. J Biol Chem. 2001;276: 7027–32. doi:10.1074/jbc.M010446200

109. Weisman R, Roitburg I, Schonbrun M, Harari R, Kupiec M. Opposite effects of tor1 and tor2 on nitrogen starvation responses in fission yeast. Genetics. 2007;175: 1153–62. doi:10.1534/genetics.106.064170

110. Matsuo T, Otsubo Y, Urano J, Tamanoi F, Yamamoto M. Loss of the TOR kinase Tor2 mimics nitrogen starvation and activates the sexual development pathway in fission yeast. Mol Cell Biol. 2007;27: 3154–64. doi:10.1128/MCB.01039-06

111. Alvarez B, Moreno S. Fission yeast Tor2 promotes cell growth and represses cell differentiation. J Cell Sci. 2006;119: 4475–85. doi:10.1242/jcs.03241

112. Hayashi T, Hatanaka M, Nagao K, Nakaseko Y, Kanoh J, Kokubu A, et al. Rapamycin sensitivity of the Schizosaccharomyces pombe tor2 mutant and organization of two highly phosphorylated TOR complexes by specific and common subunits. Genes Cells. 2007;12: 1357–70. doi:10.1111/j.1365-2443.2007.01141.x

113. Hartmuth S, Petersen J. Fission yeast Tor1 functions as part of TORC1 to control mitotic entry through the stress MAPK pathway following nutrient stress. J Cell Sci. 2009;122: 1737–46. doi:10.1242/jcs.049387

114. Ikai N, Nakazawa N, Hayashi T, Yanagida M. The reverse, but coordinated, roles of Tor2 (TORC1) and Tor1 (TORC2) kinases for growth, cell cycle and separase-mediated mitosis in Schizosaccharomyces pombe. Open Biol. 2011;1: 110007. doi:10.1098/rsob.110007

115. Davie E, Forte GMA, Petersen J. Nitrogen regulates AMPK to control TORC1 signaling. Curr Biol. The Authors; 2015;25: 445–54. doi:10.1016/j.cub.2014.12.034

116. Petersen J, Nurse P. TOR signalling regulates mitotic commitment through the stress MAP kinase pathway and the Polo and Cdc2 kinases. Nat Cell Biol. 2007;9: 1263–72. doi:10.1038/ncb1646

117. Marguerat S, Schmidt A, Codlin S, Chen W, Aebersold R, Bähler J. Quantitative analysis of fission yeast transcriptomes and proteomes in proliferating and quiescent cells. Cell. 2012;151: 671–83. doi:10.1016/j.cell.2012.09.019

9 SUPPLEMENTS

Some of the data presented in this thesis are published in enclosed publications.

Publications:

Fission Yeast CSL Transcription Factors: Mapping Their Target Genes and Biological Roles.
Převorovský M, Oravcová M, Tvarůžková J, Zach R, Folk P, Půta F, Bähler J.
PLoS One. 2015

CSL protein regulates transcription of genes required to prevent catastrophic mitosis in fission yeast.
Převorovský M, Oravcová M, Zach R, Jordáková A, Bähler J, Půta F, Folk P.
Cell Cycle. 2016